

A Sober Look at Neural Network Initializations

Ingo Steinwart

Institute for Stochastics and Applications

Faculty 8: Mathematics and Physics

University of Stuttgart

D-70569 Stuttgart Germany

ingo.steinwart@mathematik.uni-stuttgart.de

September 6, 2019

Abstract

Initializing the weights and the biases is a key part of the training process of a neural network. Unlike the subsequent optimization phase, however, the initialization phase has gained only limited attention in the literature. In this paper we discuss some consequences of commonly used initialization strategies for vanilla DNNs with ReLU activations. Based on these insights we then develop an alternative initialization strategy. Finally, we present some large scale experiments assessing the quality of the new initialization strategy.

1 Introduction

Improving and understanding the training phase of deep neural networks has attracted a lot of attention in the last couple of years. This training phase mostly consists of minimizing an empirical risk term, and due to the structure of deep neural networks, the corresponding optimization landscape is convoluted and highly non-convex. To avoid getting stuck in local minima several variants of stochastic gradient descent have been proposed and successfully applied. These success stories suggest that the initialization of neural networks, that is, choosing the starting point of the optimization, has become less important. In fact, the two commonly used heuristics proposed in [7, 9] both focus on normalizing the variance of the weights of the neural network to ensure that the gradients of deep networks do not exponentially explode or implode. So far, however, positive or negative side-effects of these initialization strategies have not been investigated in depth. This is the first goal of our paper, and the second goal is to use these insights to develop a new initialization strategy.

To be a bit more specific let $|\cdot|_+ : \mathbb{R} \rightarrow [0, \infty)$ be the ReLU function, that is $|t|_+ := \max\{0, t\}$. For $d \in \mathbb{N}$, a single neuron is then given by

$$\begin{aligned} h : \mathbb{R}^d &\rightarrow [0, \infty) \\ x &\mapsto |\langle a, x \rangle + b|_+, \end{aligned}$$

where $a \in \mathbb{R}^d$ and $b \in \mathbb{R}$ are the weight vector and the bias of the neuron. A layer of width m is a function $H : \mathbb{R}^d \rightarrow [0, \infty)^m$, whose coordinate functions are neurons. Finally, a deep neural network is the composition of layers followed by an affine linear function, that is, a function $g : \mathbb{R}^d \rightarrow \mathbb{R}$ of the form

$$g = v \circ H_L \circ H_{L-1} \circ \cdots \circ H_1, \tag{1}$$

where $H_l : \mathbb{R}^{m_{l-1}} \rightarrow [0, \infty)^{m_l}$ are layers with $m_0 := d$ and the output neuron $v : \mathbb{R}^{m_L} \rightarrow \mathbb{R}$ is a function given by $v(x) = \langle w, x \rangle + c$, where w and c are the weight vector and the bias of the output neuron. Clearly, g is always a continuous and piecewise linear function, which is fully described by all its weight vectors and biases. Moreover, the architecture of a deep neural network is described by the number L of hidden layers, the input dimension d , and the widths m_1, \dots, m_L . In the following, we write

$$\mathcal{A}_{d, m_1, \dots, m_L, 1} := \{g : \mathbb{R}^d \rightarrow \mathbb{R} \mid g \text{ is of the form (1) with layers } H_l : \mathbb{R}^{m_{l-1}} \rightarrow [0, \infty)^{m_l} \text{ and } m_0 := d \}.$$

To train a neural network of fixed architecture, we need a labeled data set $D := ((x_1, y_1), \dots, (x_n, y_n)) \in (X \times \mathbb{R})^n$, where $X \subset \mathbb{R}^d$ is called the input space, as well as a loss function $L : \mathbb{R} \times \mathbb{R} \rightarrow [0, \infty)$. For a function $f : X \rightarrow \mathbb{R}$, we then define the empirical L -risk by

$$\mathcal{R}_{L, D}(f) := \frac{1}{n} \sum_{j=1}^n L(y_j, f(x_j)).$$

Now, training a network seeks an (approximate) empirical risk minimizer within the given architecture, that is a network $g_D \in \mathcal{A}_{d, m_1, \dots, m_L, 1}$ such that

$$\mathcal{R}_{L, D}(g_D) \approx \inf \{ \mathcal{R}_{L, D}(g) : g \in \mathcal{A}_{d, m_1, \dots, m_L, 1} \}. \quad (2)$$

Usually, the considered loss function is differentiable in its second argument and the networks $g \in \mathcal{A}_{d, m_1, \dots, m_L, 1}$ are parameterized by their weights and biases. The optimization problem is then executed on these parameters with the help of some variant of stochastic gradient descent (SGD). Consequently, the training produces a sequence $g_0, g_1, \dots, g_T \in \mathcal{A}_{d, m_1, \dots, m_L, 1}$ from which a g_D is chosen, e.g. $g_D := g_T$. Unfortunately, however, the optimization problem (2) is, in general, highly non-convex, and therefore, the final g_D may depend on the initial g_0 . Initializing the network, i.e., choosing an initial g_0 , is therefore a potentially crucial part of the entire training.

It is well-known, that initializing all weights and biases to the same value, e.g. to zero, hinders training by SGD since all neurons in the same layer will be updated in the same way. For this reason, the weights (and biases) are typically initialized randomly. More precisely, the most common initialization strategies proposed in [7] and [9] both fix some random variable A with distribution μ , that is $A \sim \mu$, and then initialize the weights of the layer H_l by realizations of independent copies of $\sigma_{m_{l-1}, m_l} A$, where σ_{m_{l-1}, m_l} is a suitable scaling factor. In fact, μ is usually either the standard normal distribution or the uniform distribution on e.g. $[-1, 1]$. Moreover, both papers propose to initialize the biases to zero, but some other heuristics also recommend a small positive value such as 0.1 or 0.01, or a some small random value, instead. We refer to [8, Ch. 8.4] for a more detailed discussion on these and other initialization strategies.

In any case, the resulting initial function g_0 is a random function, and one may ask how suitable this starting point g_0 is. So far, this question has not been answered in a satisfying manner, in fact, most papers dealing with this question only apply some heuristic arguments, mostly centered around effects on SGD updates on the weights, and report some empirical findings, mostly on a few data sets related to images.

The goal of this paper is to go beyond this by investigating how different initialization strategies influence the shape of the function g_0 . To this end, we first investigate the most simple case of one-dimension input data and one hidden layer, that is $d = L = 1$ in Section 2. Here it turns out that we can explicitly compute several key quantities such as the probability of initializing a neuron into an inactive state. As a consequence, we can also compare the effects of different initialization strategies, for example, we will see why it is better to choose a small positive value for the bias instead of a

small negative value. Finally, based on these insights, we will develop a first alternative initialization strategy. In Section 3 we will then investigate the significantly more complicated general situation. Here we will compute, for example, the influence of $\sigma_{m_l-1, m_l} A$ on the size and the direction of the weight vector, as well as on the size of the output of H_l . In addition, we will investigate the effect of different initialization strategies for the bias term. Based on these insights we will then develop a new initialization strategy that spreads the active and inactive regions of each neuron more widely across the space spanned by the input data of the layer. Finally, in Section 4 we present some experiments that compare to the new initialization strategy to the one of [9].

2 The simplest case: One-dimensional data and one hidden layer

In this section we explore the effects of different initialization strategies in the simplest case of one-dimensional input data and neural networks with one hidden layer consisting of ReLU-neurons. To be more precise, we assume that our input space X is a subset of \mathbb{R} and that our hidden layer has m neurons $h_1, \dots, h_m : \mathbb{R} \rightarrow \mathbb{R}$ of the form

$$h_i(x) = |a_i x + b_i|_+, \quad x \in \mathbb{R},$$

where $a_i, b_i \in \mathbb{R}$ are the weights and the biases of these neurons. Consequently, our network can represent exactly those functions $g : \mathbb{R} \rightarrow \mathbb{R}$ that are of the form

$$g(x) = \sum_{i=1}^m w_i |a_i x + b_i|_+ + c, \quad x \in \mathbb{R}, \quad (3)$$

where $w_1, \dots, w_m \in \mathbb{R}$ are the weights and $c \in \mathbb{R}$ is the bias of the output neuron. The goal of the training process is then to find suitable values for $a_1, b_1, \dots, a_m, b_m \in \mathbb{R}$, $w_1, \dots, w_m \in \mathbb{R}$, and $c \in \mathbb{R}$. Let us denote the set of all functions that can be represented by our network by $\mathcal{A}_{1,m,1}$, that is

$$\mathcal{A}_{1,m,1} := \{g : \mathbb{R} \rightarrow \mathbb{R} \mid g \text{ has a representation (3) for suitable } a_i, b_i, w_i \in \mathbb{R} \text{ and } c \in \mathbb{R}\}.$$

It is not hard to see that given a $g \in \mathcal{A}_{1,m,1}$, the representing parameters in (3) are anything than unique.

Now notice that for $a_i = 0$ the neuron h_i is a constant function, namely $h_i \equiv |b_i|_+$. Moreover, if $a_i \neq 0$, then h_i is a continuous, piecewise linear function with exactly one kink, and this kink is located at $x_i^* := -b_i/a_i$. Inspired by spline interpolation we call x_i^* a *knot* throughout this section. A simple calculation shows that in the case $a_i < 0$, the function h_i is given by

$$h_i(x) = \begin{cases} a_i x + b_i & \text{if } x \in (-\infty, x_i^*] \\ 0 & \text{if } x \in [x_i^*, \infty), \end{cases} \quad (4)$$

while for $a_i > 0$, it is given by

$$h_i(x) = \begin{cases} 0 & \text{if } x \in (-\infty, x_i^*] \\ a_i x + b_i & \text{if } x \in [x_i^*, \infty). \end{cases} \quad (5)$$

To describe the corresponding behavior of the function g with representation (3) we now write $I = \{1, \dots, m\}$, $I_* := \{i \in I : a_i \neq 0\}$, and

$$\begin{aligned} I_- &:= \{i \in I_* : a_i < 0\} \\ I_+ &:= \{i \in I_* : a_i > 0\}. \end{aligned}$$

Moreover, throughout the rest of this section we write $x_i^* := -b_i/a_i$ for $i \in I_*$.

Now, we immediately obtain the following result, which provides a different representation of $g \in \mathcal{A}_{1,m,1}$.

Proposition 2.1. *For $m \geq 1$ we fix a $g \in \mathcal{A}_{1,m,1}$ with the representation (3). Then for all $x \in \mathbb{R}$ we have*

$$g(x) = \sum_{i \in I_- : x \leq x_i^*} w_i(a_i x + b_i) + \sum_{i \in I_+ : x \geq x_i^*} w_i(a_i x + b_i) + \sum_{i \in I \setminus I_*} w_i |b_i|_+ + c$$

Our next goal is to derive explicit formulas for the partial derivatives considered during training of our neural network. To this end, we say that a loss function $L : \mathbb{R} \times \mathbb{R} \rightarrow [0, \infty)$ is *differentiable*, if for all $y \in \mathbb{R}$ the function

$$t \mapsto L(y, t)$$

is differentiable. In this case we write

$$L'(y, t) := \frac{\partial L}{\partial t}(y, t).$$

Since the function $t \mapsto |t|_+$ is not differentiable at 0, we formally need to exclude all occasions, at which we would need to use its derivative at 0. However, from a practical point of view this is not feasible, since there are actually realistic situations in which the “derivative” of $t \mapsto |t|_+$ at $t = 0$ is needed, see e.g. Example 2.10 below. For this reason, we pick a $\partial_0 \in [0, 1]$, which will serve as a surrogate for the missing derivative.¹ To be more precise, in all formulas involving derivatives of $t \mapsto |t|_+$ we will use ∂_0 , whenever we would actually need the derivative $t \mapsto |t|_+$ at $t = 0$. In addition, to allow for compact formulas, we define $\partial_t = 0$ for $t < 0$ and $\partial_t = 1$ for $t > 0$. Then, our approach gives

$$\frac{\partial |ax + b|_+}{\partial a}(a_0) = \partial_{a_0 x + b} \cdot x = \begin{cases} 0 & \text{if } a_0 x + b < 0 \\ \partial_0 \cdot x & \text{if } a_0 x + b = 0 \\ x & \text{if } a_0 x + b > 0, \end{cases} \quad (6)$$

where the first and third case is covered by the usual chain rule and in the second case we used ∂_0 as a formal surrogate. Similarly, we get

$$\frac{\partial |ax + b|_+}{\partial b}(b_0) = \partial_{ax + b_0} = \begin{cases} 0 & \text{if } ax + b_0 < 0 \\ \partial_0 & \text{if } ax + b_0 = 0 \\ 1 & \text{if } ax + b_0 > 0. \end{cases} \quad (7)$$

Moreover, if $f : \mathbb{R} \rightarrow \mathbb{R}$ is a differentiable function, then we formally apply the chain rule in the following sense

$$\frac{\partial f(|ax + b|_+)}{\partial a}(a_0) = f'(|a_0 x + b|_+) \cdot \frac{\partial |ax + b|_+}{\partial a}(a_0) = f'(|a_0 x + b|_+) \cdot \partial_{a_0 x + b} \cdot x \quad (8)$$

$$\frac{\partial f(|ax + b|_+)}{\partial b}(b_0) = f'(|ax + b_0|_+) \cdot \frac{\partial |ax + b|_+}{\partial b}(b_0) = f'(|ax + b_0|_+) \cdot \partial_{ax + b_0}. \quad (9)$$

In particular, given a $g \in \mathcal{A}_{1,m,1}$, these extended chain rules are used when computing partial derivatives of $\mathcal{R}_{L,D}(g)$ with respect to the parameters in (3). The next proposition executes these computations.

¹In “native” PyTorch, for example, we find $\partial_0 := 0$, see <https://github.com/pytorch/pytorch/issues/11662#issuecomment-423138052>, and the same choice is taken in Tensorflow, see https://github.com/tensorflow/tensorflow/blob/e39d8feebb9666a331345cd8d960f5ade4652bba/tensorflow/core/kernels/relu_op_functor.h#L54.

Proposition 2.2. *Let $L : \mathbb{R} \times \mathbb{R} \rightarrow [0, \infty)$ be a differentiable loss function. For $m \geq 1$ we further fix a $g \in \mathcal{A}_{1,m,1}$ with the representation (3). Then for $i \in I_-$ we have*

$$\begin{aligned}\frac{\partial \mathcal{R}_{L,D}(g)}{\partial a_i}(w, c, a, b) &= \frac{w_i}{n} \sum_{j:x_j < x_i^*} L'(y_j, g(x_j, w, c, a, b)) \cdot x_j + \frac{\partial_0 \cdot w_i \cdot x_i^*}{n} \sum_{j:x_j = x_i^*} L'(y_j, g(x_i^*, w, c, a, b)) \\ \frac{\partial \mathcal{R}_{L,D}(g)}{\partial b_i}(w, c, a, b) &= \frac{w_i}{n} \sum_{j:x_j < x_i^*} L'(y_j, g(x_j, w, c, a, b)) + \frac{\partial_0 \cdot w_i}{n} \sum_{j:x_j = x_i^*} L'(y_j, g(x_i^*, w, c, a, b)) \\ \frac{\partial \mathcal{R}_{L,D}(g)}{\partial w_i}(w, c, a, b) &= \frac{1}{n} \sum_{j:x_j < x_i^*} L'(y_j, g(x_j, w, c, a, b)) \cdot (a_i \cdot x_j + b_i).\end{aligned}$$

Moreover, for $i \in I_+$ we have

$$\begin{aligned}\frac{\partial \mathcal{R}_{L,D}(g)}{\partial a_i}(w, c, a, b) &= \frac{w_i}{n} \sum_{j:x_j > x_i^*} L'(y_j, g(x_j, w, c, a, b)) \cdot x_j + \frac{\partial_0 \cdot w_i \cdot x_i^*}{n} \sum_{j:x_j = x_i^*} L'(y_j, g(x_i^*, w, c, a, b)) \\ \frac{\partial \mathcal{R}_{L,D}(g)}{\partial b_i}(w, c, a, b) &= \frac{w_i}{n} \sum_{j:x_j > x_i^*} L'(y_j, g(x_j, w, c, a, b)) + \frac{\partial_0 \cdot w_i}{n} \sum_{j:x_j = x_i^*} L'(y_j, g(x_i^*, w, c, a, b)) \\ \frac{\partial \mathcal{R}_{L,D}(g)}{\partial w_i}(w, c, a, b) &= \frac{1}{n} \sum_{j:x_j > x_i^*} L'(y_j, g(x_j, w, c, a, b)) \cdot (a_i \cdot x_j + b_i).\end{aligned}$$

In addition, for $i \in I \setminus I_*$ we have

$$\begin{aligned}\frac{\partial \mathcal{R}_{L,D}(g)}{\partial a_i}(w, c, a, b) &= \frac{\partial_{b_i} \cdot w_i}{n} \sum_{j=1}^n L'(y_j, g(x_j, w, c, a, b)) \cdot x_j \\ \frac{\partial \mathcal{R}_{L,D}(g)}{\partial b_i}(w, c, a, b) &= \frac{\partial_{b_i} \cdot w_i}{n} \sum_{j=1}^n L'(y_j, g(x_j, w, c, a, b)) \\ \frac{\partial \mathcal{R}_{L,D}(g)}{\partial w_i}(w, c, a, b) &= \frac{|b_i|_+}{n} \sum_{j=1}^n L'(y_j, g(x_j, w, c, a, b)).\end{aligned}$$

Finally, we have

$$\frac{\partial \mathcal{R}_{L,D}(g)}{\partial c}(w, c, a, b) = \frac{1}{n} \sum_{j=1}^n L'(y_j, g(x_j, w, c, a, b)).$$

Inspired by Propositions 2.1 and Proposition 2.2 we now introduce the following classification for the state of a neuron h_i in (3).

Definition 2.3. *Let $D = ((x_1, y_1), \dots, (x_n, y_n)) \in (\mathbb{R} \times \mathbb{R})^n$ be a data set, and*

$$x_{\min} := \min_{1 \leq j \leq n} x_j \quad \text{and} \quad x_{\max} := \max_{1 \leq j \leq n} x_j,$$

and $g \in \mathcal{A}_{1,m,1}$ be a function with representation (3). For $i \in I_*$ we then say that the neuron h_i is:

- i) Fully active, if $x_{\min} < x_i^* < x_{\max}$.
- ii) Semi-active, if $i \in I_-$ and $x_i^* \geq x_{\max} > x_{\min}$, or if $i \in I_+$ and $x_i^* \leq x_{\min} < x_{\max}$.

iii) Inactive, if $i \in I_-$ and $x_i^* \leq x_{\min}$, or if $i \in I_+$ and $x_i^* \geq x_{\max}$.

Moreover, if $L : \mathbb{R} \times \mathbb{R} \rightarrow [0, \infty)$ is a differentiable loss function and $i \in I_*$, then we say that the neuron h_i is dead, if h_i is inactive and for all sub-samples D' of D we have

$$\frac{\partial \mathcal{R}_{L,D'}(g)}{\partial a_i}(w, c, a, b) = \frac{\partial \mathcal{R}_{L,D'}(g)}{\partial b_i}(w, c, a, b) = 0.$$

The following corollary shows that the state of a neuron h_i determines how h_i influences the entire function g .

Corollary 2.4. *Let $D = ((x_1, y_1), \dots, (x_n, y_n)) \in (\mathbb{R} \times \mathbb{R})^n$ be a data set and $g \in \mathcal{A}_{1,m,1}$ be a function with representation (3). Then for all $i \in I_*$ the following statements are true:*

i) *If h_i is fully active and there exists an x_{j_0} with $x_{\min} < x_{j_0} < x_{\max}$, then h_i does not behave linearly on the data set, that is, for all $\tilde{a}, \tilde{b} \in \mathbb{R}$ there exists a $j \in \{1, \dots, n\}$ such that*

$$h(x_j) \neq \tilde{a}x_j + \tilde{b}.$$

ii) *If h_i is semi-active, then h_i behaves linearly on the data set, namely for all $j = 1, \dots, n$ we have*

$$h_i(x_j) = a_i x_j + b_i.$$

iii) *The neuron h_i is inactive, if and only if for all $j = 1, \dots, n$ we have*

$$h_i(x_j) = 0.$$

Moreover, if h_i is inactive and $L : \mathbb{R} \times \mathbb{R} \rightarrow [0, \infty)$ is a differentiable loss function, then for all sub-samples $D' = ((x_{j_1}, y_{j_1}), \dots, (x_{j_k}, y_{j_k}))$ of D we have

$$\begin{aligned} \frac{\partial \mathcal{R}_{L,D'}(g)}{\partial a_i}(w, c, a, b) &= \frac{\partial_0 \cdot w_i \cdot x_i^*}{n} \sum_{l: x_{j_l} = x_i^*} L'(y_{j_l}, g(x_i^*, w, c, a, b)) \\ \frac{\partial \mathcal{R}_{L,D'}(g)}{\partial b_i}(w, c, a, b) &= \frac{\partial_0 \cdot w_i}{n} \sum_{l: x_{j_l} = x_i^*} L'(y_{j_l}, g(x_i^*, w, c, a, b)) \\ \frac{\partial \mathcal{R}_{L,D'}(g)}{\partial w_i}(w, c, a, b) &= 0. \end{aligned}$$

Consequently, h_i is dead independently of the specific choice of L , if $\partial_0 = 0$ or if $x_j \neq x_i^*$ for all $j = 1, \dots, n$.

Corollary 2.4 shows that, depending on its state, a neuron has a rather different impact on the entire network. Indeed, fully active neurons contribute in a truly non-linear manner, while semi-active neurons all contribute in a linear fashion. Once training is completed, all semi-active neurons could therefore be replaced by a single semi-active neuron weighted with new weight $w = 1$ and given by

$$h(x) := \left(\sum_{j \in I_{SA}} w_j a_j \right) \cdot x + \sum_{j \in I_{SA}} w_j b_j,$$

where I_{SA} denotes the set of all indices of semi-active neurons, and where we assume that future inputs x satisfy $x \in [x_{\min}, x_{\max}]$. In addition, all inactive neurons do not contribute to the network, and can therefore be removed after training. Finally, all dead neurons do not contribute to the

network, either, and since the partial derivatives of their parameters vanish, any training algorithm that uses these derivatives in a gradient-descent-type step will never change the parameters of these neurons. Consequently, these neurons can be removed during training without changing the final decision function $g \in \mathcal{A}_{1,m,1}$. Finally, note that if $\partial_0 = 0$, then all inactive neurons are actually dead. These observations raise the following question:

Q1. How many neurons are semi-active, inactive, or dead due to their initialization?

To answer this question, we write λ for the Lebesgue measure on \mathbb{R} and F_ν for the cumulative distribution function of a given probability measure ν on \mathbb{R} . Moreover, if ν is λ -absolutely continuous, then f_ν denotes a density of ν .

Now, we consider the following generic initialization strategy for our simple neural networks $g \in \mathcal{A}_{1,m,1}$.

Definition 2.5. Let P_a and P_w be probability measures on \mathbb{R} with $P_a(\{0\}) = P_w(\{0\}) = 0$ and P_b, P_c be probability measures on \mathbb{R} . Then we say that a $g \in \mathcal{A}_{1,m,1}$ with representation (3) is initialized by (P_w, P_c, P_a, P_b) , if the parameter vector (w, c, a, b) is a realization of a random variable with distribution $P := P_w^m \otimes P_c \otimes P_a^m \otimes P_b^m$.

Essentially all commonly used initialization methods are of the above type for suitably chosen (P_w, P_c, P_a, P_b) . We will discuss a few examples after we have investigated the generic initialization method.

Now recall that the state of a neuron h_i is defined by the position of its knot $x_i^* = -b_i/a_i$ relative to the data set D . This motivates the following definitions.

Definition 2.6. Let P and Q be two probability measures on \mathbb{R} with $Q(\{0\}) = 0$ and X, Y be two independent random variables with $X \sim P$ and $Y \sim Q$. Then the ratio distribution P/Q is the probability measure μ on \mathbb{R} that is given by

$$\frac{X}{Y} \sim \mu.$$

Moreover, we define the functions $F_{P,Q}^- : \mathbb{R} \rightarrow [0, 1]$ and $F_{P,Q}^+ : \mathbb{R} \rightarrow [0, 1]$ by

$$\begin{aligned} F_{P,Q}^-(z) &:= P \otimes Q(\{(x, y) \in \mathbb{R}^2 : x \geq zy \text{ and } y < 0\}) \\ F_{P,Q}^+(z) &:= P \otimes Q(\{(x, y) \in \mathbb{R}^2 : x \leq zy \text{ and } y > 0\}). \end{aligned}$$

To motivate the functions $F_{P,Q}^\pm$ we consider the product measure $P \otimes Q$ on \mathbb{R}^2 and the two projections $\pi_X, \pi_Y : \mathbb{R}^2 \rightarrow \mathbb{R}$ defined by $\pi_X(x, y) := x$ and $\pi_Y(x, y) := y$. Then π_X and π_Y are independent random variables and their distributions are P and Q . Using $Q(\{0\}) = 0$ this leads to

$$\begin{aligned} F_{P/Q}(z) &= P \otimes Q\left(\frac{\pi_X}{\pi_Y} \leq z\right) \\ &= P \otimes Q(\{(x, y) \in \mathbb{R}^2 : x \leq zy \text{ and } y > 0\}) + P \otimes Q(\{(x, y) \in \mathbb{R}^2 : x \geq zy \text{ and } y < 0\}) \\ &= F_{P,Q}^+(z) + F_{P,Q}^-(z) \end{aligned} \tag{10}$$

for all $z \in \mathbb{R}$. Moreover, the functions $F_{P/Q}$, $F_{P,Q}^-$, and $F_{P,Q}^+$ can be used to describe the probability for a neuron to be initialized into a fully active, semi-active, or inactive state, respectively. This is done in the following lemma.

Lemma 2.7. *Let $g \in \mathcal{A}_{1,m,1}$ be initialized by (P_w, P_c, P_a, P_b) . Then P -almost surely we have $I = I_*$. Moreover, $-x_i^*$ is, for all $i \in I_*$, a realization of a random variable with distribution P_b/P_a . In particular, if we have a data set D , then for all $i \in I_*$ we have*

$$P(\{\text{neuron } h_i \text{ is fully active}\}) = P_b/P_a((-x_{\max}, -x_{\min})).$$

Moreover, if F_{P_b/P_a} is continuous, then the following equations hold:

$$P(\{\text{neuron } h_i \text{ is fully active}\}) = F_{P_b/P_a}(-x_{\min}) - F_{P_b/P_a}(-x_{\max}), \quad (11)$$

$$P(\{\text{neuron } h_i \text{ is semi-active}\}) = P_a([0, \infty)) + F_{P_b, P_a}^-(-x_{\max}) - F_{P_b, P_a}^+(-x_{\min}), \quad (12)$$

$$P(\{\text{neuron } h_i \text{ is inactive}\}) = P_a((-\infty, 0]) + F_{P_b, P_a}^+(-x_{\max}) - F_{P_b, P_a}^-(-x_{\min}), \quad (13)$$

and, in addition, the following equivalence holds P_b/P_a -almost surely:

$$\text{neuron } h_i \text{ is inactive} \iff \text{neuron } h_i \text{ is dead.}$$

Lemma 2.7 shows that answering Question **Q1** reduces to computing the functions $F_{P/Q}$, $F_{P,Q}^-$, and $F_{P,Q}^+$. Fortunately, ratio distributions have a rather long history in probability and their first systematic treatment can be found in [3]. Consequently, computing the probability for neurons being fully active after initialization can be directly computed using those results. Distinguishing between semi-active and inactive neurons, however, also requires knowledge about $F_{P,Q}^-$ and $F_{P,Q}^+$. For this reason, Proposition A.1 collects several useful results on $F_{P/Q}$ as well as some results on $F_{P,Q}^-$ and $F_{P,Q}^+$. In particular, it is shown there Q is Lebesgue absolutely continuous and P is either also Lebesgue absolutely continuous or a Dirac distribution, then $F_{P/Q}$ is continuous, and hence (11), (12), and (13) hold. Moreover, in both cases, simplified formulas for computing $F_{P/Q}$, $F_{P,Q}^-$, and $F_{P,Q}^+$ are presented. Finally, if Q is symmetric, that is $Q(A) = Q(-A)$ for all measurable $A \subset \mathbb{R}$, then P/Q is symmetric, too.

The next theorem, which relies on both Lemma 2.7 and Proposition A.1, characterizes distributions P_b that prevent either inactive neurons or semi-active neurons during initialization.

Theorem 2.8. *Let $g \in \mathcal{A}_{1,m,1}$ be initialized by (P_w, P_c, P_a, P_b) and assume that F_{P_b/P_a} is continuous and that $P_a((-\varepsilon, \varepsilon)) > 0$ holds for all $\varepsilon > 0$. Moreover, let D be a data set with $x_{\min} \leq 0 \leq x_{\max}$. Then the following statements are equivalent:*

i) P_b only assigns positive values, that is $P_b((0, \infty)) = 1$.

ii) For all $i \in I$ we have $P(\{\text{neuron } h_i \text{ is inactive}\}) = 0$.

In addition, we also have the equivalence of the following two statements:

iii) P_b only assigns negative values, that is $P_b((-\infty, 0)) = 1$.

iv) For all $i \in I$ we have $P(\{\text{neuron } h_i \text{ is semi-active}\}) = 0$.

Note that without the continuity of F_{P_b/P_a} Theorem 2.8 does not hold in general. In particular, if P_b is the Dirac measure at zero, that is $P_b = \delta_{\{0\}}$, then $P_b/P_a = \delta_{\{0\}}$, and hence we have $x_i^* = 0$ almost surely. For data sets with $x_{\min} < 0 < x_{\max}$, all neurons are therefore fully active after initialization.

For other commonly used distributions, such as $P_b = \delta_{\{0,0.1\}}$, $P_b = \mathcal{U}[\alpha, \beta]$, or $P_b = \mathcal{N}(\mu, \sigma_b^2)$, and $P_a = \mathcal{U}[-\gamma, \gamma]$ or $P_a = \mathcal{N}(0, \sigma_a^2)$, however, the assumptions of Theorem 2.8 are satisfied. In this case, Theorem 2.8 shows that the only way to prevent inactive neurons during initialization is to enforce strictly positive biases by P_b . For such P_b , however, Theorem 2.8 further shows that the initialization

necessarily produces some semi-active neurons. By combining both equivalences of Theorem 2.8 we thus find

$$P(\{\text{neuron } h_i \text{ is fully active}\}) < 1. \quad (14)$$

However, this result requires, as already mentioned, the continuity of F_{P_b/P_a} . The next theorem in particular shows that for data sets with $x_{\min} < 0 < x_{\max}$, Inequality (14) actually holds for all $P_b \neq \delta_{\{0\}}$ and all commonly used P_a .

Theorem 2.9. *Let $g \in \mathcal{A}_{1,m,1}$ be initialized by (P_w, P_c, P_a, P_b) and assume that $P_a((-\varepsilon, 0)) > 0$ and $P_a((0, \varepsilon)) > 0$ hold for all $\varepsilon > 0$. Moreover, let D be a data set with $x_{\min} \leq 0 \leq x_{\max}$. Then for all $i \in I$ the following statements are equivalent:*

- i) $P_b(\{0\}) < 1$.
- ii) $P(\{x_i^* > x_{\max}\}) > 0$.
- iii) $P(\{x_i^* < x_{\min}\}) > 0$.

Moreover, if the data set D satisfies $x_{\min} < 0 < x_{\max}$, then these conditions are also equivalent to:

- iv) $P(\{x_i^* \geq x_{\max}\}) > 0$.
- v) $P(\{x_i^* \leq x_{\min}\}) > 0$.

For the most commonly used distributions for P_a and P_b , the ratio distribution as well as the functions $f_{P/Q}$, $F_{P/Q}$, $F_{P,Q}^-$, and $F_{P,Q}^+$ can be explicitly derived, see Examples, A.3, A.4, A.5, A.6, and A.7. Consequently, the probabilities for initializing fully active, semi-active, and inactive neurons can be explicitly with the help of Lemma 2.7. This is the goal of the next couple of examples, see also Figure 1 for the probabilities of not fully active and inactive knots and Figure 2 for the densities f_{P_b/P_a} of the knot distributions. In these examples, we restrict our considerations to data sets with $x_{\min} = 0$ and $x_{\max} = 1$, since a) this describes one of the two most commonly used data pre-scalings, and b) the non-negativity of x_{\min} will also play a key role when considering hidden layers in the middle of deeper neural networks in Section 3. In addition, considering the other commonly used data pre-scaling $x_{\min} = -1$ and $x_{\max} = 1$ in the examples below is merely more than a straight forward exercise.

The first two examples consider initialization strategies that assign constant values to the bias. These strategies are probably the most commonly used ones.²

Example 2.10 (Zero bias initialization). In recent years, the importance of proper initialization of neural networks and in particular of their weight parameters has been observed in e.g. [7] and [9]. To be more precise, in [7] it was proposed to initialize the weights of the l -th layer with the help of the following distributions $P_w := \mathcal{U}[-\alpha, \alpha]$ with $\alpha = \sqrt{6/(m_l + m_{l-1})}$, where m_{l-1} denotes the number of neurons in layer $l - 1$. Moreover, all bias entries are initialized using $\delta_{\{0\}}$. This initialization method is known as *Xavier* and is strictly speaking not for ReLUs. For this reason, [9] adapted the insights of [7] to ReLU-Functions. To be more precise, [9] proposes to initialize the weight entries of the l -th layer using a symmetric distribution whose variance is $2/m_{l-1}$. An explicitly mentioned example of such a distribution is $\mathcal{N}(0, \sigma_l^2)$ with $\sigma_l = \sqrt{2/m_{l-1}}$. Moreover, [9] again proposed to use $\delta_{\{0\}}$ for all bias entries. This initialization method is known as *He-et-al.*

²For example, [8, p. 302], writes “Typically, we set the biases for each unit to heuristically chosen constants, and initialize only the weights randomly.”

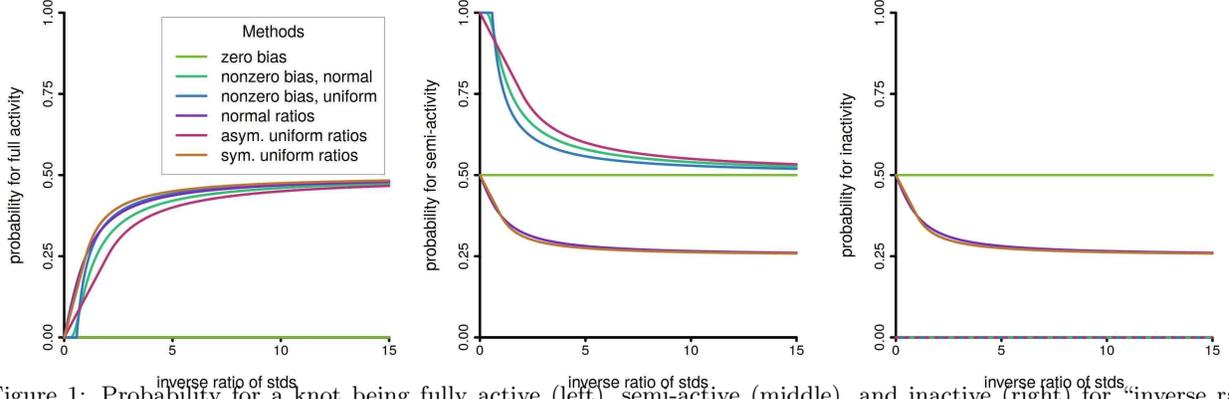


Figure 1: Probability for a knot being fully active (left), semi-active (middle), and inactive (right) for “inverse ratio of standard deviations” $\rho \in (0, 15]$ and data sets with $[x_{\min}, x_{\max}] = [0, 1]$. Six different initialization methods, which are discussed in Example 2.10 (“zero bias”), Example 2.11 (“nonzero bias . . .”), and Example 2.12 (“. . . ratios”), are displayed. For each method, the probability of initializing a fully active neuron is bounded from above by 0.5, and for typical choices of ρ this upper bound is actually almost attained. Moreover, the probability of initializing an inactive neuron is either approximately 0.25 or equal to 0. As shown in Theorem 2.8 the latter case occurs exactly for those distributions P_b , which only produce positive values for the bias.

Let us now analyze the effect of this and similar initialization methods. To this end, we consider a $g \in \mathcal{A}_{1,m,1}$, and assume that $P_b = P_c = \delta_{\{0\}}$ and that P_a and P_w are some Lebesgue-absolutely continuous, symmetric distributions. Then we have $P_b/P_a = \delta_{\{0\}}$, and therefore the initialization almost surely yields $x_i^* = 0$ for all $i = 1, \dots, m$. Moreover, we have $P_w(\{0\}) = 0$ and consequently, independent of the number of neurons m , our initialized g has almost surely exactly one knot, which is located at 0. Our next goal is to investigate the states of the neurons after initialization.

To this end we assume that our data set D is normalized such that it satisfies $[x_{\min}, x_{\max}] = [0, 1]$. Since $x_i^* = 0$, we then see that each neuron is either semi-active or inactive, and therefore Corollary 2.4 shows that for all $i = 1, \dots, m$ we either have $h_i(x_j) = 0$ for all $j = 1, \dots, n$ or $h_i(x_j) = a_i x_j + b_i$ for all $j = 1, \dots, n$. Moreover, a neuron h_i is semi-active if and only if $i \in I_+$, and it is inactive if and only if $i \in I_-$. By the symmetry of P_a we then find

$$P(\{\text{neuron } h_i \text{ is semi-active}\}) = P(\{\text{neuron } h_i \text{ is inactive}\}) = 0.5.$$

Let us now consider an inactive neuron h_i , that is $i \in I_-$. For the most commonly used choice $\partial_0 = 0$, part *iii*) of Corollary 2.4 then shows that h_i is dead. Therefore, the probability of h_i being initialized into a dead state is 0.5 and the total number $|I_{\text{dead}}|$ of neurons that are initialized as dead is a random variable with

$$|I_{\text{dead}}| \sim B(m, 0.5).$$

Let us now consider the case $\partial_0 > 0$. To this end, we first observe that for a sub-sample $D' = ((x_{j_1}, y_{j_1}), \dots, (x_{j_k}, y_{j_k}))$ of D , Corollary 2.4 and Proposition 2.2 show

$$\begin{aligned} \frac{\partial \mathcal{R}_{L,D'}(g)}{\partial a_i}(w, c, a, 0) &= \frac{\partial \mathcal{R}_{L,D'}(g)}{\partial w_i}(w, c, a, 0) = 0 \\ \frac{\partial \mathcal{R}_{L,D'}(g)}{\partial b_i}(w, c, a, 0) &= \frac{\partial_0 \cdot w_i}{n} \sum_{l: x_{j_l}=0} L'(y_{j_l}, c) \\ \frac{\partial \mathcal{R}_{L,D'}(g)}{\partial c}(w, c, a, 0) &= \frac{1}{n} \sum_{l=1}^k L'(y_{j_l}, g(x_{j_l}, w, c, a, 0)), \end{aligned} \quad (15)$$

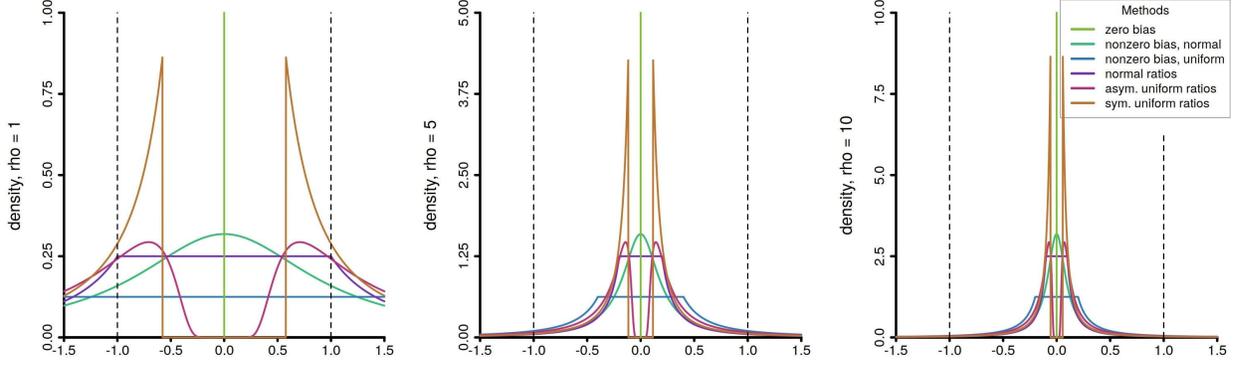


Figure 2: Densities f_{P_b/P_a} of the knot distributions for 5 different initialization strategies considered in Examples 2.11 and 2.12 and the initialization with $P_b = \delta_{\{0\}}$ of Example 2.10, which is indicated by a vertical line at $x = 0$. Left to Right: 3 inverse ratios of standard deviations $\rho = 1, 5$, and 10 as defined in the examples. For fixed P_b , distributions P_a with larger variance lead to larger ρ and, as the graphics show, to a higher concentration of P_a/P_b around zero. All densities are symmetric, and hence at least have of the initialized knots fall outside $[x_{\min}, x_{\max}] = [0, 1]$. In addition, all densities have a fat tail and are far from being uniform on $[x_{\min}, x_{\max}] = [0, 1]$.

where we used $b_i = x_i^* = 0$ and $g(x_i^*, w, c, a, 0) = g(0, w, c, a, 0) = c$. Note that our initialization actually ensures $c = 0$ but for the arguments below, we actually need general $c \in \mathbb{R}$. Let us now consider a gradient-descent type algorithm that uses a sub-sample D' of D . In the case

$$\sum_{l:x_{j_l}=0} L'(y_{j_l}, c) = 0, \quad (16)$$

this algorithm does not change the values of a_i , b_i and w_i , and hence the knots x_i^* are not changed, either. Note that (16) in particular holds, whenever the sub-sample D' does not contain a sample $x_{j_l} = 0$. Therefore let us now consider the first iteration of the training algorithm that uses sub-sample D' for which (16) does not hold. Clearly, such a D' needs to contain a sample $x_{j_l} = 0$. Our previous considerations then show that a_i , b_i and w_i have not been changed since their initialization. Without loss of generality we may thus assume that we are in the first iteration of the algorithm with c having some arbitrary value. Then (15) together with the symmetry of the distribution P_w and $P = P_w^m \otimes P_c \otimes P_a^m \otimes P_b^m$ shows that

$$P\left(\left\{(w, c, a, b) : \frac{\partial \mathcal{R}_{L, D'}(g)}{\partial b_i}(w, c, a, 0) < 0\right\}\right) = 0.5.$$

Since P_a is also symmetric we conclude that

$$\begin{aligned} 0.25 &= P\left(\left\{(w, c, a, b) : a_i < 0 \text{ and } \frac{\partial \mathcal{R}_{L, D'}(g)}{\partial b_i}(w, c, a, 0) < 0\right\}\right) \\ &= P\left(\left\{(w, c, a, b) : a_i < 0 \text{ and } \frac{\partial \mathcal{R}_{L, D'}(g)}{\partial b_i}(w, c, a, 0) > 0\right\}\right). \end{aligned}$$

In the case $a_i < 0$ and $\frac{\partial \mathcal{R}_{L, D'}(g)}{\partial b_i}(w, c, a, 0) > 0$, our gradient-descent-type algorithm will keep the values of a_i and w_i by Proposition 2.2 since we still have $x_i^* = 0$. Moreover, it will update b_i to some negative value b_i^{new} . Therefore we find $x_i^* = -b_i^{\text{new}}/a_i < 0$ after this update. Since all samples satisfy $x_j \geq 0$, we conclude by part *iii*) of Corollary 2.4 that h_i is dead after the update. Similarly, $a_i < 0$ and $\frac{\partial \mathcal{R}_{L, D'}(g)}{\partial b_i}(w, c, a, 0) < 0$, then the update yields $x_i^* > 0$ and therefore the neuron is either semi-active or fully active. The latter case occurs if the learning rate has been taken sufficiently

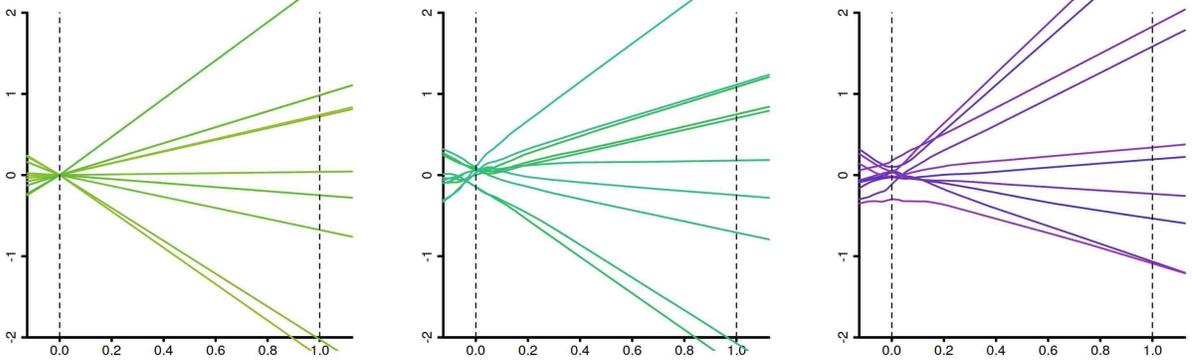


Figure 3: Ten randomly initialized predictors of a neural network with 128 hidden neurons with weights initialized by a zero-mean normal distribution with variance according to [9]. In each case, we set $c = 0$. Left: zero bias initialization, i.e. $b = 0$. Middle: nonzero bias initialization with $b = 0.1$, which leads to $\rho \approx 14.1$. Right: b is initialized by $\mathcal{N}(0, \sigma_b^2)$ with $\sigma_b = 0.1$, which again results in $\rho \approx 14.1$. As discussed in Example 2.10, the zero bias initialization lead to a linear behavior on $[0, 1]$, while the other two initialization methods only lead to an “almost” linear behavior on the right-hand side of the interval.

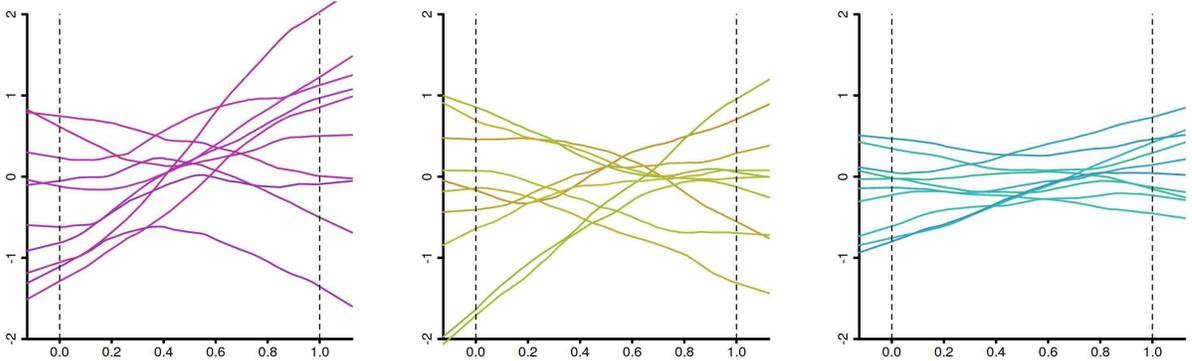


Figure 4: Ten randomly initialized predictors of a neural network with 128 hidden neurons. In all three cases, the knots $x_i^* \in [0, 1]$ are sampled from $\mathcal{U}[0, 1]$ and the weights a_i and b_i are sampled from symmetric distributions. The biases are then set to $b_i = -a_i x_i^*$ and $c = 0$. Left: Uniform weight distributions with variance according *He-et-al.*. Middle: Normal weight distributions with variance according to *He-et-al.*. Right: Weight distributions, which ensure $|a_i| = \|w\|_2 = 1$.

small, and in the following considerations we only treat this “optimistic” case. Furthermore, the two analogous sub-cases of $a_i > 0$ can be treated similarly, showing that we obtain a semi-active neuron if $\frac{\partial \mathcal{R}_{L, D'}(g)}{\partial b_i}(w, c, a, 0) < 0$, and, following our optimistic view, a fully active neuron in the remaining case.

Summing up, if $\partial_0 > 0$ and the learning rate is sufficiently small, for each neuron the probabilities of being dead or semi-active after the first iteration, in which x_i^* is changed, are 0.25 each, while the probability of having a fully active neuron is 0.5.

Example 2.11 (Non-zero bias). Initializing the weights according to [9] seems to be one of the most common strategies. Sometimes, however, the bias is initialized differently by $P_b := \delta_{\{b\}}$ for some small $b > 0$. For example, [12] uses $b = 0.01$, and [8, p. 192] discusses $b = 0.1$. Let us now investigate the consequences of this initialization method. To this end, we assume that we have fixed an arbitrary $b > 0$ and $P_b := \delta_{\{b\}}$.

Let us first consider the case $P_a := \mathcal{N}(0, \sigma_a^2)$, where σ_a can, e.g. be initialized according to [9]. Moreover, we write $\varrho := \sigma_a/b$ for the “inverse ratio of standard deviations”, where for P_b we used the

standard deviation of its symmetrized version $\frac{1}{2}(\delta_{\{b\}} + \delta_{\{-b\}})$. Note that for the method proposed by [9], we have $\sigma_a = \sqrt{2}$ and hence $b = 0.1$ leads to $\rho \approx 14.1$ and $b = 0.01$ leads to $\rho \approx 141$. By Example A.4 the distribution of each knot x_i^* has the Lebesgue density

$$f_{P_b/P_a}(z) = \frac{1}{\sqrt{2\pi}\varrho z^2} \exp\left(-\frac{1}{2\varrho^2 z^2}\right), \quad z \in \mathbb{R}.$$

and Figure 2 indicates that for $b = 0.1$ and $b = 0.01$ the corresponding distributions are highly concentrated around 0. Furthermore, Example A.4 also provides the functions F_{P_b/P_a} , and F_{P_b/P_a}^+ . For a data set with $[x_{\min}, x_{\max}] = [0, 1]$, Lemma 2.7 and Theorem 2.8 then give

$$\begin{aligned} P(\{\text{neuron } h_i \text{ is fully active}\}) &= \Phi\left(-\frac{1}{\varrho}\right), \\ P(\{\text{neuron } h_i \text{ is semi-active}\}) &= 1 - \Phi\left(-\frac{1}{\varrho}\right), \\ P(\{\text{neuron } h_i \text{ is inactive}\}) &= 0. \end{aligned}$$

Note that for $b = 0.1$ and $b = 0.01$ we have $\Phi\left(-\frac{1}{\varrho}\right) \approx 0.5$, see also Figure 1.

Let us now consider the case $P_a := \mathcal{U}[-\alpha, \alpha]$, where $\alpha > 0$. We define $\varrho := \frac{\alpha}{\sqrt{3b}}$ and note that for the method proposed by [9], we have $\sigma_a = \sqrt{2}$ and hence $b = 0.1$ again leads to $\rho \approx 14.1$ and $b = 0.01$ leads to $\rho \approx 141$. Moreover, the functions f_{P_b/P_a} , F_{P_b/P_a} , and F_{P_b/P_a}^+ are computed in Example A.7. For a data set with $[x_{\min}, x_{\max}] = [0, 1]$, Lemma 2.7 and Theorem 2.8 then give

$$\begin{aligned} P(\{\text{neuron } h_i \text{ is fully active}\}) &= \begin{cases} 0 & \text{if } \varrho \leq \frac{1}{\sqrt{3}} \\ \frac{1}{2} - \frac{1}{\sqrt{12}\varrho} & \text{if } \varrho \geq \frac{1}{\sqrt{3}} \end{cases}, \\ P(\{\text{neuron } h_i \text{ is semi-active}\}) &= \begin{cases} 1 & \text{if } \varrho \leq \frac{1}{\sqrt{3}} \\ \frac{1}{2} + \frac{1}{\sqrt{12}\varrho} & \text{if } \varrho \geq \frac{1}{\sqrt{3}} \end{cases}, \\ P(\{\text{neuron } h_i \text{ is inactive}\}) &= 0. \end{aligned}$$

Consequently, for $\rho \approx 14.1$ or $\rho \approx 141$ the probability of initializing a fully active neuron approximately equals 0.5 and the same is true for semi-active neurons, see also 1. Finally, the distribution of each knot x_i^* has the Lebesgue density

$$f_{P_b/P_a}(z) = \begin{cases} 0 & \text{if } z \in \left[-\frac{1}{\sqrt{3}\varrho}, \frac{1}{\sqrt{3}\varrho}\right] \\ \frac{1}{\sqrt{12}\varrho} \cdot z^{-2} & \text{if } z < -\frac{1}{\sqrt{3}\varrho} \text{ or } z > \frac{1}{\sqrt{3}\varrho} \end{cases},$$

and for the above mentioned values of ρ the corresponding distributions are highly concentrated around 0, see Figure 2.

Example 2.12 (Random Initializations). Another class of possible initialization strategies initialize both the weights and the biases randomly with the help of some ad-hoc distributions such as the uniform or normal distribution. These strategies are considered in this example.

Let us first investigate the case of normal distributions, that is, in the hidden layer we have $P_a := \mathcal{N}(0, \sigma_a^2)$ and $P_b := \mathcal{N}(0, \sigma_b^2)$ for some $\sigma_a, \sigma_b > 0$, and the output layer is initialized similarly

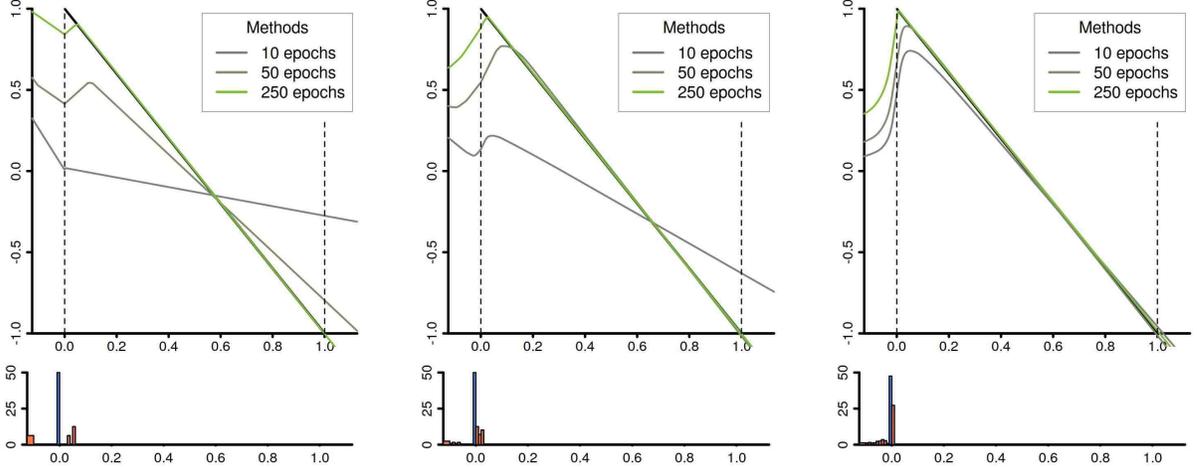


Figure 5: Training behavior for three architectures and the initialization strategy *He-et-al.* with zero mean normal distribution for the weights. The biases are set to zero as in Example 2.10. The upper row displays how well the predictors approximate the target $f^*(t) = 2 - t$ after 10, 50, and 250 training epochs. The histograms in the lower row indicate the distribution of knots in percent for $i \in I_+$ (orange bars) and $i \in I_-$ (blue bars on top of the orange ones). Left: $m = 16$ hidden neurons. Middle: $m = 128$. Right: $m = 1024$. In all cases, the target is not well approximated after 50 epochs. Also, despite the fact that the target function can be represented by single hidden neuron (or even no hidden layer at all), the already over-parameterized architecture $m = 16$ exhibits some difficulties in quickly learning the target function. Finally, the large blue bars left to zero correspond to the approximately 50 percent of dead neurons as predicted in Example 2.10.

with variances σ_w^2 and σ_c^2 , instead. Let us write $\varrho := \sigma_a/\sigma_b$ for the inverse ratio of standard deviations. For a given data set D , a combination of Lemma 2.7 and Example A.3 with (A.41) and $\arctan(-t) = -\arctan(t)$ then yields

$$\begin{aligned}
 P(\{\text{neuron } h_i \text{ is fully active}\}) &= \frac{1}{\pi} \arctan(\varrho \cdot x_{\max}) - \frac{1}{\pi} \arctan(\varrho \cdot x_{\min}), \\
 P(\{\text{neuron } h_i \text{ is semi-active}\}) &= P(\{\text{neuron } h_i \text{ is inactive}\}) \\
 &= \frac{1}{2} - \frac{1}{2\pi} \arctan(\varrho \cdot x_{\max}) + \frac{1}{2\pi} \arctan(\varrho \cdot x_{\min})
 \end{aligned}$$

for all $i \in I$. In particular, if the data is scaled to $[0, 1]$, that is $[x_{\min}, x_{\max}] = [0, 1]$ then the latter probability becomes

$$P(\{\text{neuron } h_i \text{ is inactive}\}) = \frac{1}{2} - \frac{1}{2\pi} \arctan(\varrho).$$

In addition, the distribution of each knot x_i^* has the Lebesgue density

$$f_{P_b/P_a}(z) = \frac{1}{\pi} \cdot \frac{\varrho}{\varrho^2 z^2 + 1}, \quad z \in \mathbb{R}.$$

Let us now consider the case, in which both distributions P_a and P_b are uniform distributions. We begin with the sub-case $P_b := \mathcal{U}[0, \beta]$ and $P_a := \mathcal{U}[-\alpha, \alpha]$ for some $\alpha, \beta > 0$. Again, we write $\varrho := \frac{\alpha}{\sqrt{3}} \left(\frac{\beta}{\sqrt{12}}\right)^{-1} = 2\alpha/\beta$ for the inverse ratio of standard deviations. The formula for the cumulative

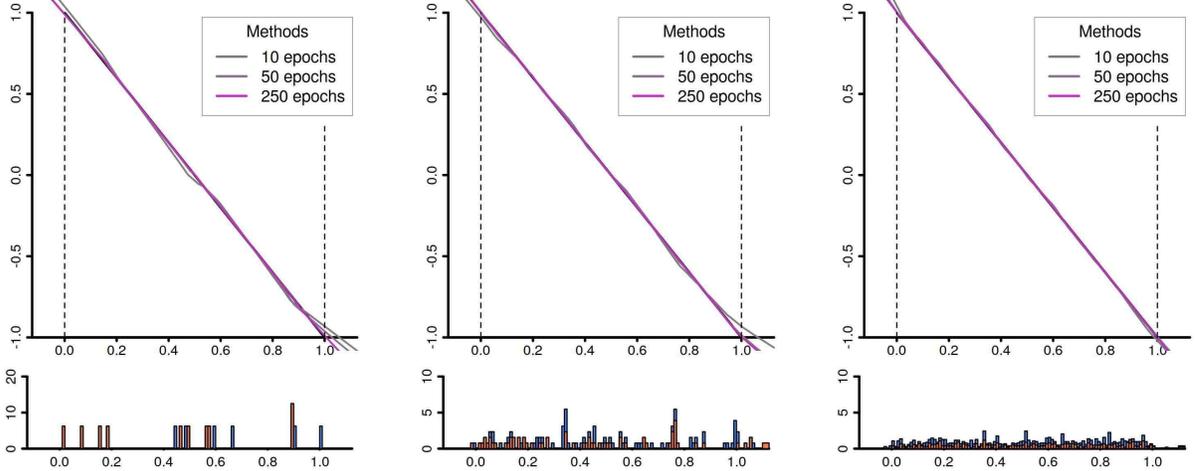


Figure 6: Training behavior for three architectures and an initialization strategy, that samples the knots x_i^* from $\mathcal{U}[0, 1]$ and that initializes the weights by a zero mean normal distribution with variances according to *He-et-al.*. The 6 graphics have a meaning analogous to Figure 5. Notice that unlike the method considered in Figure 5, the new initialization method already leads to a good approximation after 10 training epochs.

distribution function provided in Example A.5 then reads as

$$F_{P_b/P_a}(z) = \begin{cases} -\frac{1}{2\varrho z} & \text{if } z \leq -\frac{2}{\varrho} \\ \frac{4 + \varrho z}{8} & \text{if } z \in \left[-\frac{2}{\varrho}, \frac{2}{\varrho}\right] \\ 1 - \frac{1}{2\varrho z} & \text{if } z \geq \frac{2}{\varrho} . \end{cases}$$

For a data set with $[x_{\min}, x_{\max}] = [0, 1]$ we consequently find by Lemma 2.7

$$P(\{\text{neuron } h_i \text{ is fully active}\}) = \begin{cases} \frac{\varrho}{8} & \text{if } \varrho \leq 2 \\ \frac{1}{2} - \frac{1}{2\varrho} & \text{if } \varrho \geq 2 , \end{cases}$$

$$P(\{\text{neuron } h_i \text{ is inactive}\}) = 0 .$$

Finally, for both types of data sets the distribution of each knot x_i^* has the Lebesgue density

$$f_{P_b/P_a}(z) = \frac{1}{2} \cdot \min\left\{\frac{\varrho}{4}, \frac{1}{\varrho z^2}\right\}, \quad z \in \mathbb{R} .$$

Let us now consider the sub-case $P_b := \mathcal{U}[-\beta, \beta]$ and $P_a := \mathcal{U}[-\alpha, \alpha]$ for some $\alpha, \beta > 0$. Then the inverse ratio of standard deviations is $\varrho := \alpha/\beta$ and therefore Example A.6 shows that

$$F_{P_b/P_a}(z) = \begin{cases} -\frac{1}{4\varrho z} & \text{if } z \leq -\frac{1}{\varrho} \\ \frac{2 + \varrho z}{4} & \text{if } z \in \left[-\frac{1}{\varrho}, \frac{1}{\varrho}\right] \\ 1 - \frac{1}{4\varrho z} & \text{if } z \geq \frac{1}{\varrho} . \end{cases}$$

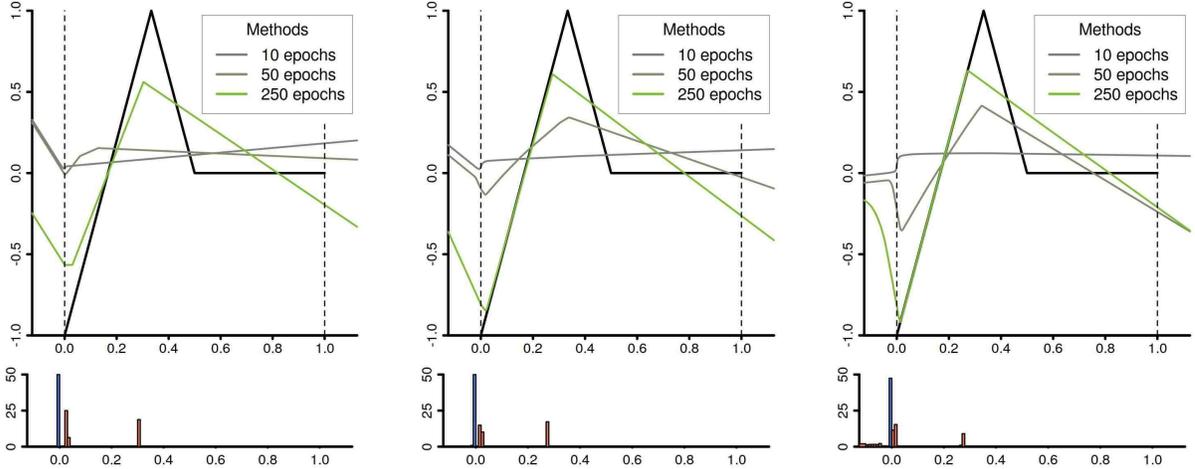


Figure 7: Training behavior as in Figure 5 for the target function $f^*(t) = 1 - 6 \cdot |x - 1/3|$, which can be represented by 2 hidden neurons with knots at $x_1^* = 1/3$ and $x_2^* = 1/2$. Clearly, the optimizer fails to learn the target function within 250 epochs. Recall that initializing with *He-et-al.* places all knots at $x = 0$ and the training algorithm apparently has significant difficulties to push even a single knot towards $x = 1/3$.

For a data set with $[x_{\min}, x_{\max}] = [0, 1]$ we consequently find by Lemma 2.7 that

$$P(\{\text{neuron } h_i \text{ is fully active}\}) = \begin{cases} \frac{\varrho}{4} & \text{if } \varrho \leq 1 \\ \frac{1}{2} - \frac{1}{4\varrho} & \text{if } \varrho \geq 1 \end{cases},$$

$$P(\{\text{neuron } h_i \text{ is inactive}\}) = \begin{cases} \frac{1}{2} - \frac{\varrho}{8} & \text{if } \varrho \leq 1 \\ \frac{1}{4} + \frac{1}{8\varrho} & \text{if } \varrho \geq 1 \end{cases}.$$

Finally, the distribution of each knot x_i^* has the Lebesgue density

$$f_{P_b/P_a}(z) = \frac{1}{4} \min\left\{\varrho, \frac{1}{\varrho z^2}\right\}, \quad z \in \mathbb{R}.$$

Let us summarize our findings we made so far: If we wish to avoid neurons to be dead right after initialization and we also want to allow weights a_i arbitrarily close to 0, then we need initialize the biases b_i with strictly positive values, see Theorem 2.8. However, such an approach necessarily produces semi-active neurons, too, and the only way to control the fraction of the latter for fixed P_a is to generate small values for b_i , only. This, however, forces the knots x_i^* to be more concentrated around 0, forcing the initial function $g(\cdot, w, c, a, b)$ of our network to be almost linear on the data set, see Figure 3. Finally, in the “limiting” case $b_i := 0$, the function $g(\cdot, w, c, a, b)$ is actually linear on the data set, and no neuron is fully active. In fact, with the usual setting $\partial_0 = 0$, half of the initialized neurons are dead.

Now recall that the goal of the learning process is to find parameters w, c, a , and b such that the resulting $g(\cdot, w, c, a, b)$ approximates the unknown target function $f_{L,P}^*$ well. For most $f_{L,P}^*$, such an approximation requires the corresponding knots to be spread over the input interval, which in our case is $[0, 1]$. Consequently, if we force the knots to be concentrated near zero for the reasons discussed above, then these knots need to be significantly moved during the training phase. This raises the question, whether such initializations really produce good starting points for the training process, or to phrase it differently:

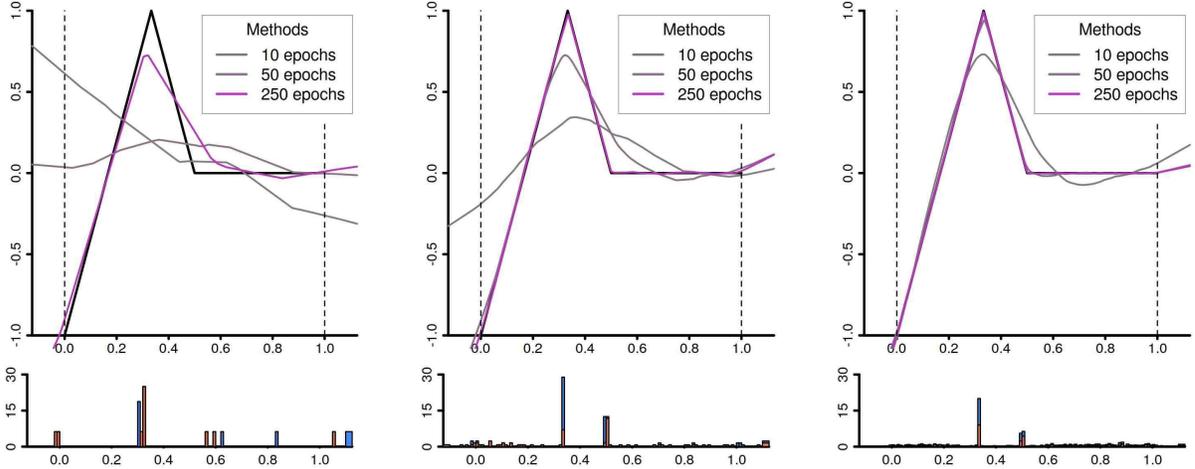


Figure 8: Learning the function of Figure 7 with the initialization method considered in Figure 6. At least for the two larger architectures, the new initialization method achieves a good approximation within 250 epochs.

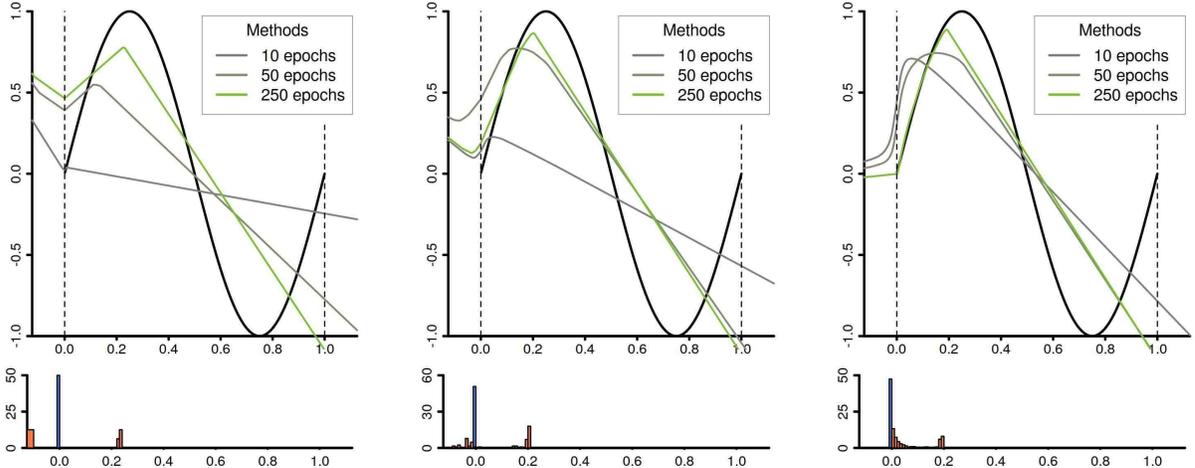


Figure 9: Training with initialization *He-et-al.* as in Figure 5 for the target function $f^*(t) = \sin(2\pi t)$. Again, the optimizer fails to produce meaningful approximations of f^* , and similar to Figure 7, the knots are not pushed beyond $1/4$. This results in a good approximation on the left, but a very poor one on the right.

Q2. Are there other initialization strategies that ensure both a large fraction of fully active neurons and a somewhat uniform distribution of the knots?

Q3. Do such initializations produce better starting points for the training process?

Let us first consider **Q2**. Our discussion above showed that the conventional initialization strategies can only partially ensure both goals simultaneously. On the other hand, these initialization strategies actually focus on initializing the weights and biases, whereas the location of the knots is merely more than a side-product of this focus. For a moment, let us therefore consider the case, in which we begin with the distribution of the knots, instead. For example, we could sample virtual knots x_i^* according to the uniform distribution on $[0, 1]$. Using the formula $x_i^* = -b_i/a_i$, we then see that we either need to initialize a_i or b_i . Moreover, the empirical success of [9] suggests that initializing a_i as in Example 2.10 should be kept. Following this, we would then initialize the biases by $b_i := -a_i x_i^*$. Obviously, for data sets with $[x_{\min}, x_{\max}] = [0, 1]$, this new initialization strategy almost surely produces fully active neurons as well as uniformly distributed knots. In other words, both aspects of **Q2** are fully satisfied

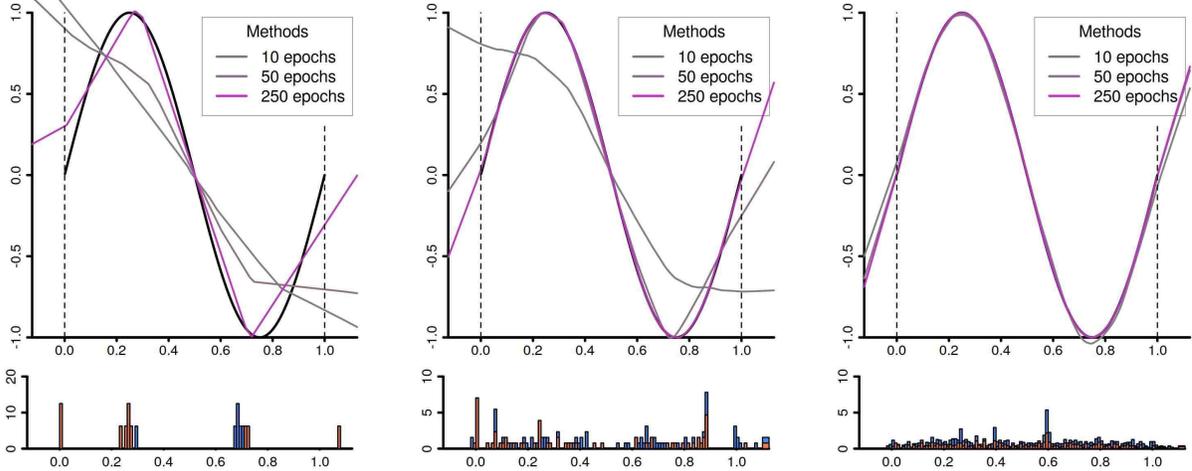


Figure 10: The situation of Figure 9 for the initialization method considered in Figure 6. At least for the two larger architectures the target function is well approximated, and for $m = 1024$ this is almost instantly achieved.

and a comparison between Figure 3 and Figure 4 shows that the resulting initial predictors are less biased towards a linear behavior.

Let us therefore investigate, whether the new initialization strategy also positively answers **Q3**. Since later in Section 3 we will investigate similar initialization strategies in more detail, we restrict our considerations to three toy examples illustrated in Figures 5 to 10. These Figures show that the new initialization strategy leads in basically all considered cases to a faster learning of the target function than initializing with *He-et-al.* and zero biases does. Moreover, *He-et-al.* with zero biases seems to have serious problems when a good approximation of the target function requires knots being located further away from 0. As a consequence, some target functions could not be learned sufficiently well with this initialization method. Based on these initial promising findings, we will generalize the new initialization method to higher dimensions.

3 The General situation

The goal of this section is to generalize the initialization strategy discussed at the end of Section 2 to higher dimensions and deeper networks. To this end, we consider throughout this section a single hidden layer within a deep architecture. To be more precise, we assume that this hidden layer follows a layer with d neurons, i.e. $d = m_{l-1}$ and that the layer itself has m neurons, i.e. $m = m_l$. In particular, if the considered hidden layer is the first hidden layer, then d equals the dimension of the input space. Moreover, to avoid notational overload, we denote the data that goes into the considered layer by x_1, \dots, x_n . In particular, we have $x_j \in \mathbb{R}^d$, and if the considered layer is not the first hidden layer, the non-negativity of the ReLU-functions applied in the previous layer actually ensures

$$x_j \in [0, \infty)^d, \quad i = 1, \dots, n. \quad (17)$$

To avoid a cumbersome distinction of cases, we assume in the following that (17) also holds for the first hidden layer, whenever we require (17) for our results. Now, the considered hidden layer consists of m neurons of the form

$$\begin{aligned} h_i : \mathbb{R}^d &\rightarrow [0, \infty) \\ x &\mapsto |\langle a_i, x \rangle + b_i|_+, \end{aligned} \quad (18)$$

where $a_1, \dots, a_n \in \mathbb{R}^d$ and $b_1, \dots, b_m \in \mathbb{R}$ are the weight vectors and biases of these neurons. To address **Q2**, which asks for “a large fraction of fully active neurons and a somewhat uniform distribution of the knots”, our first goal needs to be a translation of “fully active neurons” and “knots”.

Let us begin with the latter notion. To this end, we note that in the one-dimensional case $d = 1$ the knot is defined by the equation $a_i x_i^* + b_i = 0$, and the obvious generalization to $d > 1$ is

$$x_i^* := \{x \in \mathbb{R}^d : \langle a_i, x \rangle + b_i = 0\}$$

provided that $a_i \neq 0$. Clearly, x_i^* is the affine hyperplane that separates the two sets

$$\begin{aligned} A_i^+ &:= \{x \in \mathbb{R}^d : \langle a_i, x \rangle + b_i > 0\} \\ A_i^- &:= \{x \in \mathbb{R}^d : \langle a_i, x \rangle + b_i < 0\}. \end{aligned}$$

In the following, we call x_i^* the *edge of the neuron h_i* , and A_i^+ , A_i^- its *region of activity* and *inactivity*, respectively. In the one-dimensional case the region of activity of a neuron with $a_i > 0$ is (x_i^*, ∞) , see (4), while its region of inactivity is $(-\infty, x_i^*)$. With this information it is easy to see that the following definition generalizes the one-dimensional case considered in Definition 2.3.

Definition 3.1. *Let $D = (x_1, \dots, x_n)$ be a data set in \mathbb{R}^d and $h_i : \mathbb{R}^d \rightarrow [0, \infty)$ be a neuron of the form (18) with $a_i \neq 0$. Moreover, let x_i^* , A_i^+ , and A_i^- be as above. Then we say that h_i is:*

- i) Fully active, if we have $D \cap A_i^+ \neq \emptyset$ and $D \cap A_i^- \neq \emptyset$.
- ii) Semi-active, if $D \subset x_i^* \cup A_i^+$ and $D \not\subset x_i^*$ hold.
- iii) Inactive, if $D \subset x_i^* \cup A_i^-$ holds.

Note that each neuron with $a_i \neq 0$ is in exactly one of these states. Our next goal is provide an alternative characterization of fully active neurons, which in the sequel make it possible to describe initialization strategies. To this end, recall that the convex hull $\text{co } A$ of a set $A \subset \mathbb{R}^d$ is the smallest convex set containing the set A . For a finite set $A = \{y_1, \dots, y_k\}$ we further define

$$\text{ico } A := \left\{ y \in \mathbb{R}^d : \exists \lambda_1, \dots, \lambda_k > 0 \text{ with } \lambda_1 + \dots + \lambda_k = 1 \text{ and } y = \sum_{j=1}^k \lambda_j y_j \right\}.$$

It can be shown that $\text{ico } A$ is the interior of $\text{co } A$ relative to the affine hull of A , but since we do not need this, we skip the details. Moreover, we clearly have $\text{ico } A \subset \text{co } A$ and equality only holds if $|A| = 1$. Moreover, it is not hard to see that $\text{ico } A$ is convex and that the closure of $\text{ico } A$ equals $\text{co } A$, that is $\overline{\text{ico } A} = \text{co } A$. Finally, for a data set $D = (x_1, \dots, x_n)$ we write $\text{ico } D := \text{ico}\{x_1, \dots, x_n\}$. The next lemma characterizes fully active neurons with the help of $\text{ico } D$.

Lemma 3.2. *Let $D = (x_1, \dots, x_n)$ be a data set in \mathbb{R}^d with $n \geq 2$ and $h_i : \mathbb{R}^d \rightarrow [0, \infty)$ be a neuron of the form (18) with $a_i \neq 0$ and edge x_i^* . Then the following statements are equivalent:*

- i) The neuron h_i is fully active.
- ii) We have both $x_i^* \cap \text{ico } D \neq \emptyset$ and $\text{ico } D \not\subset x_i^*$.

Our next goal is to generalize Corollary 2.4, which described how the state of a neuron influences its behavior on the data set. Clearly, if a neuron h_i is inactive, then we have $h_i(x_j) = 0$ for all $j = 1, \dots, n$, and if h_i is semi-active, then $h_i(x_j) = \langle a_i, x_j \rangle + b_i$ for all $j = 1, \dots, n$. Consequently, the remarks made after Corollary 2.4 remain valid for these types of neurons. The next lemma shows that the assertion of Corollary 2.4 for fully active neurons is also true in the case $d > 1$.

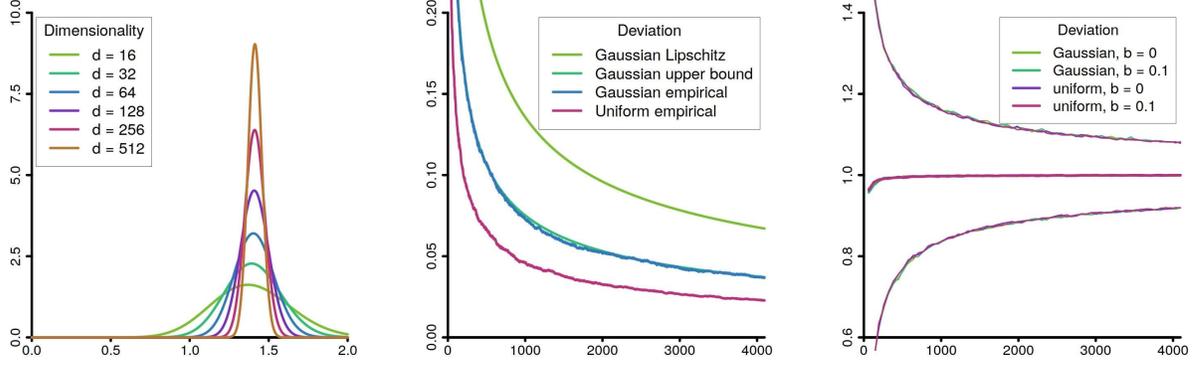


Figure 11: Left: Densities of $\|A\|_2$, where $A = (A_1, \dots, A_d)$ is a vector of i.i.d. random variables with $A_i \sim \mathcal{N}(0, 2/d)$. Middle: Plots for estimates of the smallest $\delta > 0$ satisfying $P(\|A\|_2 \geq \sqrt{2} + \delta) \leq 0.01$ for $d = 1, \dots, 4096$. The descriptors “Gaussian Lipschitz” and “Gaussian upper bound” refer to the theoretical estimates (20) and (22), respectively. The two empirical estimates are based on 50,000 repetitions. The upper bound (22) is on average 2% off. In contrast, (20) captures the asymptotics but is, on average, by a factor of about 1.8 too large. Right: Average value and 1%, respectively 99% percentile of $(\frac{d}{m})^{1/2} \|(h_1(x), \dots, h_m(x))\|_2$ for a fixed input vector $x \in \mathbb{R}^d$ with $d = 64$ and $m = 1, \dots, 4096$. The values are empirical estimates based upon 10,000 repetitions.

Lemma 3.3. *Let $D = (x_1, \dots, x_n)$ be a data set in \mathbb{R}^d with $n \geq 2$ for which there is a $j_0 \in \{1, \dots, n\}$ with $x_{j_0} \in \text{ico } D$. Moreover, let $h_i : \mathbb{R}^d \rightarrow [0, \infty)$ be a neuron of the form (18) with $a_i \neq 0$. Then the following statements are equivalent:*

i) *The neuron h_i is fully active.*

ii) *The neuron h_i does not behave linearly on D , that is, for all $\tilde{a} \in \mathbb{R}^d$, $\tilde{b} \in \mathbb{R}$, there exists a $j \in \{1, \dots, n\}$ such that*

$$h(x_j) \neq \langle \tilde{a}, x_j \rangle + \tilde{b}.$$

Our next goal is to investigate initialization strategies that initialize each weight vector a_i by some probability distribution P_a^d on \mathbb{R}^d , that is, each coordinate of a_i is independently sampled from the distribution P_a on \mathbb{R} . As in the one-dimensional case, we assume that P_a is symmetric and satisfies $P_a(\{0\}) = 0$. Obviously, the latter implies $P_a^d(\{0\}) = 0$ and some simple considerations show that P_a^d is symmetric in the sense of $P_a^d(A) = P_a^d(-A)$ for all measurable $A \subset \mathbb{R}^d$.

In the following two remarks we investigate the size and the direction of the initialized weight vector, respectively. To this end, we assume that we have i.i.d. random variables A_1, \dots, A_d with $A_i \sim P_a$, where P_a is as above. In other words, the random variables A_1, \dots, A_d describe our random initialization of a single neuron, say h_1 . We additionally assume $\text{Var } A_i < \infty$ and write $A := (A_1, \dots, A_d)$.

Remark 3.4 (Size of the weight vector). In the following we investigate the size $\|A\|_2$ of the random weight vector A for the initialization method *He-et-al.*. To this end, we first note that the random variables $Z_i := \frac{d}{2} A_i^2$ are i.i.d. with $\mathbb{E} Z_i = \frac{d}{2} \text{Var } A_i = 1$, and hence the strong law of large numbers shows that, for $d \rightarrow \infty$, we have

$$\|A\|_2^2 = \sum_{i=1}^d A_i^2 = \frac{2}{d} \sum_{i=1}^d Z_i \rightarrow 2 \quad \text{almost surely.}$$

In other words, for sufficiently large d we have $\|A\|_2 \approx \sqrt{2}$. Under additional assumptions on A_i this approximation can be also quantified. For example, if we have a symmetric sub-Gaussian random

variable Y and assume that A_1, \dots, A_d are independent copies of αY with $\alpha^2 := \frac{2}{d \text{Var} Y}$, then Theorem D.6 applied to $X_i := \sqrt{d/2} \cdot A_i \sim (\text{Var} Y)^{-1/2} \cdot Y$ yields

$$P\left(\left|\|X\|_2 - \sqrt{d}\right| \geq t\right) \leq 2 \exp(-C_Y t^2), \quad t > 0,$$

where C_Y is a constant only depending on $\text{Var} Y$ and the sub-Gaussian norm $\|Y\|_{\Psi_2}$ of Y . Using the definition of X_i and $\tau := C_Y t^2$, we thus find

$$P\left(\left|\|A\|_2 - \sqrt{2}\right| \geq \sqrt{\frac{2\tau}{C_Y d}}\right) \leq 2e^{-\tau} \quad (19)$$

for all $d \geq 1$ and $\tau > 0$.

Let us finally consider the specific case $A_i \sim \mathcal{N}(0, \sigma^2)$. Combining Lemma D.3 with Lemma D.1 we then find

$$\sigma \sqrt{d-1/2} \leq \mathbb{E}\|A\|_2 \leq \sigma \sqrt{d-1/4} \quad \text{and} \quad \sigma^2/4 \leq \text{Var}\|A\|_2 \leq \sigma^2/2,$$

and for the choice $\sigma^2 = 2/d$ of the strategy *He-et-al.* we thus have

$$\sqrt{2} \cdot \sqrt{1 - \frac{1}{2d}} \leq \mathbb{E}\|A\|_2 \leq \sqrt{2} \cdot \sqrt{1 - \frac{1}{4d}} \quad \text{and} \quad \frac{1}{2d} \leq \text{Var}\|A\|_2 \leq \frac{1}{d}.$$

In particular, we have $\mathbb{E}\|A\|_2 < \sqrt{2}$ for all $d \geq 1$, but $\mathbb{E}\|A\|_2 \rightarrow \sqrt{2}$ for $d \rightarrow 0$. In fact, even for moderate sizes of d we actually have $\mathbb{E}\|A\|_2 \approx \sqrt{2}$. For example, for $d = 64$ the estimates guarantee $0.996 \cdot \sqrt{2} \leq \mathbb{E}\|A\|_2 \leq 0.9981 \cdot \sqrt{2}$. In addition, (19) can be made more explicit. For example, a well-known concentration inequality for Lipschitz continuous functions acting on a standard normal vector, see e.g. [2, Inequalities (A.5)], shows

$$P\left(\|A\|_2 \geq \mathbb{E}\|A\|_2 + \sqrt{\frac{\tau}{d}}\right) \leq e^{-\tau/4} \quad \text{and} \quad P\left(\|A\|_2 \leq \mathbb{E}\|A\|_2 - \sqrt{\frac{\tau}{d}}\right) \leq e^{-\tau/4}. \quad (20)$$

However, the Lebesgue density of the random variable $\|A\|_2$ can also be explicitly computed, see Lemma D.3 for details, and Figure 11 shows the shape of this density for different values of d . For example, using this explicit form of the density, we see by considering Equation (D.58) of Lemma D.3 for $\delta \geq -1$, $\sigma^2 = 2/d$ and $s := \sqrt{2} + \delta$, that

$$P(\|A\|_2 \geq \sqrt{2} + \delta) = \frac{\Gamma(\frac{d}{2}, (1 + \sqrt{2}\delta + \frac{\delta^2}{2}) \cdot \frac{d}{2})}{\Gamma(\frac{d}{2})}, \quad (21)$$

where $\Gamma(\cdot, \cdot)$ and $\Gamma(\cdot)$ denote the (incomplete) gamma function. Combining Stirling's formula (D.54) for the gamma function with (D.56) we further have for $d \geq 3$ and $\alpha > 0$:

$$\frac{\Gamma(\frac{d}{2}, (1 + \alpha)\frac{d}{2})}{\Gamma(\frac{d}{2})} \leq \frac{2}{2 + d\alpha} \cdot \left(\frac{(1 + \alpha)d}{2}\right)^{d/2} e^{-\frac{(1+\alpha)d}{2}} \sqrt{\frac{d}{\pi}} \cdot \left(\frac{2e}{d}\right)^{\frac{d}{2}} = \frac{1}{\sqrt{\pi}} \cdot \frac{\sqrt{d}}{2 + d\alpha} \cdot \left(\frac{1 + \alpha}{e^\alpha}\right)^{\frac{d}{2}},$$

and applying this estimate for $\alpha := \sqrt{2}\delta + \frac{\delta^2}{2}$ in (21) gives

$$P(\|A\|_2 \geq \sqrt{2} + \delta) \leq \frac{1}{\sqrt{\pi}} \cdot \frac{2\sqrt{d}}{4 + 2\sqrt{2}d\delta + d\delta^2} \cdot \left(\frac{1 + \sqrt{2}\delta + \delta^2/2}{e^{\sqrt{2}\delta + \delta^2/2}}\right)^{\frac{d}{2}} \quad (22)$$

Similar considerations can be made for the the probability of $\|A\|_2 \geq \sqrt{2} + \delta$, and some simple empirical experiment suggest that this probability has behavior that is a very similar to the one for the upper bound. We skip the the details but refer to Figure 11 for a comparison between (20), (22), and empirically found bounds. ◀

Remark 3.5 (Direction of the weight vector). Unlike in Remark 3.4 we are now interested in the Euclidean direction of weight vector $A := (A_1, \dots, A_d)$ of h_1 . To this end, we denote the Euclidean sphere in \mathbb{R}^d by \mathbb{S}^{d-1} , that is $\mathbb{S}^{d-1} := \{x \in \mathbb{R}^d : \|x\|_2 = 1\}$. Moreover, we write σ^{d-1} for the surface measure on \mathbb{S}^{d-1} . In particular, we have, see e.g. [5, Beispiel 14.9]

$$\sigma^{d-1}(\mathbb{S}^{d-1}) = \frac{2\pi^{d/2}}{\Gamma(d/2)} = d \operatorname{vol}_d(B_{\ell_2^d}), \quad (23)$$

and it is well-known that by normalizing σ^{d-1} we obtain the uniform distribution on \mathbb{S}^{d-1} .

Let us first consider the case $A_i \sim \mathcal{N}(0, \sigma^2)$ for some $\sigma > 0$. Then it is well-known, see e.g. [4, page 227], that the normalized vector $A/\|A\|_2$ is uniformly distributed on \mathbb{S}^{d-1} . Consequently, all orientations of the hyperplanes described by the weight vector A are equally likely.

Let us now consider the case $A_i \sim \mathcal{U}[-\alpha, \alpha]$ for some $\alpha > 0$. Then $f := (2\alpha)^{-d} \mathbf{1}_{[-\alpha, \alpha]^d}$ is the Lebesgue density of distribution of $A := (A_1, \dots, A_d)$, and Theorem D.5 shows that the σ^{d-1} -density of the distribution of the normalized vector $A/\|A\|_2$ is given by

$$h(\xi) = \int_0^\infty f(r\xi) r^{d-1} dr, \quad \xi \in \mathbb{S}^{d-1}.$$

Now observe that we have $r\xi \in [-\alpha, \alpha]^d$ if and only if $r\|\xi\|_\infty \leq \alpha$, and hence we obtain

$$h(\xi) = (2\alpha)^{-d} \int_0^\infty \mathbf{1}_{[-\alpha, \alpha]^d}(r\xi) r^{d-1} dr = (2\alpha)^{-d} \int_0^{\alpha/\|\xi\|_\infty} r^{d-1} dr = \frac{1}{d 2^d \|\xi\|_\infty^d}, \quad \xi \in \mathbb{S}^{d-1}.$$

In particular, the distribution of $A/\|A\|_2$ is independent of α and does *not* equal the uniform distribution on \mathbb{S}^{d-1} . In fact, since we have $d^{-1/2} \leq \|\xi\|_\infty \leq 1$ for all $\xi \in \mathbb{S}^{d-1}$, we find

$$\frac{1}{d 2^d} \leq h(\xi) \leq \frac{d^{d/2}}{d 2^d}$$

and both the lower and the upper bound are attained. In fact, for disjoint $J_+, J_- \in \{1, \dots, d\}$ and

$$\xi_{J_+, J_-} := \frac{1}{\sqrt{l}} \left(\sum_{j \in J_+} e_j - \sum_{j \in J_-} e_j \right),$$

where $l := |J_+ \cup J_-|$, we have both $\|\xi_{J_+, J_-}\|_2 = 1$ and $\|\xi_{J_+, J_-}\|_\infty = l^{-1/2}$, and hence the above formula reduces to

$$h(\xi_{J_+, J_-}) = \frac{l^{d/2}}{d 2^d}. \quad (24)$$

For $l = 1$, respectively $l = d$, the lower and upper bound are thus attained. Let us investigate the relation between h and the uniform distribution on \mathbb{S}^{d-1} in a bit more detail. To this end, let g be the density of the uniform distribution with respect to σ^{d-1} . Equation (23) then shows

$$g(\xi) = \frac{\Gamma(d/2)}{2\pi^{d/2}}, \quad \xi \in \mathbb{S}^{d-1}.$$

Now using Stirling's formula (D.54) for the gamma function we have

$$\Gamma(d/2) = 2\sqrt{\frac{\pi}{d}} \cdot \left(\frac{d}{2e}\right)^{d/2} \cdot e^{\mu(d)},$$

where $\mu(d)$ satisfies $0 < \mu(d) < \frac{1}{6d}$. Consequently, $\xi \in \mathbb{S}^{d-1}$ satisfies $g(\xi) = h(\xi)$ if and only if

$$\frac{1}{d 2^d \|\xi\|_\infty^d} = \sqrt{\frac{\pi}{d}} \cdot \left(\frac{d}{2e\pi}\right)^{d/2} \cdot e^{\mu(d)},$$

and the latter is equivalent to

$$\|\xi\|_\infty = \left(\frac{1}{d 2^d} \cdot \sqrt{\frac{d}{\pi}} \cdot \left(\frac{2e\pi}{d}\right)^{d/2} \cdot e^{-\mu(d)}\right)^{1/d} = \sqrt{\frac{e\pi}{2}} \cdot (\pi d)^{-\frac{1}{2d}} \cdot e^{-\nu(d)} \cdot \frac{1}{\sqrt{d}},$$

where $\nu(d)$ satisfies $0 < \nu(d) < \frac{1}{6d^2}$. Now, some numerical calculations show $\sqrt{\frac{e\pi}{2}} \approx 2.066365676$ and it is well known that $(\pi d)^{-\frac{1}{2d}} \cdot e^{-\nu(d)} \leq 1$ for all $d \geq 1$ and $(\pi d)^{-\frac{1}{2d}} \cdot e^{-\nu(d)} \rightarrow 1$ for $d \rightarrow \infty$. In fact, for our purposes, this convergence is somewhat fast, for example for $d \geq 86$, respectively $d \geq 1024$, we already have

$$\sqrt{\frac{e\pi}{2}} \cdot (\pi d)^{-\frac{1}{2d}} \cdot e^{-\nu(d)} > 2 \quad \text{and} \quad \sqrt{\frac{e\pi}{2}} \cdot (\pi d)^{-\frac{1}{2d}} \cdot e^{-\nu(d)} > 2.05823276.$$

If $d \geq 86$ and $\|\xi\|_\infty \leq 2/\sqrt{d}$, we thus find $h(\xi) > g(\xi)$, and consequently such directions ξ are preferred when sampling $A_i \sim \mathcal{U}[-\alpha, \alpha]$ instead of sampling $A_i \sim \mathcal{N}(0, \sigma^2)$. Conversely, for all $d \geq 1$ our calculations above show that $\|\xi\|_\infty \geq 2.06636568/\sqrt{d}$ implies $h(\xi) < g(\xi)$ and hence such directions ξ are disrated by sampling $A_i \sim \mathcal{U}[-\alpha, \alpha]$ compared to the sampling $A_i \sim \mathcal{N}(0, \sigma^2)$.

In particular, if the previous layer was sufficiently wide in the sense of $d \geq 86$, then the directions ξ_{J_+, J_-} given by (24) are preferred if $l \geq d/4$ and disrated if $l \leq d/4.2698672$.

◀

Remark 3.6 (Size of the output vector). In this remark, we again assume that the weights of neuron h_i are initialized by a realization of the vector $A_i = (A_{i,1}, \dots, A_{i,d})$. In addition, we consider an input sample $x = (x_1, \dots, x_d)$ and first ask for the distribution of the size of the initial output $(h_1(x), \dots, h_m(x))$. To be more precise, we have

$$h_i(x) = \left| \sum_{k=1}^d A_{i,k} x_k + b_i \right|_+, \quad i = 1, \dots, m,$$

where we assume that there is a $b \in \mathbb{R}$ with $b_i = b$ for all $i = 1, \dots, m$, and we are interested in the distribution of $\|(h_1(x), \dots, h_m(x))\|_2$. To this end let us fix i.i.d. symmetric random variables $A_{i,k}$ with $\text{Var} A_{i,k} = \sigma^2$. Then, the random variables $Y_i := \sum_{k=1}^d A_{i,k} x_k + b$ are i.i.d. with $\mathbb{E}Y_i = b$ and $\text{Var} Y_i = \sigma^2 \|x\|_2^2$. Moreover, we find

$$\mathbb{E}\|(h_1(x), \dots, h_m(x))\|_2^2 = \mathbb{E} \sum_{i=1}^m \left| \sum_{k=1}^d A_{i,k} x_k + b \right|_+^2 = \sum_{i=1}^m \mathbb{E}|Y_i|_+^2 = m \mathbb{E}|Y_1|_+^2,$$

and for $m \rightarrow \infty$, the strong law of large numbers gives

$$\frac{\|(h_1(x), \dots, h_m(x))\|_2^2}{m} = \frac{1}{m} \sum_{i=1}^m \left| \sum_{k=1}^d A_{i,k} x_k + b \right|_+^2 = \frac{1}{m} \sum_{i=1}^m |Y_i|_+^2 \rightarrow \mathbb{E}|Y_1|_+^2$$

almost surely. In particular, for $b = 0$ Lemma D.7 shows that $2\mathbb{E}|Y_i|_+^2 = \mathbb{E}Y_i^2 = \sigma^2 \|x\|_2^2$, and for the choice $\sigma^2 = 2/d$ of the strategy *He-et-al.* we thus obtain

$$\frac{\|(h_1(x), \dots, h_m(x))\|_2^2}{m} \rightarrow \mathbb{E}|Y_1|_+^2 = \frac{\|x\|_2^2}{d}.$$

With high probability, see Figure 11 for some empirical estimates, we consequently have

$$\frac{\|(h_1(x), \dots, h_m(x))\|_2}{\sqrt{m}} \approx \frac{\|x\|_2}{\sqrt{d}}.$$

Note that if we define the *normalized* Euclidean norm on \mathbb{R}^k by $\|x\|_2 := \frac{\|x\|_2}{\sqrt{k}}$, then the above approximation reads as $\|(h_1(x), \dots, h_m(x))\|_2 \approx \|x\|_2$. In other words, the size of the output of the layer is approximately equal to the size of its input, if both are measured in $\|\cdot\|_2$. Clearly, this approximate equality remains unchanged by compositions of several layers, in other words the normalized output of sample x_j at the l -th layer is approximately equal to the normalized norm of x_j at the input layer.

To investigate the case $b \neq 0$, we restrict our considerations to the case $A_{i,k} \sim \mathcal{N}(0, \sigma^2)$. Our previous considerations then show that $Y_i \sim \mathcal{N}(b, \tau^2)$, where $\tau^2 = \sigma^2 \|x\|_2^2$. This yields

$$\begin{aligned} \mathbb{E}|Y_1|_+^2 &= \frac{1}{\sqrt{2\pi\tau^2}} \int_0^\infty e^{-\frac{(s-b)^2}{2\tau^2}} s^2 ds \\ &= \frac{1}{\sqrt{2\pi\tau^2}} \int_{-b}^\infty e^{-\frac{s^2}{2\tau^2}} (s+b)^2 ds \\ &= \frac{1}{\sqrt{2\pi\tau^2}} \int_{-b}^\infty e^{-\frac{s^2}{2\tau^2}} s^2 ds + \frac{2b}{\sqrt{2\pi\tau^2}} \int_{-b}^\infty e^{-\frac{s^2}{2\tau^2}} s ds + \frac{b^2}{\sqrt{2\pi\tau^2}} \int_{-b}^\infty e^{-\frac{s^2}{2\tau^2}} ds \\ &= \frac{2\tau^2}{\sqrt{\pi}} \int_{-\frac{b}{\sqrt{2\tau}}}^\infty e^{-s^2} s^2 ds + 2b\sqrt{\frac{2\tau^2}{\pi}} \int_{-\frac{b}{\sqrt{2\tau}}}^\infty e^{-s^2} s ds + \frac{b^2}{\sqrt{\pi}} \int_{-\frac{b}{\sqrt{2\tau}}}^\infty e^{-s^2} ds. \end{aligned}$$

Now, for $c > 0$ we have

$$\begin{aligned} \int_{-c}^\infty e^{-s^2} s^2 ds &= \int_0^c e^{-s^2} s^2 ds + \int_0^\infty e^{-s^2} s^2 ds = \frac{1}{2} \int_0^{c^2} e^{-s} s^{1/2} ds + \frac{1}{2} \int_0^\infty e^{-s} s^{1/2} ds \\ &= \Gamma\left(\frac{3}{2}\right) - \frac{1}{2}\Gamma\left(\frac{3}{2}, c^2\right) \\ &= \frac{\sqrt{\pi}}{2} - \frac{1}{4}\Gamma\left(\frac{1}{2}, c^2\right) - \frac{c e^{-c^2}}{2}, \end{aligned}$$

where in the last step we used the well known identities $\Gamma(x+1) = x\Gamma(x)$, and $\Gamma(1/2) = \sqrt{\pi}$, as well as the recurrence formula $\Gamma(a+1, x) = a\Gamma(a, x) + e^{-x}x^a$ of the incomplete gamma function, see e.g. [15, Lemma A.1.1]. Moreover, we have

$$\int_{-c}^\infty e^{-s^2} s ds = - \int_0^c e^{-s^2} s ds + \int_0^\infty e^{-s^2} s ds = -\frac{1}{2} \int_0^{c^2} e^{-s} ds + \frac{1}{2} \int_0^\infty e^{-s} ds = \frac{1}{2} e^{-c^2}$$

and

$$\int_{-c}^\infty e^{-s^2} ds = \int_{-\infty}^c e^{-s^2} ds = \sqrt{\pi} \Phi(\sqrt{2} \cdot c),$$

the Φ denotes the cumulative distribution function of $\mathcal{N}(0, 1)$. By combining these equations for

$c := \frac{b}{\sqrt{2}\tau}$, that is, $c^2 = \frac{b^2}{2\tau^2}$, we obtain

$$\begin{aligned}\mathbb{E}|Y_1|_+^2 &= \frac{2\tau^2}{\sqrt{\pi}} \cdot \left(\frac{\sqrt{\pi}}{2} - \frac{1}{4}\Gamma\left(\frac{1}{2}, \frac{b^2}{2\tau^2}\right) - \frac{b e^{-\frac{b^2}{2\tau^2}}}{2\sqrt{2}\tau} \right) + 2b \cdot \sqrt{\frac{2\tau^2}{\pi}} \cdot \frac{1}{2} \cdot e^{-\frac{b^2}{2\tau^2}} + \frac{b^2}{\sqrt{\pi}} \cdot \sqrt{\pi} \cdot \Phi\left(\frac{b}{\tau}\right) \\ &= \tau^2 - \frac{\tau^2}{2\sqrt{\pi}} \cdot \Gamma\left(\frac{1}{2}, \frac{b^2}{2\tau^2}\right) - \tau \cdot \frac{b e^{-\frac{b^2}{2\tau^2}}}{\sqrt{2}\pi} + 2\tau \cdot \frac{b e^{-\frac{b^2}{2\tau^2}}}{\sqrt{2}\pi} + b^2 \cdot \Phi\left(\frac{b}{\tau}\right) \\ &= \tau^2 - \frac{\tau^2}{2\sqrt{\pi}} \cdot \Gamma\left(\frac{1}{2}, \frac{b^2}{2\tau^2}\right) + \tau \cdot \frac{b e^{-\frac{b^2}{2\tau^2}}}{\sqrt{2}\pi} + b^2 \cdot \Phi\left(\frac{b}{\tau}\right).\end{aligned}$$

Now using $\tau^2 = \sigma^2 \|x\|_2^2$ and restricting our considerations to the strategy *He-et-al.*, that is $\sigma^2 = \frac{2}{d}$, we find

$$\begin{aligned}\mathbb{E}|Y_1|_+^2 &= \frac{\|x\|_2^2}{d} \left(2 - \frac{1}{\sqrt{\pi}} \cdot \Gamma\left(\frac{1}{2}, \frac{b^2 d}{4\|x\|_2^2}\right) \right) + \frac{\|x\|_2}{\sqrt{d}} \cdot \frac{b}{\sqrt{\pi}} \cdot \exp\left(-\frac{b^2 d}{4\|x\|_2^2}\right) + b^2 \cdot \Phi\left(\frac{b\sqrt{d}}{\sqrt{2}\|x\|_2}\right) \\ &= \|x\|_2^2 \cdot \left(2 - \frac{1}{\sqrt{\pi}} \cdot \Gamma\left(\frac{1}{2}, \frac{b^2}{4\|x\|_2^2}\right) \right) + \|x\|_2 \cdot \frac{b}{\sqrt{\pi}} \cdot \exp\left(-\frac{b^2}{4\|x\|_2^2}\right) + b^2 \cdot \Phi\left(\frac{b}{\sqrt{2}\|x\|_2}\right) \\ &=: \Psi(\|x\|_2, b).\end{aligned}$$

To obtain an intuitive understanding of this result, assume for a moment, that the previous layer is actually the input layer, and that the data was normalized during pre-processing, e.g. to $[-1, 1]^d$ or $[0, 1]^d$. Then we have $\|x\|_2 \leq 1$ and for $\|x\|_2 = 0$ we easily find $(\mathbb{E}|Y_1|_+^2)^{1/2} = \sqrt{\Psi(0, b)} = b$. Moreover, for e.g. $b = 0.1$ some numerical calculations show that $\|x\|_2 \mapsto \sqrt{\Psi(\|x\|_2, b)} - \|x\|_2$ is monotonically decreasing on $[0, 1]$ with $\sqrt{\Psi(1, b)} - 1 \approx 0.057323$. Consequently, such a moderate choice of $b > 0$ does not lead to output vectors whose normalized norm is significantly larger than 1. For larger values of b , however, the influences may be more pronounced. For example, for $\|x\|_2 = 1$ and $b \rightarrow \infty$, the function $\sqrt{\Psi(1, b)}$ behaves like $\sqrt{2 + b^2}$, that is, like b . ◀

Our next goal is to investigate the effect of different initialization strategies for the offsets. We begin with the zero-bias initialization, that is, each b_i is set to $b_i = 0$. Note that in this case, x_i^* is almost surely a linear subspace with $\dim x_i^* = d - 1$, and this observation will significantly simplify our considerations below. In these considerations, we will require the dual cone of a set $A \subset \mathbb{R}^d$, which is defined by

$$A^* := \{y \in \mathbb{R}^d : \langle y, x \rangle \geq 0 \text{ for all } x \in A\}.$$

Some properties of this and other geometric set construction are summarized in Appendix B. For now, we only recall that A^* is always a convex, closed cone, and that $A \subset B$ implies $B^* \subset A^*$. Now assume that the neuron h_i is inactive, that is $D \subset x_i^* \cup A_i^-$. Since $b_i = 0$, this is equivalent to

$$\langle a_i, x_j \rangle \leq 0, \quad x_j \in D,$$

and the latter condition means $-a_i \in D^*$. A similar consideration for semi-active neurons together with some considerations dealing with the condition $D \not\subset x_i^*$ leads to the following result, which is shown in Subsection 5.2.

Theorem 3.7. *Let $D = (x_1, \dots, x_n)$ be a data set in \mathbb{R}^d in which there exists a sample $x_j \neq 0$. Moreover, let P_a be a symmetric distribution on \mathbb{R} that is Lebesgue absolutely continuous and let $h_i : \mathbb{R}^d \rightarrow [0, \infty)$ be a neuron of the form (18). If a_i is sampled from P_a^d and $b_i = 0$, then we have*

$$\begin{aligned}P_a^d(\{\text{neuron } h_i \text{ is inactive}\}) &= P_a^d(\{\text{neuron } h_i \text{ is semi-active}\}) = P_a^d(D^*) \\ P_a^d(\{\text{neuron } h_i \text{ is fully active}\}) &= 1 - 2P_a^d(D^*).\end{aligned}$$

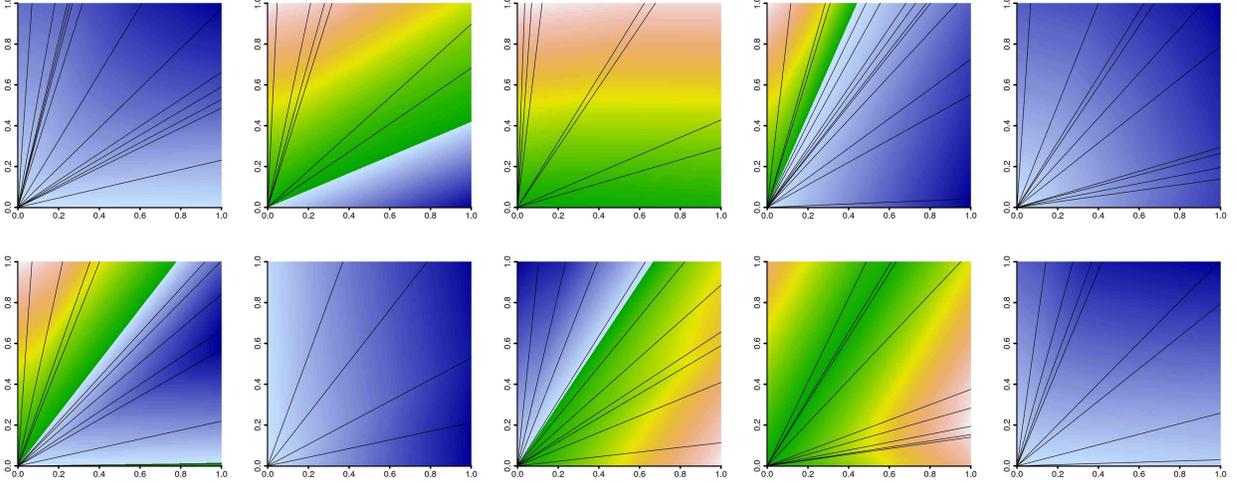


Figure 12: Ten randomly initialized predictors of a neural network with one layer of 20 hidden neurons. The weights were sampled from $\mathcal{N}(0, \sigma^2)$ with $\sigma^2 = 2/d = 1$ according to *He-et-al.* and the biases are set to zero. The color scheme is similar to those of geographic maps. Namely, blue colors indicate negative outputs and darker blues correspond to smaller values. Conversely, green colors indicate small positive values and yellow, brown, and white colors correspond to larger values. The black lines show the edges x_i^* of the neurons.

To illustrate this result, let us recall from the beginning of this section that we are mostly interested in data sets $D \subset [0, \infty)^d$. Now assume that the conical hull $\text{coni } D$ of D , that is, the smallest convex cone that contains D , satisfies

$$\text{coni } D = [0, \infty)^d. \quad (25)$$

Using some properties listed in Appendix B, we then have $D^* = (\text{coni } D)^* = ([0, \infty)^d)^* = [0, \infty)^d$, and $P_a(\{0\}) = 0$ together with the symmetry of P_a then yields

$$P_a^d(\{\text{neuron } h_i \text{ is inactive}\}) = P_a^d(D^*) = P_a^d([0, \infty)^d) = 2^{-d}. \quad (26)$$

In other words, if (25) is satisfied, then even for moderate sizes $d = m_{l-1}$ of the previous layer we can essentially ignore the problem of initializing a neuron into an inactive or semi-active state. On the other hand, Lemma B.1 shows that (25) is satisfied if and only if the data set contains, modulo positive constants, all vectors of the standard ONB of \mathbb{R}^d . In other words, for each $k = 1, \dots, d$, there needs to be a sample x_{j_k} whose precursor in the previous layer *only* falls into the region of activity of the k -neuron. Unfortunately, estimating the probability of such events is rather complicated as the following remark, which describes the transformation of the data set by a single, randomly initialized neuron, shows.

Remark 3.8 (Functions with zero bias). Recall, that a function $f : \mathbb{R}^d \rightarrow \mathbb{R}^m$ is positively homogeneous, if for all $\alpha > 0$ and all $x \in \mathbb{R}^d$ we have

$$f(\alpha x) = \alpha f(x).$$

We will now show that if we initialize all biases of our network of arbitrary depth and width with 0, then the resulting function represented by the entire network is positively homogeneous. We begin by showing that an arbitrary hidden layer $H_l : \mathbb{R}^d \rightarrow \mathbb{R}^m$ is positively homogeneous. To this end, let

$h_1, \dots, h_m : \mathbb{R}^d \rightarrow \mathbb{R}$ be the neurons of the hidden layer. Since they are initialized with $b_i = 0$, we then have

$$h_i(x) = |\langle a_i, x \rangle|_+, \quad x \in \mathbb{R}^d.$$

Combining the examples of positively homogeneous functions listed in Appendix C with Lemma C.2, we easily see that each h_i is positively homogeneous and another application of Lemma C.2 then shows that $H_l = (h_1, \dots, h_m) : \mathbb{R}^d \rightarrow \mathbb{R}^m$ is also positively homogeneous. Moreover, Lemma C.2 further recalls that the composition of positively homogeneous is positively homogeneous, and therefore, the composition of all hidden layers is positively homogeneous. Finally, the output layer is linear and thus positively homogeneous, so that another application of Lemma C.2 shows that the function represented by the entire network is positively homogeneous. Figure 12 presents a few such random functions.

We have already seen in the one-dimensional case that a zero-bias-initialization leads to a very restrictive function class on e.g. $[0, 1]$, namely linear functions. Obviously, such functions cannot approximate a nonlinear continuous function arbitrarily well. Now, in the general case, our network with zero biases is able to represent more general functions, namely positively homogeneous, continuous functions. There could thus be some hope that such a network is able to approximate suitably large classes of functions. Unfortunately, this is not true. Indeed, Corollary C.5 shows that for every compact $X \subset \mathbb{R}^d$ and every continuous function $g \in C(X)$ that is *not* positively homogeneous there is an $\varepsilon > 0$ such that

$$\|g - f\|_\infty \geq \varepsilon$$

for all functions $f : X \rightarrow \mathbb{R}$ that can be represented by an *arbitrary* network with ReLU-activation functions. Moreover, Corollary C.6 shows that the same result remains valid if we replace $C(X)$ with its norm $\|\cdot\|_\infty$ by $L_p(P)$ and $\|\cdot\|_{L_p(P)}$, where $p \in [1, \infty)$ and P is an arbitrary probability measure on \mathbb{R}^d provided that the target function g does not P -almost surely coincide with a positively homogeneous function. Consequently, considering ReLU-networks without bias violates any sort of universal approximation property in a very strong sense, and initializing ReLU-networks with zero biases requires updating the biases during training for basically all interesting target functions. ◀

Our next goal is to investigate the effects of non-zero bias initialization strategies. We begin by presenting the following lemma that considers deterministic initializations of the bias.

Lemma 3.9. *Let $D = (x_1, \dots, x_n)$ be a data set in \mathbb{R}^d , P_a be a symmetric distribution on \mathbb{R} that is Lebesgue absolutely continuous, and $b_-, b_+ \in \mathbb{R}$ with $b_- < b_+$. Moreover, let $h_i : \mathbb{R}^d \rightarrow [0, \infty)$ be a neuron of the form (18). If its weight a_i is sampled from P_a^d and its bias is initialized by either b_- or b_+ then we have*

$$\begin{aligned} P_a^d \otimes \delta_{b_-}(\{ \text{neuron } h_i \text{ is inactive} \}) &\geq P_a^d \otimes \delta_{b_+}(\{ \text{neuron } h_i \text{ is inactive} \}) \\ P_a^d \otimes \delta_{b_-}(\{ \text{neuron } h_i \text{ is semi-active} \}) &\leq P_a^d \otimes \delta_{b_+}(\{ \text{neuron } h_i \text{ is semi-active} \}). \end{aligned}$$

Remark 3.10 (Functions with non-zero bias). By applying Lemma 3.9 in the case $b_+ = 0$, we see that, compared to a zero-bias initialization, the probability of obtaining an inactive neuron increases if we choose a negative deterministic bias. Similarly, by considering $b_- = 0$, we observe that the probability of obtaining an inactive neuron decreases when we choose a positive deterministic bias. This may explain the fact that some popular initialization heuristics prefer a positive deterministic bias, but to the best of our knowledge, there is no initialization heuristic described in the literature that chooses a negative deterministic bias. Finally recall that in the one-dimensional case, Theorem 2.8 provided a significantly stronger result, if $0 \in \text{co } D$. In fact, one could also reproduce Theorem 2.8 for $d > 1$ if $0 \in \text{co } D$. However, we are mostly interested in data sets D contained in $[0, \infty)^d$, and for

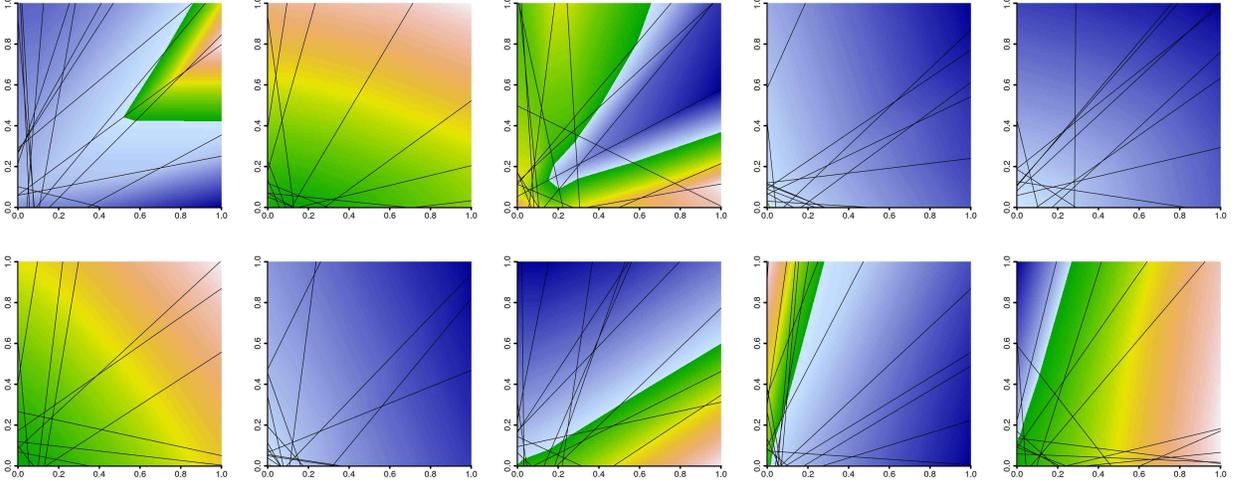


Figure 13: Ten randomly initialized predictors of a neural network with one layer of 20 hidden neurons. The weights were sampled from $\mathcal{N}(0, \sigma^2)$ with $\sigma^2 = 1$ according to *He-et-al.* and the biases are set to $b = 0.1$. The color scheme equals that of Figure 12. Compared to the zero-bias-initialization depicted in Figure 12 we see that the edges no longer contain the origin, but most edges are still in the vicinity of the origin.

such D , the condition $0 \in \text{co } D$ is equivalent to $x_{j_0} = 0$ for some $j_0 \in \{1, \dots, \}$. In other words, there needs to be at least one sample that is mapped to 0 by all neurons of the previous layer. So far, it is unclear to us, how likely this situation occurs, and hence we omitted the generalization of Theorem 2.8 to the case $d > 1$.

Another consequence of Lemma 3.9 is that using deterministic bias initialization we cannot simultaneously decrease the probabilities of inactive and semi-active neurons. This is in alignment with the one-dimensional situation described in Theorem 2.8.

Now recall that the distance of the hyperplane x_i^* can be computed by $|b_i|/\|a_i\|_2$. Moreover, we have already seen in Remark 3.4 that e.g. the initialization strategy *He-et-al.* results in $\|a_i\|_2 \approx \sqrt{2}$ with high probability. Consequently, the distance of x_i^* concentrates around $|b_i|/\sqrt{2}$ with high probability. For the usual choices $b_i = 0.1$ and $b_i = 0.01$, this shows that most hyperplanes are very close to the origin. Figure 13 illustrates this in the case $d = 2$. ◀

The final goal of this section is to develop an initialization strategy for the offsets that addresses Question **Q2**. To this end, let us quickly summarize our findings that relate to **Q2**.

- Lemma 3.2 essentially shows that the edge x_i^* of a fully active neurons h_i (needs to) intersect the convex hull of the data.
- For the zero-bias initialization, Theorem 3.7 exactly computes the probability of initializing a neuron in an inactive, semi-active, or fully active state respectively. Unfortunately, the key quantity $P_a^d(D^*)$ for these computations depends on the unknown random geometry of the data. Under some ideal assumptions on the data (25), however, the probability of an inactive neuron, may be negligible, see (26).
- Deterministic, non-zero bias initializations change the probability of inactive neurons, and Lemma 3.9 shows that larger values for the bias are preferable.
- Initializing all biases with zero forces the initial function represented by the network to be

positively homogeneous as discussed in Remark 3.8. Such functions have, independent of the network width and depth, very bad approximations properties.

- Small positive initial values for the biases create functions that are in general not positively homogeneous, but at each layer, the edges of the neurons remain in the vicinity of 0 as discussed in Remark 3.10. As a result, the initial function represented by the network is close to a positively homogeneous function.

In summary, the probability of inactive neurons highly depends, unlike in the one-dimensional case, on the geometry of the data, and therefore empirical investigations seem to be suitable to determine, if too many inactive neurons are actually created. Moreover, initializing the biases with either zero or a small positive value leads to functions with restricted approximation properties. Whether this hinders the training process needs to be investigated empirically, too. To this end, however, we first need to develop an alternative initialization strategy. In view of our findings above, such a new strategy should ensure that *a)* each edge x_i^* intersects the convex hull of the data; and *b)* the edges are not concentrated in the vicinity of the origin. One way to ensure both conditions is to (randomly) pick a point $x_i^* \in \text{ico } D$ for each neuron h_i and to initialize the bias by $b_i := -\langle a_i, x_i^* \rangle$, where the weight vector $a_i \in \mathbb{R}^d$ of h_i is initialized by a common strategy such as *He-et-al.*. Indeed, a simple calculation shows $x_i^* \in x_i^*$, and the distance of x_i^* to the origin is given by

$$d(x_i^*, 0) = \frac{|\langle a_i, x_i^* \rangle|}{\|a_i\|_2}.$$

We refer to Figure 14 for some illustrations in the case of $\text{ico } D = (0, 1)^2$. It thus remains to develop methods for picking $x_i^* \in \text{ico } D$. One such method would be to use the uniform distribution on the set $\text{ico } D$. Unfortunately, however, this choice would require to find all extreme points of $\text{ico } D$, which is, even for moderate values of n and d , prohibitive. For this reason, we consider cheap “approximations” of this approach. Namely, we first pick N random samples x_{j_1}, \dots, x_{j_N} from D , and then choose x_i^* according to the uniform distribution on $\text{ico}\{x_{j_1}, \dots, x_{j_N}\}$. For computational reasons, N should be small, and in our experiments reported in the following section we therefore consider both fixed $N = 5$, denoted by **hull +5** in the experiments, and randomly chosen $N \sim \mathcal{U}(\{1, \dots, 5\})$, denoted by **hull -5**.

Moreover note that with the new strategy discussed so far, the bias $b_i := -\langle a_i, x_i^* \rangle$ may be significantly larger than 0 and therefore we also investigate alternative scalings for the distribution from which the weights a_i are initialized. These include a scaling called **sphere** that first uses the normal distribution to generate the entries of a weight vector a_i , and then normalizes this weight vector with respect to the Euclidean norm. As a result, each weight vector is uniformly sampled from \mathbb{S}^{d-1} , where d is the input dimension of the initialized neuron. A second scaling called **ball** multiplies the weight vector obtained by **sphere** by another random number $R \sim \mathcal{U}[0, 2]$. As a result the weight vector of **ball** is an element of the ball with radius 2 and its expected norm equals 1.

4 Experiments

In this section we present some experiments assessing the quality of the new initialization method and comparing it to the standard approach *He-et-al.*. Let us begin by briefly describing the key aspects of our experiments.

Data. We downloaded all data sets from the UCI repository, that have between 2,500 and 50,000 samples of dimension not exceeding 1,000, that were labeled as classification or regression task, and

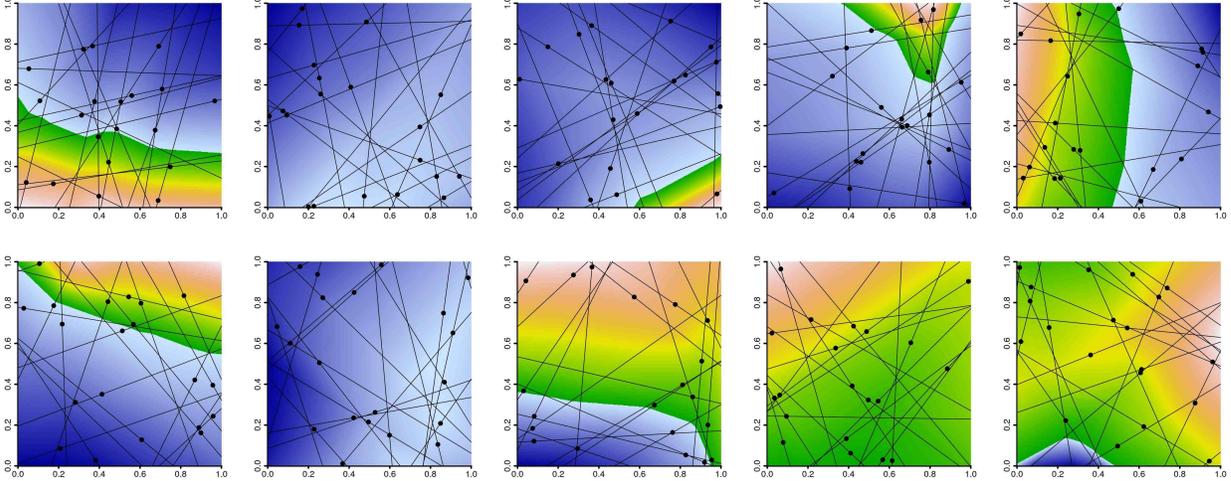


Figure 14: Ten randomly initialized predictors of a neural network with one layer of 20 hidden neurons. The weight vectors were uniformly sampled from \mathbb{S}^1 and the biases we determined by $b_i := -\langle a_i, x_i^* \rangle$, where the points x_i^* depicted as black spots were sampled from $\mathcal{U}[0, 1]^2$. The color scheme equals that of Figure 12. Compared to the initializations shown in Figures 12 and 13, we see that the edges are longer in the vicinity of the origin.

whose description made it straightforward to convert the original data set into a numeric .csv format. During this conversion, rows with missing values were removed, and we kept only those data sets that still had at least 2,500 samples. Since we were only interested in regression and binary classification, we extracted the largest two classes from the multi-class data sets and only kept the resulting binary classification data set if it still had at least 2,500 samples. Some data sets are labeled both as regression and classification data sets, in which case we used them for both. Also, some data sets contained different versions, and since we were hesitating to choose one, we used them all. Altogether this resulted in 40 for regression and 61 data sets for binary classification. Tables 2 and 3 summarize key characteristics of these data sets. Finally, we collected some data sets from other sources to conduct some in-front experiments for the identification of the most promising variants of the new initialization strategy introduced at the end of Section 3.

Hardware and Software. We had seven desktops with varying hardware at our disposal: one with a GTX Titan, one with both a GTX 1060 and a GTX 1070, one with two GTX 1080, one with a GTX 1060, and three with a GTX 1080. Except the desktop with the single GTX 1060, all desktops had 64GB RAM, and the first four desktops were running `Tensorflow 1.4`, while the 3 identical computers were running `Tensorflow 1.10`. All computers were solely used for the experiments to ensure that the timing is as exact as possible.

Initial Experiments for Exploration. So far we used the least squares loss for the regression-type data sets and the logistic loss for the classification-type data sets. For the least squares loss we initially considered, besides the scalings `sphere` and `ball`, some other but similar scalings, too. However, since these showed inferior performance on some initial, less structured experiments on the additional data, we abandoned these alternatives quickly. As a result of these initial experiments we decided to only consider the variants `sphere hull -5`, `sphere hull +5`, `ball hull -5`, and `ball hull +5` in all subsequent experiments. However, considering all four alternatives in the experiments would have been too expensive, and in addition, it would have changed the character of the experiments from the validation of one initialization method to an exploration of different initialization methods. To

Architecture Number	Depth	Widths
1	2	256 – 128
2	2	512 – 256
3	2	1024 – 512
4	3	512 – 256 – 128
5	3	1024 – 512 – 256
6	3	2048 – 1024 – 512
7	4	512 – 256 – 128 – 64
8	4	1024 – 512 – 256 – 128
9	4	2048 – 1024 – 512 – 256
10	8	512 – 512 – 256 – 256 – 128 – 128 – 64 – 64
11	8	1024 – 1024 – 512 – 512 – 256 – 256 – 128 – 128
12	8	2048 – 2048 – 1024 – 1024 – 512 – 512 – 256 – 256

Table 1: Considered network architectures. Each number in the right column stands for the width of one layer, and the first hidden layer corresponds to the most left number.

pick one of the four variants for each loss function, we thus conducted structured experiments on the additional data sets.

Main Experiments. Every data set we used from the UCI repository was randomly split into 60% samples for training, 20% samples for validation, and 20% samples for testing. On the training samples we trained networks of twelve architectures with depth varying between 2 and 8, see Table 1 for details. All methods and architectures received the same splitting of the data sets.

The optimization of the network parameters was performed by the function `AdamOptimizer` provided by `Tensorflow`. The optimizer was run with its default values and a batch size of 128. After k batches, we computed both the validation and the test error, where

$$k = \max\left\{\left\lfloor \frac{\lceil n/128 \rceil}{10} \right\rfloor, 5\right\}$$

and n is the size of the training set. Consequently, for training sets with $n < 7680$ we checked the validation error after five batches, whereas for larger training sets we waited for more than 5 batches. We kept training until the validation error did not decrease for 15 epochs, but a post analysis of the training log data suggested that 5 epochs would have sufficed. For this reasons, all experimental results we report are actually based on a patience of 5 epochs, which is possible, because we computed the test error whenever we computed the validation error. All timings, however, do not include the time needed for computing the test error.

The training described so far yields a pair of validation and test error for each architecture, that is, 12 pairs altogether. We then chose the pair with the smallest validation error and saved the corresponding test error. This entire procedure was repeated 50 times with different random splits, and the errors reported are the average test errors over these 50 repetitions. More precisely, the reported for each method on the i -th data set is

$$\text{ATE}_i(\text{method}) := \frac{1}{50} \sum_{j=1}^{50} \text{TE}_{i,j}(\text{method}), \quad (27)$$

where $\text{TE}_{i,j}(\text{method})$ denotes either the classification error or the root mean squared error of the considered method on the j -th split of the i -th data set.

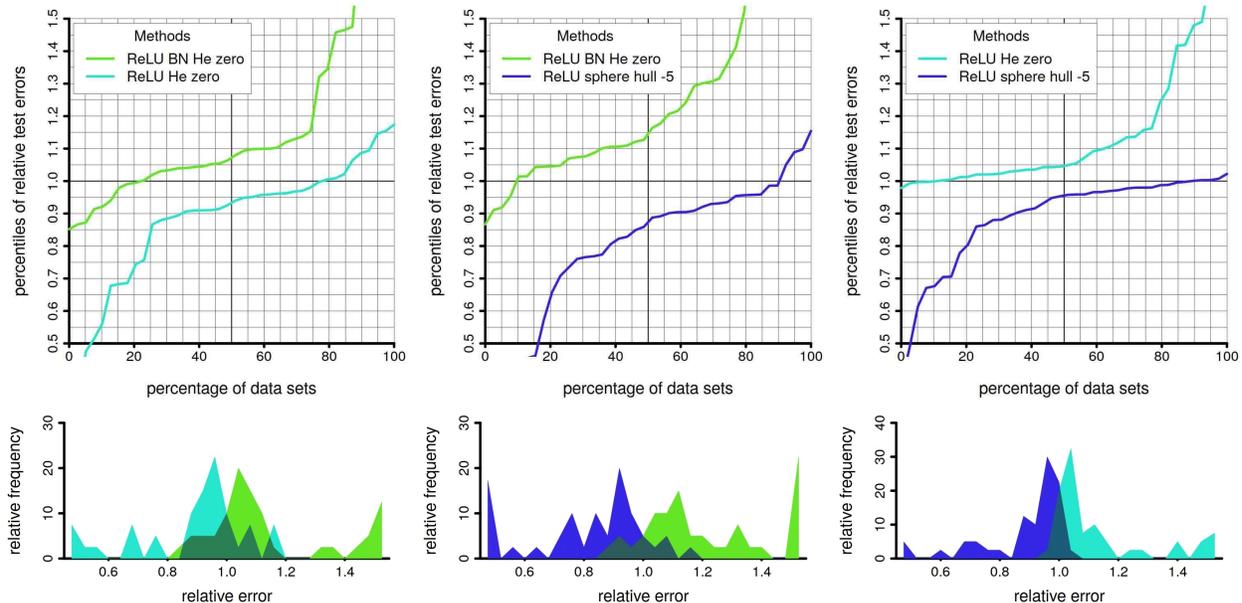


Figure 15: Pairwise comparisons of old and new methods for regression with ReLU activation function in terms of test errors. In the first row, each column displays the empirical percentile functions of the “observations” $y_i := \text{RATE}_i(\text{colored method, other method})$ for $i = 1, \dots, 40$, where $\text{RATE}_i(\text{colored method, other method})$ denotes the modification (29) of the relative error $\text{ATE}_i(\text{colored method})/\text{ATE}_i(\text{other method})$ and where ATE_i denotes the usual average test error, see (27). Note that the colored method is better than the other method on the i -th data set, if and only if the $y_i < 1$. Consequently, colored methods, whose percentile functions stay significantly below 1 for a large range on the horizontal, achieve significantly better results on a large portion of the data sets compared to the competing method. For example, the first column shows that **ReLU He zero** outperforms **ReLU BN He zero** by at least 10% on about 35% percent of the data sets, while conversely **ReLU BN He zero** is only able to outperform **ReLU He zero** by at least 10% on about 6% of the data sets. Similarly, the behavior of the percentile above 1 describes to which extend and on how many data sets the colored method was outperformed by the competing method. In general, colored methods with small percentiles on the left of the diagram achieve significant gains over the competing method, whereas colored methods with small percentiles on the right do not suffer from corresponding significant losses. The second row of each column displays a density estimate of the distributions of $\tilde{y}_1, \dots, \tilde{y}_{40}$, where for reasons of presentation we considered the clipped values $\tilde{y}_i := \max\{0.45, \min\{1.55, y_i\}\}$. The density estimate is based on histograms with a bin width of 0.04. A method, whose density estimate has a significant portion on $(0, 1]$, achieves corresponding gains against its competitor, while a significant portion on $[1, \infty)$ stands for corresponding losses. The first column shows that **ReLU He zero** significantly outperforms **ReLU BN He zero**, while the second and third column show that our new strategy **ReLU sphere hull -5** clearly outperforms both **ReLU BN He zero** and **ReLU He zero**.

Besides our methods we also considered some baseline methods in the experiments. To describe them, we write **ReLU** if the network uses the ReLU activation function and **SeLU** for Self-Normalizing Neural Networks proposed in [11]. Moreover, weight initialization according to *He-et-al.* with normal distributions is denoted by **He**, and the modification for SeLUs proposed in [11] is denoted by **SNN**. Initializing the bias to zero is indicated by **zero**, and if batch normalization is used in the ReLU networks we additionally write **BN**. Now, for the classification tasks we considered **ReLU BN He zero**, **ReLU He zero**, and **SeLU SNN zero** as baseline methods, **ReLU ball hull +5** and **SeLU ball hull -5** as our new methods for the two types of activation functions, as well as **ReLU He hull -5** for illustrating the differences between **ReLU He zero** and **ReLU ball hull +5**. Similarly, for the regression tasks we considered **ReLU BN He zero**, **ReLU He zero**, and **SeLU SNN zero** as baseline methods and **ReLU sphere hull -5** and **SeLU ball hull -5** as new methods.

In summary, each initialization strategy required 600 training runs for each data set from the UCI repository, that is, 37,800 runs for the classification data sets and 24,000 runs for the regression

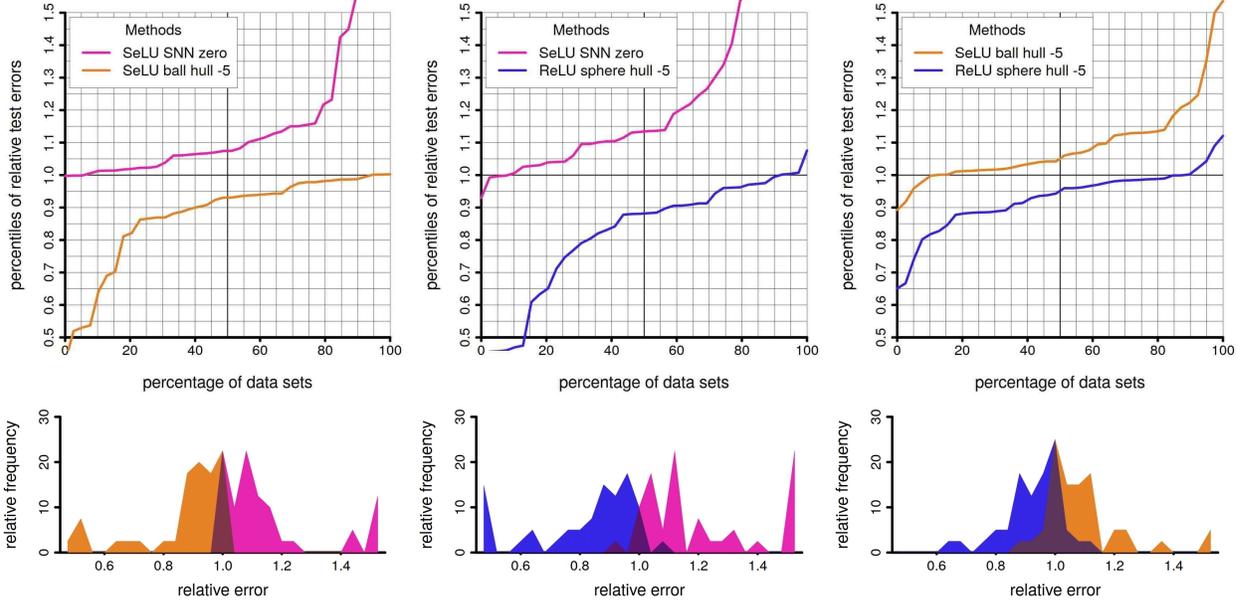


Figure 16: Pairwise comparisons of old and new methods for regression with self-normalizing activation function in terms of test errors. The graphics have the same interpretation as the ones in Figure 15. The first column shows that the original **SeLU SNN zero** proposed in [11] is clearly outperformed by our new initialization strategy for self-normalizing neural networks, namely **SeLU ball hull -5**. The second column shows that **SeLU SNN zero** is also outperformed by **ReLU ball hull -5**, and the third column shows that **ReLU ball hull -5** also outperforms **SeLU ball hull -5**.

data sets. For the classification task, we considered 6 different methods, so that in summary 225,600 networks were trained, whereas for the regression tasks, we have only considered 5 different methods so far, which results in another 120,000 networks. Together the log files comprise almost 20GB of data, which can potentially be used for further investigations, and the entire experiments took between 4 and 5 months.

Aspects of the Analysis. It is common knowledge, that in many cases the (average) test errors greatly vary over different data sets, and that this variation is mostly due to difference in the data sets. This phenomenon also occurred in our experiments: In the regression case reported in Table 4, for example, all methods achieved an average test error of about 0.027 on the data set `ONLINE-NEWS-POPULARITY`, while on the data set `SKILL-CRAFT`, the average test errors were around 1.0. Similarly, in the classification case reported in Table 5, all methods achieved zero test error on `MUSHROOM`, while on `WINE-QUALITY-ALL`, the test errors of all methods were around 0.29. For this reason, one often considers either the rank of each method on a fixed data set, or the relative errors, e.g.

$$\text{ATE}(\text{Method 1}) / \text{ATE}(\text{Method 2}) \quad (28)$$

for each data set. In the following, we report both, but mostly with the following modifications:

- i) There are several data sets, on which $\text{ATE}(\text{Method X}) = 0$ or $\text{ATE}(\text{Method X}) \approx 0$ for several methods X, see Table 5. For such data sets, the plain ratio (28) is either not defined, or may be highly misleading, and for this reason, we call the modification

$$\text{RATE}_i(\text{Method 1}, \text{Method 2}) := \frac{\text{ATE}_i(\text{Method 1}) + 0.0001}{\text{ATE}_i(\text{Method 2}) + 0.0001} \quad (29)$$

the *relative average test error* of Method 1 compared to Method 2 on the i -th data set. In the following, relative errors always refer to RATE instead of (28).

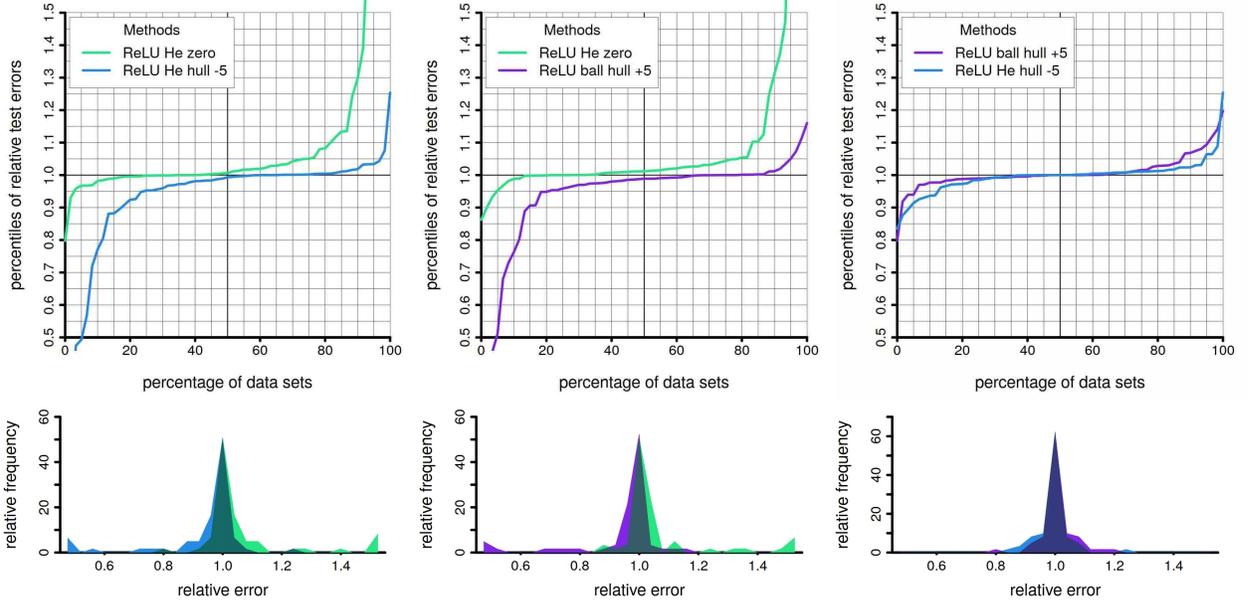


Figure 17: Pairwise comparisons of old and new methods without batch normalization for binary classification in terms of test errors. The graphics have the same interpretation as the ones in Figure 15, but this time we used the results on the 61 binary classification data sets from the UCI repository. The figures show that **ReLU He zero** is outperformed by both **ReLU ball hull +5** and **ReLU He hull -5**, and in the direct comparison of the latter two methods, **ReLU He hull -5** has a slight edge over **ReLU ball hull +5**. Also note that for each pairwise comparison there is a considerable fraction of data sets, on which both methods achieve an essentially equal performance. In fact, the central peak in the density estimates is always located in the bin $[0.98, 1.02]$, and the graphics thus show that between 50% and 60% of the data sets fall into this bin. In other words, on 50% to 60% of the data sets, the difference between the considered two methods is minimal in the sense of $\text{RATE}_i(\text{colored method}, \text{other method}) \in [0.98, 1.02]$.

ii) There are also several data sets, on which most of the methods performed not exactly equally, but at least essentially equally. For example, in Table 5 we see that on the data set POLISH-COMPANIES-BANKRUPTCY-2YEAR, three methods achieved either an average test error of .03932 or .03933. Note that this data set contains 10173 samples, and hence about 2035 samples are used for testing. If we have two predictors that only differ on exactly one test sample, then the resulting test error differs by $1/2035 \approx 0.00049$. All smaller differences in the average test errors are therefore a result of averaging over 50 runs. To be more precise, a simple calculation ignoring possible rounding errors in the average test errors shows that the method achieving an average test error of .03932 predicted exactly one sample in exactly one of the fifty runs better than the methods achieving an average test error of .03933. We do not believe that such a small difference should result in different rankings of the methods, in particular, since these small differences may also result from aspects not related to the considered methods, e.g. an unfortunate pick of the architecture based on the validation error. For this reason, we considered the following adjustment: If Method 1 performed worse than Method 2 on the i -th data set, that is $\text{RATE}_i(\text{Method 1}, \text{Method 2}) > 1$, but we also have

$$\text{RATE}_i(\text{Method 1}, \text{Method 2}) \leq 1.001 \quad (30)$$

then Method 1 was viewed to have the same performance as Method 2. As a result, there are several data sets, in particular for the classification case, in which more than one method is considered best, even if these methods have different average test errors, see Table 5. Moreover, to apply this notion of equal performance to ranking, we proceeded as follows on each data

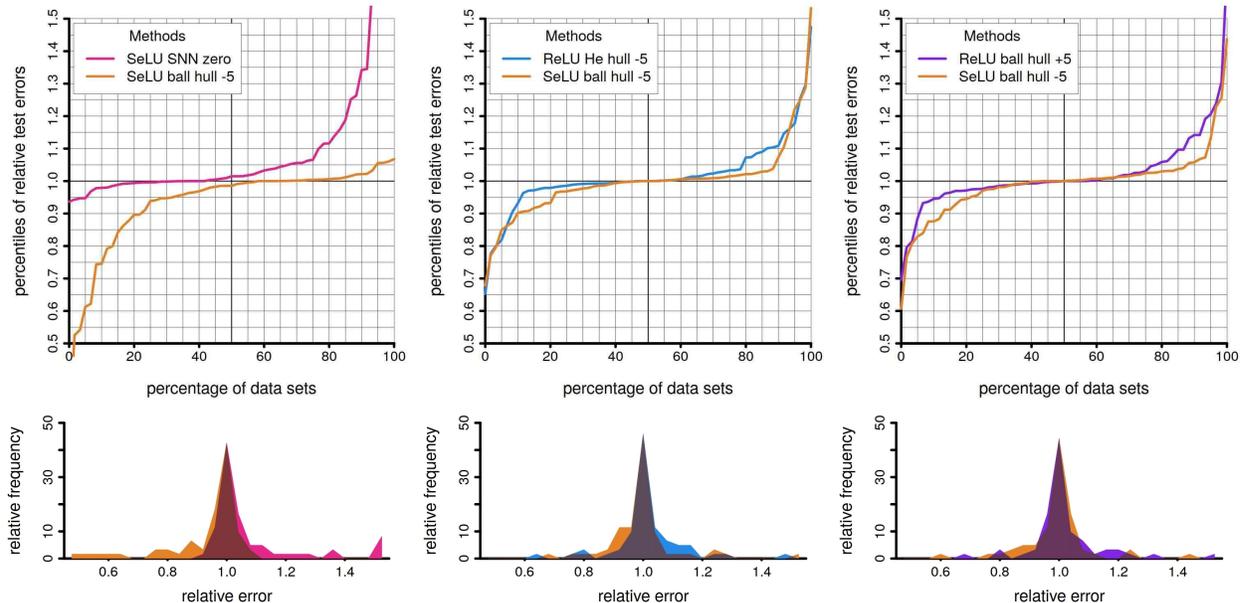


Figure 18: Pairwise comparisons for binary classification methods with self-normalizing activation function in terms of test errors. The graphics have the same interpretation as the ones in Figure 17. The first column shows that the original **SeLU SNN zero** proposed in [11] is clearly outperformed by our new initialization strategy for self-normalizing neural networks, namely **SeLU ball hull -5**. The second and third column show that **SeLU ball hull -5** slightly outperforms both **ReLU He hull -5** and **ReLU ball hull +5**. Not surprisingly, analogous comparisons between **SeLU SNN zero** and **ReLU ball hull +5**, respectively **ReLU He hull -5**, which are not displayed here for brevity’s sake, show that **SeLU SNN zero** is also outperformed by the latter two methods.

set: First we sorted the methods according to their average test errors, and assigned them a temporary rank according to their position in the sorted list. Then we adjusted these temporary ranks by iteratively going from the best to the worst method. More precisely, we assigned all methods that did not achieve the best average test error, but that achieved (30) also the rank = 1. Then we applied the same procedure to the remaining methods and so on. Finally, to ensure that the adjusted ranks of the considered M methods sum up to standard value $M(M + 1)/2$, we applied R’s `rank` function to the adjusted ranks with the default “average” method for ties. In the Tables 4 and 5 we report both, a “usual” or “raw” ranking that ignores the situation (30) as well as the adjusted ranking described above. On the regression data sets, both types of ranking led to almost identical average rankings, which is not surprising since the situation (30) does not occur very often in the regression case. On the classification data sets, the two types of rankings led to more pronounced differences, yet the largest difference of both rankings was an average raw rank of 3.811 compared to an average adjusted rank of 3.885. Moreover, the ordering of the 6 considered methods with respect to the average (adjusted) rank did not change. Thus it seems fair to say that both types of ranking led to essentially the same results.

Tables of the form of Table 4 and Table 5 are certainly the most common way of reporting experimental results in the machine learning community. However, in most cases significantly less data sets are considered and in such cases, tables together with some simple statistics such as average rank are still comprehensible as a whole. For more extended experiments, however, this may change. For example, Table 5 reports 366 average test errors, and even by highlighting the best and worst average test errors with the help of a color code, it is still rather difficult to draw conclusions from Table 5. Indeed, a full understanding of the performance of different methods requires, besides rankings and an emphasis on best and worst behavior, also an understanding of the distribution of relative average test

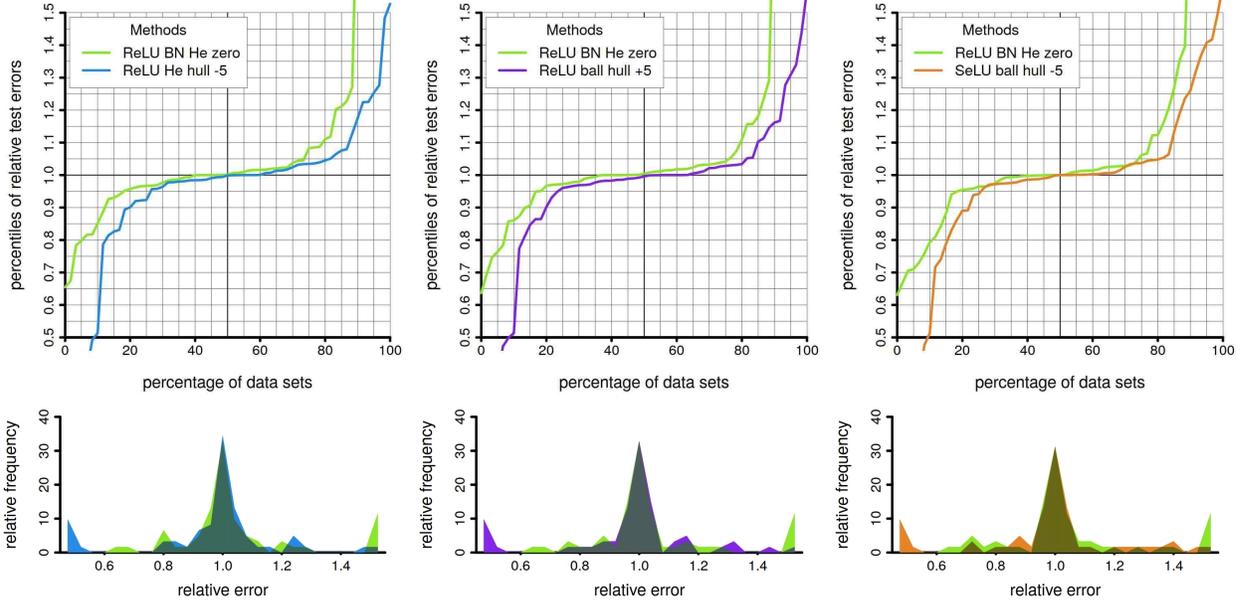


Figure 19: Pairwise comparisons against batch normalization with standard initialization in terms of test errors on the binary classification data sets. The three columns, which have the same meaning as in Figure 17, show that ReLUs with batch normalization and standard initialization are outperformed by all three new initialization strategies. In particular, all three new strategies achieve at least a 10% gain on at least 20% of the data sets. Conversely, **ReLU BN He zero** only achieves a little less than a 5% gain over its competitors on at least 20% of the data sets.

errors. To be more specific, consider the results on the data set AVILA reported in Table 5. Here, the method **ReLU ball hull -5** scores third, while **SeLU SNN zero** scores fourth. Consequently, neither of the two methods are highlighted in 5 and their ranking on this data set does not substantially influence their average ranking. Nonetheless, their performance drastically differs since **ReLU ball hull -5** achieves an average test error of 0.10157, while **SeLU SNN zero** only achieves an average test error of 0.14361. Consequently, we have

$$\text{RATE}_6(\mathbf{ReLU\ ball\ hull\ -5}, \mathbf{SeLU\ SNN\ zero}) \approx 1.413,$$

that is, on AVILA, the average test error of **SeLU SNN zero** is more than 40% worse than that of **ReLU ball hull -5**. Of course, all this information is contained in Table 5, but it requires at least substantial effort to extract and comprehend this information. For this reason, we also display pairwise comparisons of selected methods with the help of percentile functions on the relative average test errors. We refer to Figure 15 for a detailed explanation of these graphics and to Figures 16, 17, 18, and 19 for further pairwise comparisons.

Findings. Let us now have a look at some of the results to assess the quality of the new initialization strategies. To this end, we focus on the following aspects:

- i)* Average test errors
- ii)* Training costs in number of iterations and training time
- iii)* Influence of the considered architectures on the test errors

i). Let us first consider average test errors. In the regression case, Table 4 immediately shows that the two new methods **ReLU sphere hull -5** and **SeLU ball hull -5** are ranked first and second, and that **ReLU sphere hull -5**, which is ranked first, actually achieves the best average test error of

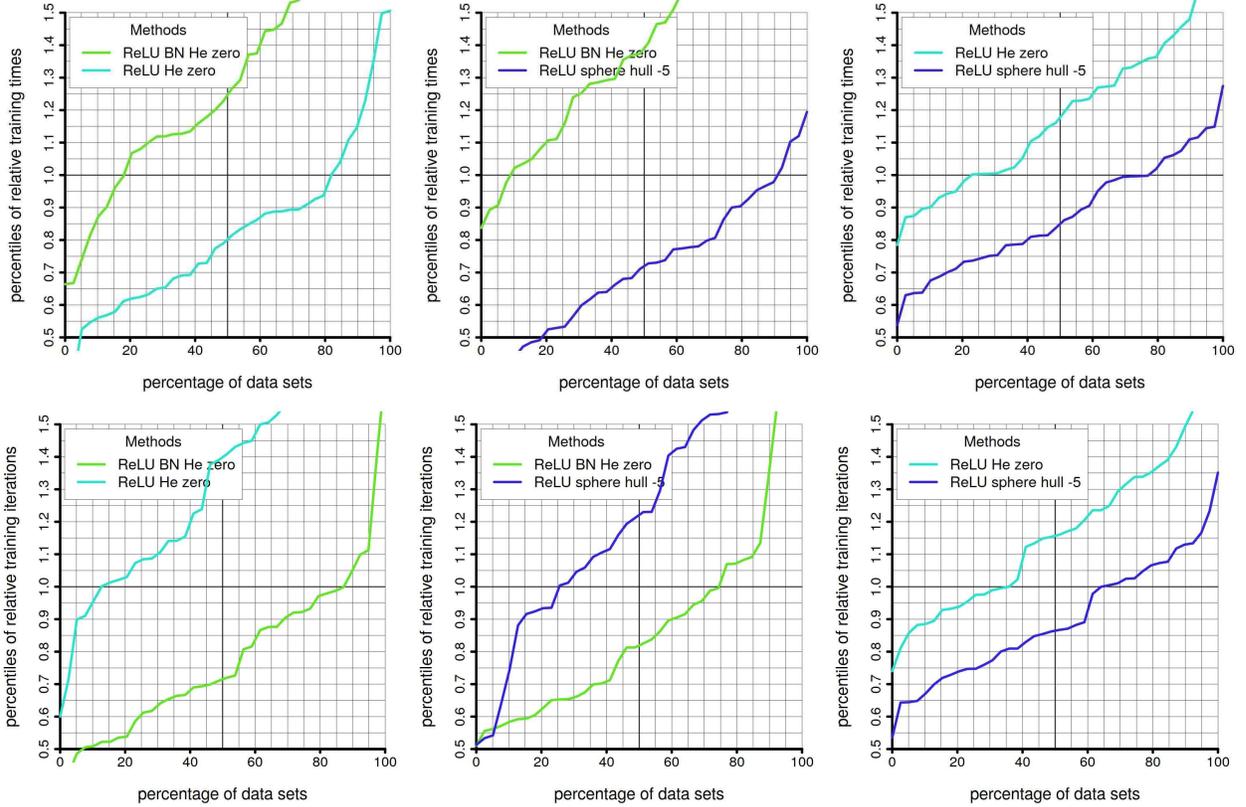


Figure 20: Pairwise comparisons of old and new methods for regression with ReLU activation functions in terms of computational resources. The first row displays the percentile curves of the “observations” $y_i = \text{ATT}_i(\text{colored method}) / \text{ATT}_i(\text{other method})$ for $i = 1, \dots, 40$, where ATT_i denotes the average training time of the considered method on the i -th data set. The second row displays the percentile curves of the “observations” $y_i = \text{ATI}_i(\text{colored method}) / \text{ATI}_i(\text{other method})$ for $i = 1, \dots, 40$, where ATI_i denotes the average number of training iterations of the considered method on the i -th data set. Consequently, the second columns shows that **ReLU sphere hull -5** was faster than **ReLU BN He zero** on more than 90% of the data sets, despite the fact that **ReLU BN He zero** required less training iterations than **ReLU sphere hull -5** on 75% of the data sets.

all methods on 75% of the data sets. In most cases, these test errors are statistically significant better than the second best test errors. Moreover, Figure 15 shows that the new initialization strategy **ReLU sphere hull -5** outperforms both **ReLU BN He zero** and **ReLU He zero** on around 90% of the data sets, and on a considerable number of data sets, the gains achieved by **ReLU sphere hull -5** is very substantial. Finally, Figure 16 shows that self-normalizing networks with standard initialization, that is **SeLU SNN zero**, are almost uniformly outperformed by both of the new initialization strategies, i.e. **ReLU sphere hull -5** and **SeLU ball hull -5**. This figure further shows that **ReLU sphere hull -5** outperforms **SeLU ball hull -5** on around 90% of the data sets.

For the classification data sets, Table 5 shows that our new three initialization strategies **ReLU He hull -5**, **ReLU ball hull +5**, and **SeLU ball hull -5** achieve the second, first, and third rank, respectively. However, a closer look reveals that unlike in the regression case, the situation is a bit more diffuse. For example, **ReLU BN He zero**, which is ranked fourth, achieves the adjusted first rank on around 40% of the data sets, whereas the three new methods are only ranked first on around 20%, 25%, and 30% of the data sets, respectively. To better understand the situation let us therefore consider Figures 17, 18, and 19. For example, Figure 17 shows that on more than 80% of the data

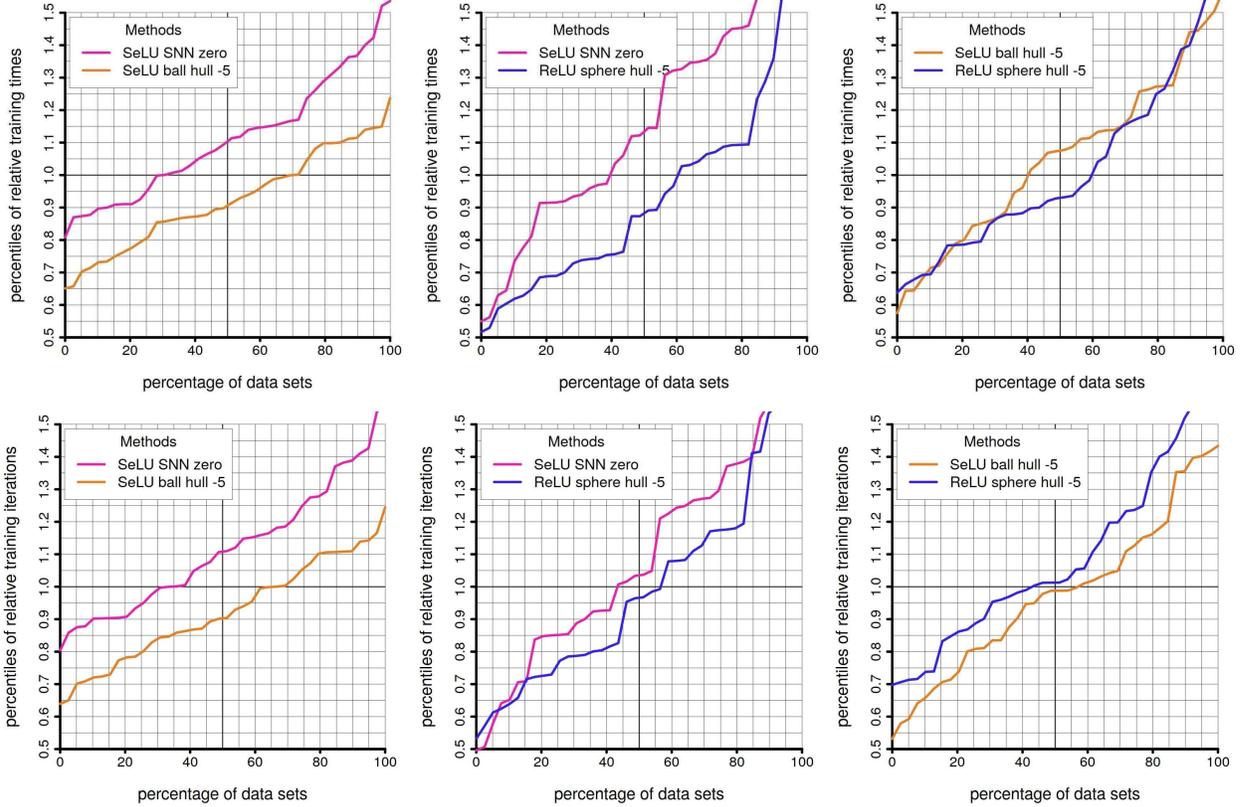


Figure 21: Pairwise comparisons of old and new methods for regression with self-normalizing activation function in terms of computational resources. The graphics, which have the same meaning as those in Figure 20, show that our new initialization strategy **SeLU ball hull -5** leads to substantially faster training of self-normalizing networks, but it is not as fast as **ReLU sphere hull -5** despite the fact that it requires less iterations than **ReLU sphere hull -5**.

sets we have

$$0.97 \leq \text{RATE}(\text{ReLU He hull -5}, \text{ReLU ball hull +5}) \leq 1.03.$$

Therefore, these two methods have a very similar performance on the vast majority of data sets. In comparison, Figure 19 shows that we have

$$0.97 \leq \text{RATE}(\text{ReLU BN He zero}, \text{ReLU He hull -5}) \leq 1.03$$

and

$$0.97 \leq \text{RATE}(\text{ReLU BN He zero}, \text{ReLU ball hull +5}) \leq 1.03.$$

on around on around 40% of the data sets, only. In this respect note that on HUMAN-ACTIVITY-SMARTPHONE, MUSHROOM, and SMARTPHONE-HUMAN-ACTIVITY-POSTURAL, that is on 5% of the data sets, almost all the methods achieved zero average test errors, while on INSURANCE-BENCHMARK, on the data sets POLISH-COMPANIES-BANKRUPTCY-1YEAR to POLISH-COMPANIES-BANKRUPTCY-5YEAR, and on SEISMIC-BUMPS, THYROID-ALL-HYPO, and THYROID-DIS, that is on around 15% of all data sets, all tested methods, as well as SVMs tested as a sanity check, were not able to outperform the naive classifier that simply predicts all new labels by the majority of the labels found in the training set, see Tables 5 and 3. In other words, around 20% of the considered data sets were either particularly simple or hard to learn from and on these data sets one can expect most classification methods to perform very similarly. To sum up this discussion, we conclude that **ReLU He hull -5** and **ReLU ball hull +5** win or loose in most cases together, whereas **ReLU BN He zero** exhibits strengths and weaknesses

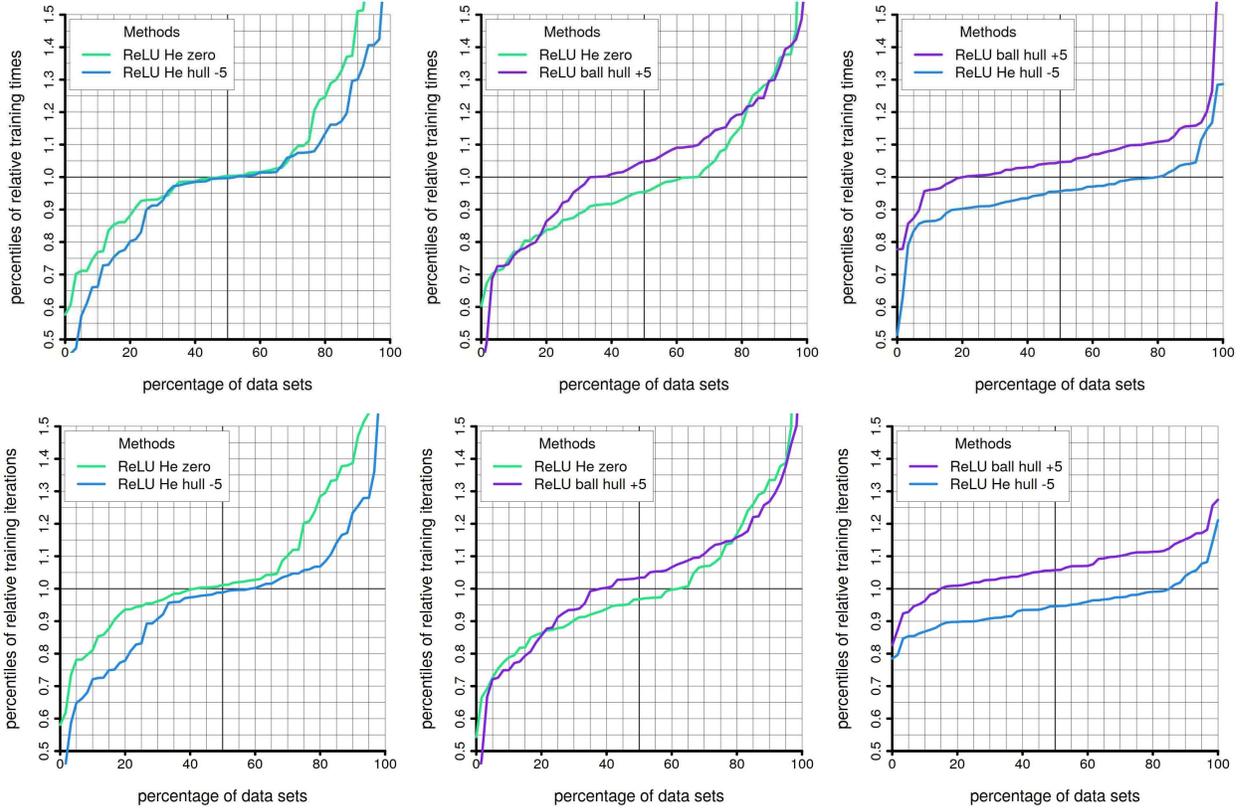


Figure 22: Pairwise comparisons of old and new methods without batch normalization for binary classification in terms of computational resources. The graphics, which have the same meaning as those in Figure 20, show that our new initialization strategy **ReLU He hull -5** leads to faster training compared to standard **ReLU He zero** and the new **ReLU ball hull +5**.

that are rather different from the aforementioned new initialization strategies. Consequently, if one is willing to consider two initialization strategies during the selection phase, it seems to be more beneficial to consider one of the new initialization strategies plus **ReLU BN He zero** instead of considering the two new initialization strategies. Finally, Figure 18 shows that for self-normalizing networks the new initialization strategy **SeLU ball hull -5** substantially outperforms the standard initialization strategy **SeLU SNN zero**. Figure 18 further shows that **SeLU ball hull -5** slightly outperforms both **ReLU He hull -5** and **ReLU ball hull +5**. In this sense, **SeLU ball hull -5** can be viewed as the best performing method, while in terms of raw and adjusted ranking it is only placed third. *In any case, whether it is in terms of ranking ranking or of pairwise comparisons with the help of percentiles of $\text{RATE}_i(\cdot, \cdot)$, all three new initialization strategies clearly outperform the standard initialization strategies.*

ii). Let us now consider the computational resources the different methods required. Again, we begin with the regression case. Here, Figure 20 shows that **ReLU sphere hull -5** is e.g. on 90% of the data sets faster than **ReLU BN He zero**, and on 70% of the data sets it requires less than 80% of the training time **ReLU BN He zero** used. Moreover, the new **ReLU sphere hull -5** is also faster than **ReLU He zero** on around 75% of the data sets, and on 40% of the data sets it requires less than 80% of the training time **ReLU He zero** uses. Similar, yet less pronounced, observations can be made in terms of training iterations the latter two methods run, which is not surprising, since the training time per epoch should be equal for both methods. In contrast, **ReLU BN He zero** requires significantly less iterations than the latter two methods, and this indicates that the training

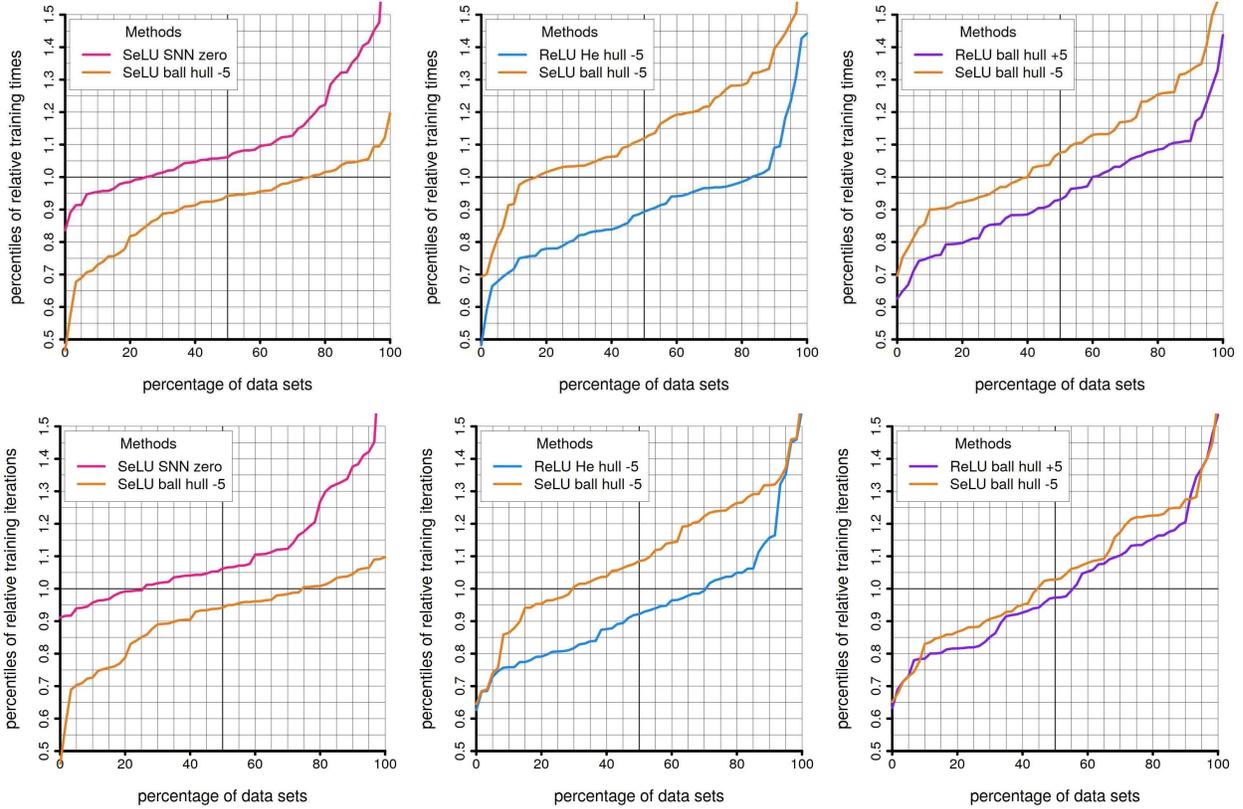


Figure 23: Pairwise comparisons for methods with self-normalizing activation function for binary classification in terms of computational resources. The graphics, which have the same meaning as those in Figure 20, show that our new initialization strategy **SeLU ball hull -5** leads to substantially faster training compared to standard **SeLU SNN zero**. However, **SeLU SNN zero** is slower than **ReLU He hull -5** and **ReLU ball hull +5**.

time per iteration needs to be substantially longer for **ReLU BN He zero** compared to e.g. **ReLU sphere hull -5**. This is, however, not overly surprising as batch normalization adds quite a few extra computations to every step of stochastic gradient descent. When comparing to self-normalizing networks, Figure 21 shows that our new **SeLU ball hull -5** is considerably faster than the standard initialization in terms of both time and iterations. However, only on 40% of the data sets **SeLU ball hull -5** is faster than **ReLU sphere hull -5**, despite the fact that it requires less iterations on $> 55\%$ of the data sets. Again, this is not overly surprising as self-normalizing networks also add computations to each iteration of gradient descent. *In summary, **ReLU sphere hull -5** is not only by far the best method in terms of test errors, but it is also the most efficient method in terms of training time. In the same sense, **SeLU ball hull -5** outperforms the standard initialization **SeLU SNN zero** for self-normalizing networks.*

Let us now have a look on the results for binary classification. Here, Figure 22 shows that the new **ReLU He hull -5** is slightly faster than both the standard **ReLU He zero** and our new **ReLU ball hull +5**, and not surprisingly this behavior can also be found in terms of training iterations. When combining these observations with Figure 17 we thus conclude that ***ReLU He hull -5** outperforms both **ReLU He zero** and **ReLU ball hull +5** in terms of test errors and required computational resources.* Moreover, when considering self-normalizing networks, Figure 23 shows that, as in the regression case, our new initialization **SeLU ball hull -5** leads to substantially faster training than the standard **SeLU SNN zero**. By combining this with Figure 18 we thus conclude that *our new **SeLU ball hull -5** outperforms the standard **SeLU SNN zero** in terms of both tests errors and*

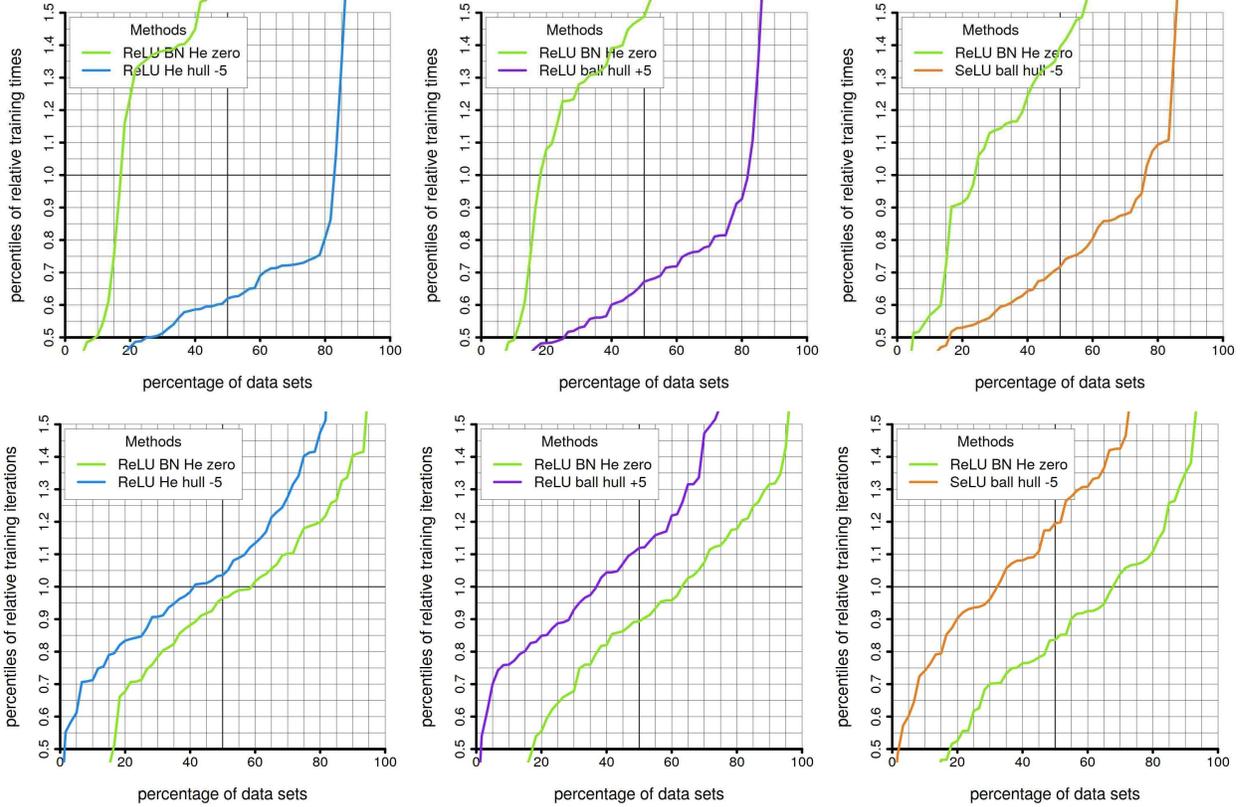


Figure 24: Pairwise comparisons against batch normalization with standard initialization for binary classification in terms of computational resources. The graphics, which have the same meaning as those in Figure 20, show that our new initialization strategies require substantially less training time than **ReLU BN He zero** does despite the fact that the latter needs less training iterations.

computational requirements. In contrast, when comparing **SeLU ball hull -5** with **ReLU He hull -5** and **ReLU ball hull +5**, we see that **SeLU ball hull -5** requires more computational resources than the latter two methods, and therefore, the slight advantage of **SeLU ball hull -5** in terms of tests errors reported in Figure 18 comes with a price tag. In any case, Figure 24 shows that all three new methods **ReLU He hull -5**, **ReLU ball hull +5**, and **SeLU ball hull -5** are also considerably faster than the standard **ReLU BN He zero**. *In summary, all three of our new initialization strategies outperform the standard methods in terms of both test errors and computational requirements.*

iii). Let us finally investigate, how the chosen architectures influence our findings. In the regression case, Figure 25 shows that all methods based on ReLU networks tend to pick deeper architectures and to some extent this is also true for **SeLU ball hull -5**. In contrast, **SeLU SNN zero** prefers narrower networks. One could thus ask, whether **SeLU SNN zero** would have better performed in the comparisons if only architectures in favor of it would have been considered. Interestingly, a comparison between Figures 16 and 26 shows that **SeLU SNN zero** does benefit from such a choice of architectures, but the effect is rather minimal. In fact, **SeLU SNN zero** is still almost uniformly outperformed by both **ReLU sphere hull -5** and **SeLU ball hull -5**.

In the classification case, the picture is again a bit more interesting. Here, Figure 27 shows that **ReLU He hull -5** and **ReLU ball hull +5** tend to prefer wider architectures, while **SeLU SNN zero** again prefers narrower architectures. In addition, **ReLU BN He zero** slightly prefers shallower architectures, while the remaining two methods **ReLU He zero** and **SeLU ball hull -5** do not have a clear tendency. Interestingly, Figure 28 shows that the standard **ReLU BN He zero** is

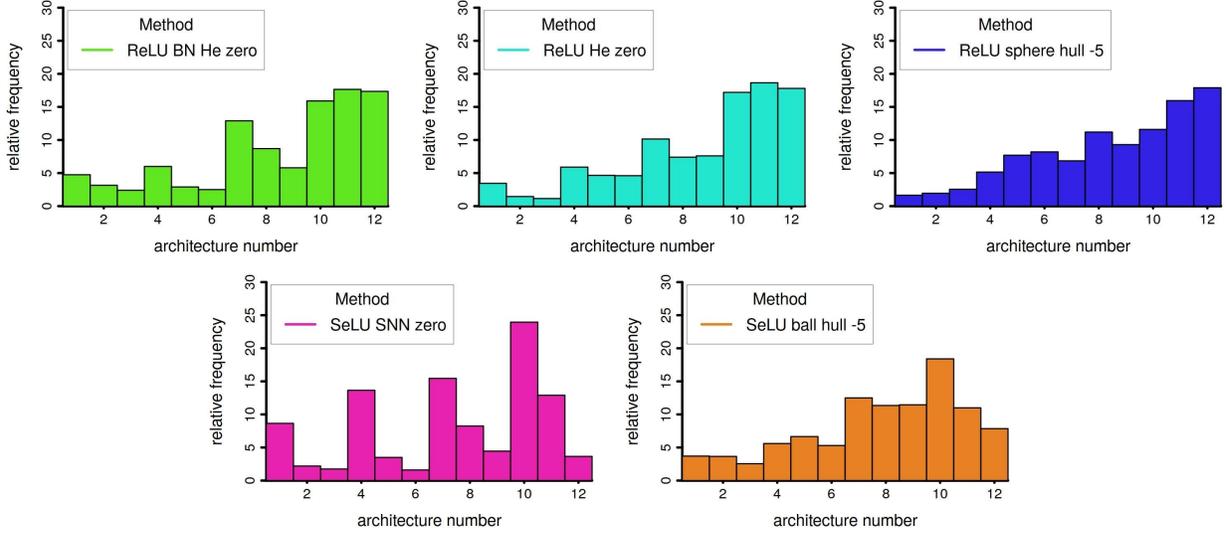


Figure 25: Relative frequency of the architecture picked on the basis of the validation error for the regression data sets. The histograms are based on the $40 \times 50 = 2000$ runs, and the architecture numbers in Table 1. The ReLU networks have the tendency to pick deeper architectures, while **SeLU SNN zero** prefers to pick narrower architectures. In addition, **ReLU BN He zero** slightly prefers shallower architectures. **SeLU ball hull -5** also has the tendency to pick deeper architectures but compared to the ReLU networks this tendency is less pronounced.

still outperformed by all three new initialization strategies **ReLU He hull -5**, **ReLU ball hull +5**, and **SeLU ball hull -5** if the architectures are restricted in favor of **ReLU BN He zero**. In fact, if only the shallowest three architectures, which are preferred by **ReLU BN He zero**, are considered, then **ReLU BN He zero** seems to perform even slightly worse against **ReLU He hull -5** and **ReLU ball hull +5**. Moreover, if these two methods are penalized by restricting to narrow architectures, **ReLU BN He zero** seem to slightly benefit against **ReLU He hull -5** and **ReLU ball hull +5**, yet the effect is minimal **ReLU BN He zero** is still outperformed. In contrast, if **ReLU He hull -5** and **ReLU ball hull +5** are favored by allowing the widest architectures only, then the gap between these two methods and **ReLU BN He zero** clearly widens compared to the set-up that includes all architectures and which is shown in Figure 19. Finally, Figure 29 illustrates the effects when favoring or penalizing **SeLU SNN zero**: If **SeLU SNN zero** is favored by considering the narrowest architectures, only, then **SeLU SNN zero** is still outperformed by all three new initialization methods, however, the gap between e.g. **SeLU SNN zero** and **SeLU ball hull -5** narrows a bit as a comparison between Figures 18 and 29 show. On the other hand, if **SeLU SNN zero** is penalized by considering the widest architectures, then all three new initialization strategies substantially and almost uniformly outperform **SeLU SNN zero**.

In summary, our overall results we obtained by considering all 12 architectures are rather insensitive against changes in the allowed architectures.

5 Proofs

5.1 Proofs for Section 2

For the proof of Proposition 2.2 we need the following trivial lemma.

Lemma 5.1. *Let $X \neq \emptyset$, $D := ((x_1, y_1), \dots, (x_n, y_n)) \in (X \times \mathbb{R})^n$ be a data set, $L : \mathbb{R} \times \mathbb{R} \rightarrow [0, \infty)$ be differentiable loss function, and $g : X \times \mathbb{R}^p \rightarrow \mathbb{R}$ be a function. Furthermore, let $v_0 \in \mathbb{R}^p$ be a*

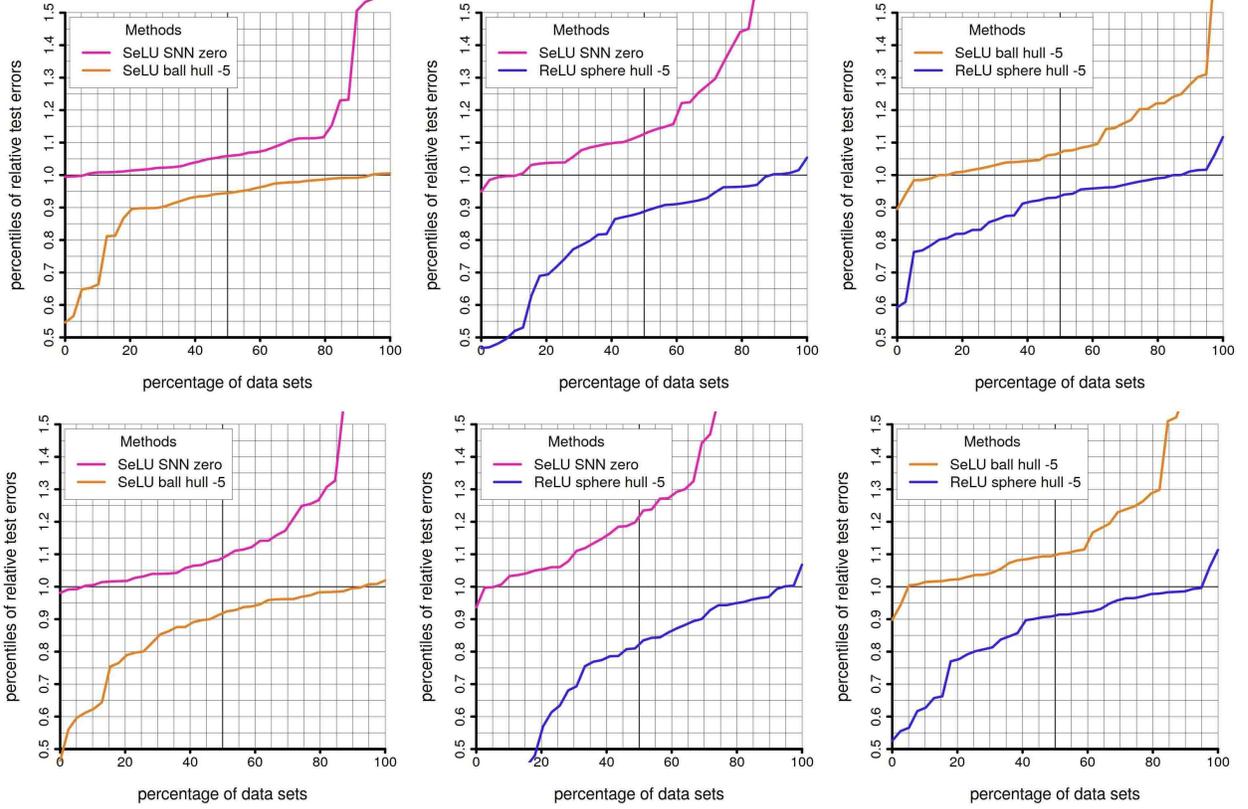


Figure 26: Pairwise comparisons of old and new methods for regression with self-normalizing activation function and different subsets of architectures. The first row displays the percentiles of RATE_i if only the most narrow architectures of each depth are considered during the selection phase, while the second row shows the corresponding results for the widest architectures of each depth. Although **SeLU SNN zero** heavily prefers the narrow architectures, it is still almost uniformly outperformed by **ReLU sphere hull -5** and **SeLU ball hull -5** if only the narrow architectures are allowed. Conversely, considering the widest architectures only, widens the gap between **SeLU SNN zero** and the other two methods as expected.

point such that $v \mapsto g(x_j, v)$ is differentiable in v_0 for all $j = 1, \dots, n$. Then $v \mapsto \mathcal{R}_{L,D}(g(\cdot, v))$ is differentiable at v_0 and we have

$$\frac{\partial \mathcal{R}_{L,D}(g(\cdot, v))}{\partial v}(v_0) = \frac{1}{n} \sum_{j=1}^n L'(y_j, g(x_j, v_0)) \cdot \frac{\partial g}{\partial v}(x_j, v_0).$$

Proof of Lemma 5.1: Using the chain rule we obtain

$$\frac{\partial L(y_j, g(x_j, v))}{\partial v}(v_0) = L'(y_j, g(x_j, v_0)) \cdot \frac{\partial g}{\partial v}(x_j, v_0),$$

for all $j = 1, \dots, n$. From this we easily derive the assertion. \square

Proof of Proposition 2.2: Our goal is to apply Lemma 5.1 in a version that is extended in the sense of (8) and (9) to $g \in \mathcal{A}_{1,m,1}$. To this end, we define $p := 3m+1$, and for $(w, c, a, b) \in \mathbb{R}^m \times \mathbb{R} \times \mathbb{R}^m \times \mathbb{R}^m = \mathbb{R}^p$ we write $g(\cdot, w, c, a, b) : \mathbb{R} \rightarrow \mathbb{R}$ for the function given by (3), that is

$$g(x, w, c, a, b) = \sum_{i=1}^m w_i |a_i x + b_i|_+ + c, \quad x \in \mathbb{R}.$$

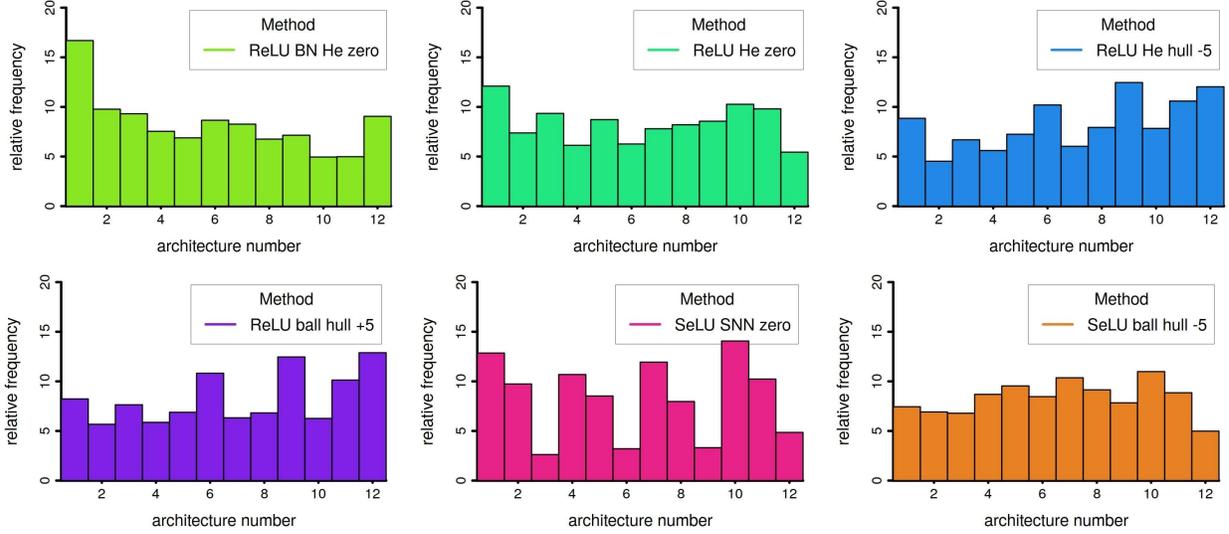


Figure 27: Relative frequency of the architecture picked on the basis of the validation error for the binary classification data sets. The histograms are based on the $61 \times 50 = 3050$ runs, and architecture numbers of those of Table 1. The strategies **ReLU He hull -5** and **ReLU ball hull +5** have the tendency to pick wider architectures of a given depth, while **SeLU SNN zero** has the tendency to pick narrower architectures. In addition, **ReLU BN He zero** slightly prefers shallower architectures. For the remaining initialization strategies there is no clear and simple tendency.

Now recall from Proposition 2.1 that for all $x \in \mathbb{R}$ we have

$$\begin{aligned}
g(x, w, c, a, b) &= \sum_{i \in I_- : x \leq x_i^*} w_i(a_i x + b_i) + \sum_{i \in I_+ : x \geq x_i^*} w_i(a_i x + b_i) + \sum_{i \in I \setminus I_*} w_i |b_i|_+ + c \\
&= \sum_{i \in I_- : x \leq x_i^*} w_i |a_i x + b_i|_+ + \sum_{i \in I_+ : x \geq x_i^*} w_i |a_i x + b_i|_+ + \sum_{i \in I \setminus I_*} w_i |a_i x + b_i|_+ + c.
\end{aligned}$$

For $i \in I_-$, we thus find by (6) and (7)

$$\begin{aligned}
\frac{\partial g}{\partial a_i}(x, w, c, a, b) &= w_i \cdot x \cdot \mathbf{1}_{(-\infty, x_i^*)}(x) + \partial_0 \cdot w_i \cdot x \cdot \mathbf{1}_{\{x_i^*\}}(x), \\
\frac{\partial g}{\partial b_i}(x, w, c, a, b) &= w_i \cdot \mathbf{1}_{(-\infty, x_i^*)}(x) + \partial_0 \cdot w_i \cdot \mathbf{1}_{\{x_i^*\}}(x), \\
\frac{\partial g}{\partial w_i}(x, w, c, a, b) &= (a_i \cdot x + b_i) \cdot \mathbf{1}_{(-\infty, x_i^*)}(x).
\end{aligned}$$

Analogously, for $i \in I_+$ we obtain

$$\begin{aligned}
\frac{\partial g}{\partial a_i}(x, w, c, a, b) &= w_i \cdot x \cdot \mathbf{1}_{(x_i^*, \infty)}(x) + \partial_0 \cdot w_i \cdot x \cdot \mathbf{1}_{\{x_i^*\}}(x) \\
\frac{\partial g}{\partial b_i}(x, w, c, a, b) &= w_i \cdot \mathbf{1}_{(x_i^*, \infty)}(x) + \partial_0 \cdot w_i \cdot \mathbf{1}_{\{x_i^*\}}(x) \\
\frac{\partial g}{\partial w_i}(x, w, c, a, b) &= (a_i \cdot x + b_i) \cdot \mathbf{1}_{(x_i^*, \infty)}(x).
\end{aligned}$$

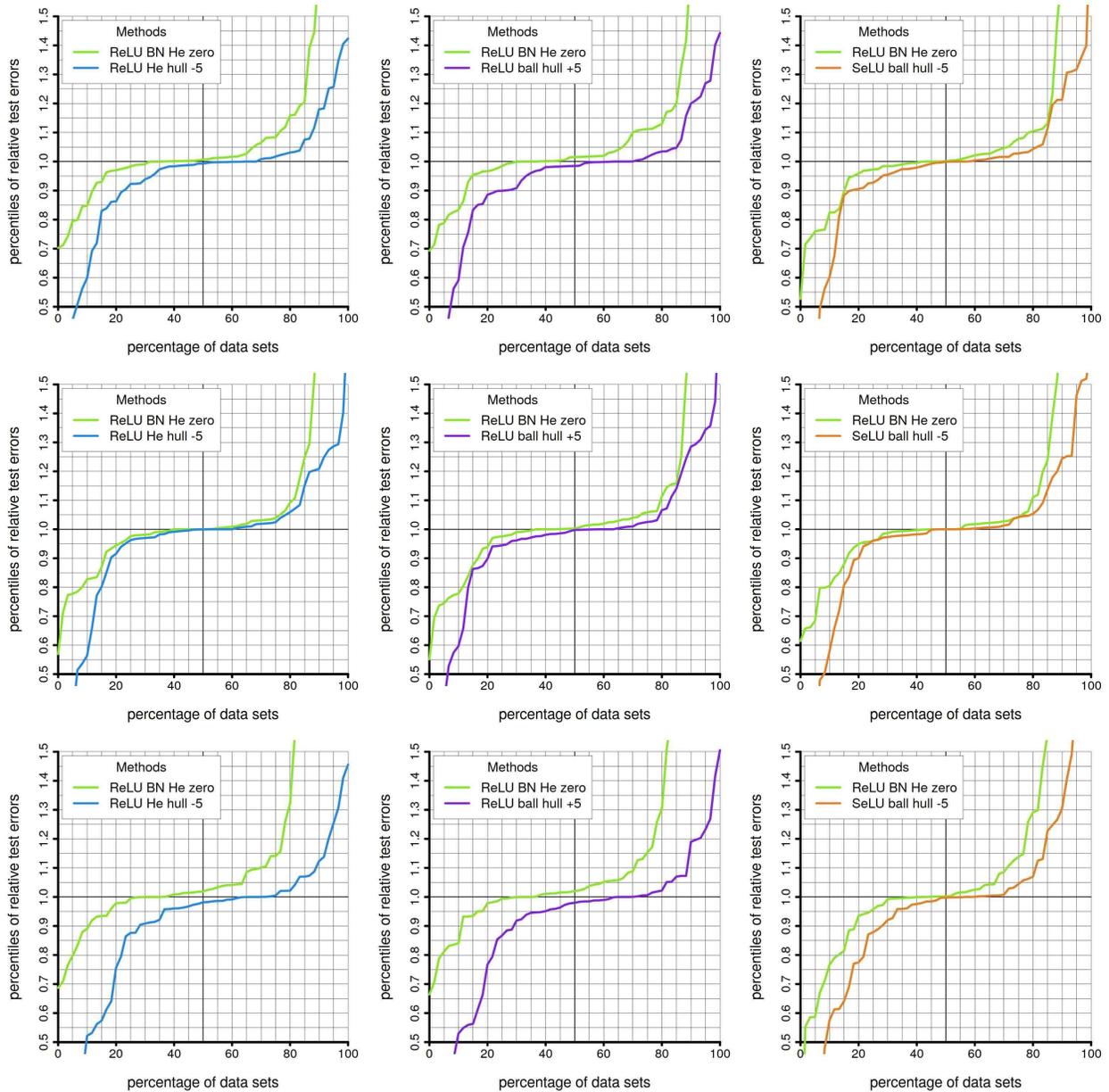


Figure 28: Pairwise comparisons against batch normalization with standard initialization and different subsets of used architectures in the case of binary classification. The first row displays the results if only the architectures with two hidden layers are considered. According to Figure 27, these architectures are the ones that are most often picked with by **ReLU BN He zero**. The second row displays the results if only the architectures with the most narrow widths of each depth are considered. According to Figure 27, these architectures are the ones that are less often picked by **ReLU He hull -5** and **ReLU ball hull +5**. The third row displays the results if only the architectures with the widest widths of each depth are considered. According to Figure 27, these architectures are the ones that are most often picked by **ReLU He hull -5** and **ReLU ball hull +5**. Together, the graphics show that the new initialization strategies outperform **ReLU BN He zero** even if the architectures are chosen in favor of **ReLU BN He zero**. Moreover, if the architectures are chosen in favor of **ReLU He hull -5** and **ReLU ball hull +5**, then the difference between these methods and **ReLU BN He zero** becomes more pronounced.

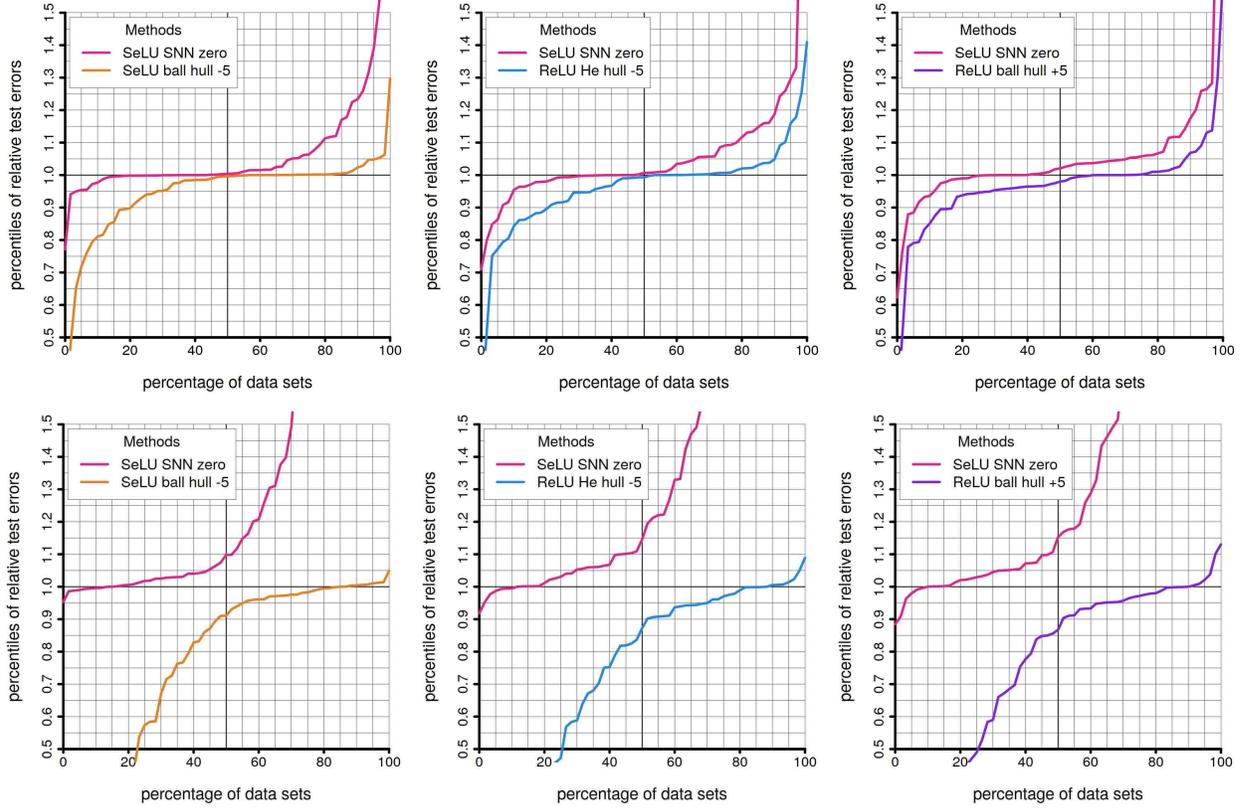


Figure 29: Pairwise comparisons against self-normalizing networks with standard initialization and different subsets of used architectures in the case of binary classification. The first row displays the results if only the architectures with the most narrow widths of each depth are considered. According to Figure 27, these architectures are the ones that are most often picked by **SeLU SNN zero**. The second row displays the results if only the architectures with the widest widths of each depth are considered. According to Figure 27, these architectures are the ones that are most often picked by **ReLU He hull -5** and **ReLU ball hull +5**. Together, the graphics show that the new initialization strategies outperform **SeLU SNN zero** even if the architectures are chosen in favor of **SeLU SNN zero**. Moreover, if the architectures are chosen in favor of **ReLU He hull -5** and **ReLU ball hull +5**, then all three new initialization strategies almost uniformly outperform **SeLU SNN zero**.

Moreover, for $i \in I \setminus I_*$ we find

$$\begin{aligned} \frac{\partial g}{\partial a_i}(x, w, c, a, b) &= w_i \cdot \partial_{b_i} \cdot x, \\ \frac{\partial g}{\partial b_i}(x, w, c, a, b) &= w_i \cdot \partial_{b_i}, \\ \frac{\partial g}{\partial w_i}(x, w, c, a, b) &= |b_i|_+. \end{aligned}$$

Finally, we have

$$\frac{\partial g}{\partial c}(x, w, c, a, b) = 1.$$

Let us now fix an $i \in I_-$. Then, for all samples (x_j, y_j) with $x_j > x_i^*$ our formulas above yield

$$\frac{\partial g}{\partial a_i}(x_j, w, c, a, b) = \frac{\partial g}{\partial b_i}(x_j, w, c, a, b) = \frac{\partial g}{\partial w_i}(x_j, w, c, a, b) = 0,$$

and consequently, Lemma 5.1 extended in the sense of (8) and (9) together with our above formulas for the partial derivatives of g for $x_j \leq x_i^*$ shows the first three formulas. Analogously, for $i \in I_+$ and

all samples (x_j, y_j) with $x_j < x_i^*$ our formulas above yield

$$\frac{\partial g}{\partial a_i}(x_j, w, c, a, b) = \frac{\partial g}{\partial b_i}(x_j, w, c, a, b) = \frac{\partial g}{\partial w_i}(x_j, w, c, a, b) = 0,$$

and consequently, we obtain the formulas in the second case. The remaining assertions follow even more directly from the extended version of Lemma 5.1 and the formulas derived for the partial derivatives of g . \square

Proof of Corollary 2.4: *i*). Without loss of generality we may assume that $x_1 = x_{\min}$, $x_2 = x_{\max}$ and $x_1 < x_3 < x_2$. Since h_i is fully active, we then have $x_1 < x_i^* < x_2$. By symmetry it suffices to consider the case $i \in I_+$. Now assume that there were some $\tilde{a}, \tilde{b} \in \mathbb{R}$ with

$$h(x_j) = \tilde{a}x_j + \tilde{b} \quad (31)$$

for $j = 1, 2, 3$. Since $x_1 < x_i^*$ we also have $h_i(x_1) = 0$ by (5) and $x_2 > x_i^*$ analogously gives

$$h_i(x_2) = a_i x_2 + b_i \neq 0. \quad (32)$$

Now, if $x_3 \leq x_i^*$, then we have $h_i(x_3) = 0$ by (5), and by (31) this implies $\tilde{a} = \tilde{b} = 0$. Hence (31) would give $h_i(x_2) = 0$, which contradicts (32). Moreover, if $x_3 > x_i^*$, then we have $h_i(x_3) = a_i x_3 + b_i$, and by (32) we find $\tilde{a} = a_i$ and $\tilde{b} = b_i$. Equation (31) then gives $h(x_1) = a_i x_1 + b_i \neq 0$ since $x_1 \neq x_i^*$, which again is a contradiction.

ii). If $i \in I_-$, then have $x_i^* \geq x_{\max}$ and hence the assertion follows from (4). The case $i \in I_+$ leads to $x_i^* \leq x_{\min}$ and (5) gives the assertion.

iii). Let us first assume that h_i is inactive. If $i \in I_-$, we then have $x_i^* \leq x_{\min}$, and therefore we find $h_i(x_j) = 0$ for all $j = 1, \dots, n$ by (4). Moreover, for the subsample D' we have $x_{j_l} \geq x_i^*$ for all $l = 1, \dots, k$ and therefore the formulas for the gradients follow from Proposition 2.2. The case $i \in I_+$ can be shown analogously.

Let us now assume that we have $h_i(x_j) = 0$ for all $j = 1, \dots, n$. Moreover, $i \in I_*$ ensures $i \in I_- \cup I_+$ and $a_i \neq 0$. Now let $i \in I_-$ and assume that h_i was not inactive. By definition, there would then exist a sample x_j with $x_j < x_i^*$, and hence (4) together with $a_i < 0$ gives $h_i(x_j) = a_i x_j + b_i > a_i x_i^* + b_i = 0$. This contradicts $h_i(x_j) = 0$. The case $i \in I_+$ can be shown analogously. \square

Proof of Lemma 2.7: The first two assertions are obvious. To show the first equation, we note that h_i is fully active, if and only if $-b_i/a_i \in (x_{\min}, x_{\max})$, and this is equivalent to $b_i/a_i \in (-x_{\max}, -x_{\min})$. This yields

$$\begin{aligned} P(\{\text{neuron } h_i \text{ is fully active}\}) &= P_b \otimes P_a \left(\{(b_i, a_i) \in \mathbb{R}^2 : -b_i/a_i \in (x_{\min}, x_{\max})\} \right) \\ &= P_b/P_a((-x_{\max}, -x_{\min})). \end{aligned}$$

If F_{P_b/P_a} is continuous, this equation immediately implies (11). To establish (12), we first note that h_i is semi-active if $a_i < 0$ and $-b_i/a_i \geq x_{\max}$ or if $a_i > 0$ and $-b_i/a_i \leq x_{\min}$. Now observe that in the case $a_i < 0$ the condition $-b_i/a_i \geq x_{\max}$ is equivalent to $b_i \geq -x_{\max}a_i$, while in the case $a_i > 0$ the condition $-b_i/a_i \leq x_{\min}$ is equivalent to $b_i \geq -x_{\min}a_i$. Consequently, we obtain

$$\begin{aligned} P(\{\text{neuron } h_i \text{ is semi-active}\}) &= P_b \otimes P_a(\{(b_i, a_i) \in \mathbb{R}^2 : b_i \geq -x_{\max}a_i \text{ and } a_i < 0\}) \\ &\quad + P_b \otimes P_a(\{(b_i, a_i) \in \mathbb{R}^2 : b_i \geq -x_{\min}a_i \text{ and } a_i > 0\}) \\ &= F_{P_b, P_a}^-(-x_{\max}) + P_b \otimes P_a(\{(b_i, a_i) \in \mathbb{R}^2 : a_i > 0\}) \\ &\quad - P_b \otimes P_a(\{(b_i, a_i) \in \mathbb{R}^2 : b_i < -x_{\min}a_i \text{ and } a_i > 0\}) \\ &= F_{P_b, P_a}^-(-x_{\max}) + P_a([0, \infty)) - F_{P_b, P_a}^+(-x_{\min}), \end{aligned}$$

where in the last step we used $P_a(\{0\}) = 0$ and the continuity of F_{P_b/P_a} , which ensures

$$P_b \otimes P_a(\{(b_i, a_i) \in \mathbb{R}^2 : b_i = -x_{\min} a_i \text{ and } a_i > 0\}) \leq P_b/P_a(\{-x_{\min}\}) = 0.$$

Equation (13) immediately follows from (10), (11), (12), and $P_a(\{0\}) = 0$, since each neuron h_i is P -almost surely either fully active, or semi-active, or inactive.

Finally, the implication “ \Leftarrow ” is part of the definition of dead neurons. Conversely, since F_{P_b/P_a} is continuous, we have $P_b/P_a(\{x_j\}) = 0$ for all $j = 1, \dots, n$, and hence part *iii* of Lemma 2.4 gives the implication “ \Rightarrow ”. \square

Proof of Theorem 2.8: *i*) \Rightarrow *ii*). Since $-x_{\max} \leq 0$ we find by (A.38)

$$F_{P_b, P_a}^+(-x_{\max}) = \int_{(0, \infty)} P_b((-\infty, -x_{\max}t]) dP_a(t) = 0$$

and analogously, $-x_{\min} \geq 0$ implies

$$F_{P_b, P_a}^-(-x_{\min}) = \int_{(-\infty, 0)} P_b([-x_{\min}t, \infty)) dP_a(t) = \int_{(-\infty, 0)} P_b((0, \infty)) dP_a(t) = P_a((-\infty, 0]),$$

where in the last step we used $P_a(\{0\}) = 0$. Now *ii*) follows from (13).

ii) \Rightarrow *i*). Let us assume that *i*) is not satisfied. Then we have $P_b((-\infty, 0]) > 0$ and consequently it holds $P_b(\{0\}) > 0$ or there exists a $z_0 < 0$ such that $F_{P_b}(z) > 0$ for all $z > z_0$. If $P_b(\{0\}) > 0$, then (A.37) gives $P_b/P_a(\{0\}) > 0$, and hence F_{P_b/P_a} is not continuous. Since this behavior is excluded in the assumptions of our theorem, it suffices to consider the second case. To this end, we define

$$t_+ := \begin{cases} -z_0/x_{\max} & \text{if } x_{\max} > 0 \\ \infty & \text{if } x_{\max} = 0. \end{cases}$$

Let us fix a $t \in (0, t_+)$. Then we have $-x_{\max}t > z_0$, and hence we find $F_{P_b}(-x_{\max}t) > 0$ as well as

$$F_{P_b, P_a}^+(-x_{\max}) = \int_{(0, \infty)} F_{P_b}(-x_{\max}t) dP_a(t) \geq \int_{(0, t_+)} F_{P_b}(-x_{\max}t) dP_a(t),$$

where in the first step we used (A.38). Similarly, we define

$$t_- := \begin{cases} -z_0/x_{\min} & \text{if } x_{\min} > 0 \\ -\infty & \text{if } x_{\min} = 0. \end{cases}$$

For $t \in (t_-, 0)$ we then obtain $-x_{\min}t > z_0$. This yields $P_b((-\infty, -x_{\min}t)) > 0$ and, by incorporating (A.38), also

$$\begin{aligned} F_{P_b, P_a}^-(-x_{\min}) &= \int_{(-\infty, 0)} P_b([-x_{\min}t, \infty)) dP_a(t) = \int_{(-\infty, 0)} 1 - P_b((-\infty, -x_{\min}t)) dP_a(t) \\ &\leq P_a((-\infty, 0]) - \int_{(t_-, 0)} P_b((-\infty, -x_{\min}t)) dP_a(t). \end{aligned}$$

Let us fix an $\varepsilon > 0$ with $\varepsilon \leq \min\{t_+, -t_-\}$. Plugging both estimates into (13) we then obtain

$$\begin{aligned} P(\{\text{neuron } h_i \text{ is inactive}\}) &= P_a((-\infty, 0]) + F_{P_b, P_a}^+(-x_{\max}) - F_{P_b, P_a}^-(-x_{\min}) \\ &\geq \int_{(t_-, 0)} P_b((-\infty, -x_{\min}t)) dP_a(t) + \int_{(0, t_+)} F_{P_b}(-x_{\max}t) dP_a(t) \\ &\geq \int_{(-\varepsilon, \varepsilon)} \min\{P_b((-\infty, -x_{\min}t)), F_{P_b}(-x_{\max}t)\} dP_a(t) \\ &> 0. \end{aligned}$$

In other words, *ii*) does not hold.

iii) \Leftrightarrow *iv*). This equivalence can be shown analogously. In addition, note, that for symmetric P_a it immediately follows from considering $(P_b)_-$ in the already established equivalence $i) \Leftrightarrow ii)$ in combination with the formulas (12), (13), and (A.40). \square

Proof of Theorem 2.9: We first note that $P_b(\{0\}) = 1$ implies $P_b/P_a = \delta_{\{0\}}$, and hence we have $P(\{x_i^* = 0\}) = 1$. Consequently, we shown both $ii) \Rightarrow i)$ and $iii) \Rightarrow i)$, and for data sets satisfying $x_{\min} < 0 < x_{\max}$ also $iv) \Rightarrow i)$ and $v) \Rightarrow i)$.

$i) \Rightarrow ii)$. By the assumed $P_b(\{0\}) < 1$ we conclude that there exists a $z_0 > 0$ with

$$P((-\infty, -z_0]) + P([z_0, \infty)) > 0. \quad (33)$$

We define $z := x_{\max} + 1$ and $\varepsilon := z_0/z$. By (A.47) we then obtain

$$\begin{aligned} P(\{x_i^* > x_{\max}\}) &\geq P(\{x_i^* \geq z\}) = P(\{-x_i^* \leq -z\}) \\ &\geq P_b([z_0, \infty)) \cdot P_a([- \varepsilon, 0]) + P_b(-\infty, -z_0] \cdot P_a((0, \varepsilon]), \end{aligned}$$

and (33) thus yields the assertion.

$i) \Rightarrow ii)$. We first note that we again have (33). We define $z := x_{\min} - 1$ and $\varepsilon := -z_0/z$. Using (A.48) we then obtain

$$P(\{x_i^* < x_{\min}\}) \geq P(\{-x_i^* \geq -z\}) \geq P_b([z_0, \infty)) \cdot P_a((0, \varepsilon]) + P_b(-\infty, -z_0] \cdot P_a([- \varepsilon, 0]),$$

and by (33) we thus find the assertion.

Finally, the implications $ii) \Rightarrow iv)$ and $iii) \Rightarrow v)$ are trivial. \square

5.2 Proofs for Section 3

Proof of Lemma 3.2: $ii) \Rightarrow i)$. Let us fix an $x \in x_i^* \cap \text{ico } D$. Then we have $h_i(x) = 0$ and, by the definition of $\text{ico } D$, there exist $\lambda_1, \dots, \lambda_n > 0$ with $\lambda_1 + \dots + \lambda_n = 1$ and $x = \sum_{j=1}^n \lambda_j x_j$. Moreover, since $\text{ico } D \not\subset x_i^*$ there exists a $j_1 \in \{1 \dots, n\}$ with $x_{j_1} \notin x_i^*$, since otherwise the convexity of x_i^* would imply $\text{ico } D \subset \text{co } D \subset x_i^*$. Consequently, we have $x_{j_1} \in A_i^+ \cup A_i^-$. Let us first assume that $x_{j_1} \in A_i^+$. Then there exists a $j_2 \in \{1 \dots, n\}$ with $x_{j_2} \in A_i^-$, since otherwise we would find

$$0 = h_i(x) = \langle a_i, x \rangle + b = \sum_{j=1}^n \lambda_j (\langle a_i, x_j \rangle + b_i) \geq \lambda_{j_1} (\langle a_i, x_{j_1} \rangle + b_i) > 0.$$

Similarly, if $x_{j_1} \in A_i^-$, then there also needs to exist a $j_2 \in \{1 \dots, n\}$ with $x_{j_2} \in A_i^+$, since otherwise we would find

$$0 = h_i(x) = \langle a_i, x \rangle + b = \sum_{j=1}^n \lambda_j (\langle a_i, x_j \rangle + b_i) \leq \lambda_{j_1} (\langle a_i, x_{j_1} \rangle + b_i) < 0.$$

Consequently, we have shown the existence of the desired $j_1, j_2 \in \{1 \dots, n\}$.

$i) \Rightarrow ii)$. Clearly, $\text{ico } D \subset x_i^*$ is impossible, since this would imply $D \subset \text{co } D = \overline{\text{ico } D} \subset \overline{x_i^*} = x_i^*$, which contradicts e.g. $D \cap A_i^+ \neq \emptyset$. Therefore, it remains to show $x_i^* \cap \text{ico } D \neq \emptyset$. To this end, we define $D^+ := D \cap A_i^+$, $D^- := D \cap A_i^-$ and $D^0 := D \cap x_i^*$. Moreover, for $t \in [0, 1]$ and $j = 1, \dots, n$ we define

$$\lambda_j(t) := \begin{cases} \frac{1-t}{|D^+|} & \text{if } x_j \in D^+ \\ t & \text{if } x_j \in D^- \cup D^0. \end{cases}$$

It is easy to check that $\lambda_1(t) + \dots + \lambda_n(t) = 1$ and that $\lambda_j(t) \in (0, 1)$ whenever $t \in (0, 1)$. Let us now consider the function

$$H : [0, 1] \rightarrow \mathbb{R}$$

$$t \mapsto \sum_{j=1}^n \lambda_j(t) \cdot (\langle a_i, x_j \rangle + b_i)$$

Obviously, the function H is continuous and since $|D^+| \geq 1$ we further have

$$H(0) = \frac{1}{|D^+|} \sum_{x_j \in D^+} (\langle a_i, x_j \rangle + b_i) > 0.$$

Analogously, $|D^-| \geq 1$ implies

$$H(1) = \frac{1}{|D^- \cup D^0|} \sum_{x_j \in D^- \cup D^0} (\langle a_i, x_j \rangle + b_i) = \frac{1}{|D^- \cup D^0|} \sum_{x_j \in D^-} (\langle a_i, x_j \rangle + b_i) < 0.$$

The intermediate value theorem then gives a $t^* \in (0, 1)$ with $H(t^*) = 0$ and for $x^* := \sum_{j=1}^n \lambda_j(t^*) \cdot x_j$ we then find both $x^* \in \text{ico } D$ and

$$\langle a_i, x^* \rangle + b_i = \sum_{j=1}^n \lambda_j(t^*) \cdot (\langle a_i, x_j \rangle + b_i) = H(t^*) = 0.$$

This shows $x^* \in x_i^*$, which completes the proof. \square

Proof of Lemma 3.3: $i) \Rightarrow ii)$. Assume that there exist $\tilde{a} \in \mathbb{R}^d$ and $\tilde{b} \in \mathbb{R}$ such that for all $j = 1, \dots, n$ we have

$$\langle \tilde{a}, x_j \rangle + \tilde{b} = h_i(x_j) = \begin{cases} \langle a_i, x_j \rangle + b_i & \text{if } x_j \in A_i^+ \\ 0 & \text{else.} \end{cases} \quad (34)$$

Since h_i is fully active, we find $j_1, j_2 \in \{1, \dots, n\}$ with $x_{j_1} \in A_i^+$ and $x_{j_2} \in A_i^-$, and the additional assumption $x_{j_0} \in \text{ico } D$ gives us some $\lambda_1, \dots, \lambda_n > 0$ with $\lambda_1 + \dots + \lambda_n = 1$ and $x_{j_0} = \sum_{j=1}^n \lambda_j x_j$. Hence, a simple calculation together with (34) shows

$$\langle \tilde{a}, x_{j_0} \rangle + \tilde{b} = \sum_{j=1}^n \lambda_j (\langle \tilde{a}, x_j \rangle + \tilde{b}) = \sum_{x_j \in A_i^+} \lambda_j (\langle \tilde{a}, x_j \rangle + \tilde{b}) = \sum_{x_j \in A_i^+} \lambda_j (\langle a_i, x_j \rangle + b_i) > 0, \quad (35)$$

where in the last step we used that $A_i^+ \neq \emptyset$, $\lambda_j > 0$ for all $j = 1, \dots, n$, and $\langle a_i, x_j \rangle + b_i > 0$ for all $x_j \in A_i^+$. By (34) we conclude that $x_{j_0} \in A_i^+$. Moreover, a combination of (34) and (35) yields

$$\sum_{j=1}^n \lambda_j (\langle a_i, x_j \rangle + b_i) = \langle a_i, x_{j_0} \rangle + b_i = \langle \tilde{a}, x_{j_0} \rangle + \tilde{b} = \sum_{x_j \in A_i^+} \lambda_j (\langle a_i, x_j \rangle + b_i),$$

and this implies

$$0 = \sum_{x_j \notin A_i^+} \lambda_j (\langle a_i, x_j \rangle + b_i) \leq \lambda_{j_2} (\langle a_i, x_{j_2} \rangle + b_i) < 0,$$

i.e. we have found a contradiction. Consequently, (34) cannot be true.

ii) \Rightarrow i). Assume that h_i was not fully active. Then it is either semi-active or inactive, but in both cases we have shown in front of Lemma 3.3 that h_i would then behave linearly on D . \square

Proof of Theorem 3.7: In front of Theorem 3.7 we have already seen that h_i is inactive if and only if $a_i \in -D^*$. By the symmetry of P_a^d this shows the formula for inactive neurons. Moreover, the formula for fully active neurons follows as soon as we have established the formula for semi-active neurons. To show the latter formula, we first observe that the condition $D \subset x_i^* \cup A_i^+$ is equivalent to $a_i \in D^*$, and hence it suffices to show that

$$P_a^d(\{a_i : D \not\subset x_i^*\}) = 1. \quad (36)$$

To this end, we first observe that x_i^* is a linear subspace due to our initialization $b_i = 0$. Consequently, $D \subset x_i^*$ is equivalent to $\text{span } D \subset x_i^*$. Moreover, $\text{span } D \subset x_i^*$ is also equivalent to $\langle a_i, x \rangle = 0$ for all $x \in \text{span } D$, and this condition simply means $a_i \in (\text{span } D)^\perp$. Now, the sample $x_j \neq 0$ ensures $\dim(\text{span } D)^\perp < d$, which in turn yields $\lambda^d((\text{span } D)^\perp) = 0$. Since P_a^d is absolutely continuous with respect to λ^d , we conclude that $P_a^d((\text{span } D)^\perp) = 0$, and the equivalences discussed previously then lead to (36). \square

Proof of Lemma 3.9: We first show the inequality for inactive neurons. To this end, we consider an $a_i \in \mathbb{R}^d$ such that the neuron described by (a_i, b_+) is inactive. Then we have

$$\langle a_i, x_j \rangle + b_+ \leq 0, \quad j = 1, \dots, n.$$

Since $b_- < b_+$ we then see that $\langle a_i, x_j \rangle + b_- \leq 0$ for all samples x_j , and consequently, the neuron described by (a_i, b_-) is inactive, too. This shows the first inequality.

The proof of the second inequality is similar: Indeed, assume that we have an $a_i \in \mathbb{R}^d$ such that the neuron described by (a_i, b_-) is semi-active. Then, for all samples x_j we have

$$\langle a_i, x_j \rangle + b_- \geq 0,$$

and there is one sample x_{j_0} such that we even have $\langle a_i, x_{j_0} \rangle + b_- > 0$. Using $b_+ > b_-$ we conclude that $\langle a_i, x_j \rangle + b_+ > 0$ for all samples x_j , and this shows that neuron described by (a_i, b_+) is also semi-active. \square

References

- [1] J. M. Borwein and O-Y. Chan. Uniform bounds for the complementary incomplete gamma function. *Math. Inequal. Appl.*, 12:115–121, 2009.
- [2] S. Chatterjee. *Superconcentration and Related Topics*. Springer, Cham, 2014.
- [3] J. H. Curtiss. On the distribution of the quotient of two chance variables. *Ann. Math. Statistics*, 12:409–421, 1941.
- [4] L. Devroye. *Non-Uniform Random Variate Generation*. Springer, New York, 1986.
- [5] O. Forster. *Analysis 3*. Springer Spektrum, Wiesbaden, 8th revised edition, 2017.
- [6] W. Gautschi. Some elementary inequalities relating to the gamma and incomplete gamma function. *Journal of Mathematics and Physics*, 38:77–81, 1959.

- [7] X. Glorot and Y. Bengio. Understanding the difficulty of training deep feedforward neural networks. In *JMLR W&CP: Proceedings of the Thirteenth International Conference on Artificial Intelligence and Statistics (AISTATS 2010)*, volume 9, pages 249–256, 2010.
- [8] I. Goodfellow, Y. Bengio, and A. Courville. *Deep Learning*. MIT Press, Cambridge, MA, 2016.
- [9] K. He, X. Zhang, S. Ren, and J. Sun. Delving deep into rectifiers: Surpassing human-level performance on imagenet classification. In *Proceedings of the 2015 IEEE International Conference on Computer Vision (ICCV)*, pages 1026–1034, Washington, DC, USA, 2015. IEEE Computer Society.
- [10] D. Kershaw. Some extensions of W. Gautschi’s inequalities for the gamma function. *Math. Comp.*, 41:607–611, 1983.
- [11] G. Klambauer, T. Unterthiner, A. Mayr, and S. Hochreiter. Self-normalizing neural networks. In I. Guyon, U. V. Luxburg, S. Bengio, H. Wallach, R. Fergus, S. Vishwanathan, and R. Garnett, editors, *Advances in Neural Information Processing Systems 30*, pages 971–980. Curran Associates, Inc., 2017.
- [12] A. Krizhevsky, I. Sutskever, and G. E. Hinton. Imagenet classification with deep convolutional neural networks. In F. Pereira, C. J. C. Burges, L. Bottou, and K. Q. Weinberger, editors, *Advances in Neural Information Processing Systems 25*, pages 1097–1105. 2012.
- [13] G. G. Magaril-II’yaev and V. M. Tikhomirov. *Convex Analysis: Theory and Applications*. American Mathematical Society, Providence, RI, 2003.
- [14] P. Natalini and B. Palumbo. Inequalities for the incomplete gamma function. *Math. Inequal. Appl.*, 3:69–77, 2000.
- [15] I. Steinwart and A. Christmann. *Support Vector Machines*. Springer, New York, 2008.
- [16] R. Vershynin. *High-Dimensional Probability*. Cambridge University Press, Cambridge, 2018.

A Appendix: Ratio Distributions

The goal of this appendix is to collect some, probably known, results about ratio distributions as well as some new results about $F_{P,Q}^-$ and $F_{P,Q}^+$.

We begin with a proposition that collects various structural properties. For its formulation we define, for a given probability measure ν on \mathbb{R} , the probability measure ν_- on \mathbb{R} by

$$\nu_-(A) := \mu(-A), \quad \text{for all measurable } A \subset \mathbb{R}.$$

Obviously, ν is symmetric if $\nu_- = \nu$.

Proposition A.1. *Let P and Q be two probability measures on \mathbb{R} with $Q(\{0\}) = 0$. Then it holds*

$$P/Q(\{0\}) = P(\{0\}) \tag{A.37}$$

and, for all $z \in \mathbb{R}$, we have

$$F_{P,Q}^-(z) = \int_{(-\infty, 0)} P([zt, \infty)) dQ(t) \quad \text{and} \quad F_{P,Q}^+(z) = \int_{(0, \infty)} P((-\infty, zt]) dQ(t). \tag{A.38}$$

Moreover, the following statements are true:

i) If Q is symmetric, then P/Q is symmetric and we have

$$F_{P/Q}(z) = \begin{cases} \frac{1}{2} - \int_{(0,\infty)} P((zt, -zt)) dQ(t) & \text{if } z < 0 \\ \frac{1}{2} + \int_{(0,\infty)} P([-zt, zt]) dQ(t) & \text{if } z \geq 0 \end{cases}. \quad (\text{A.39})$$

Moreover, for all $z \in \mathbb{R}$ we have

$$F_{P_-/Q}^+(z) = F_{P/Q}^-(z), \quad F_{P_-/Q}^-(z) = F_{P/Q}^+(z), \quad F_{P_-/Q}(z) = F_{P/Q}(z). \quad (\text{A.40})$$

In particular, if, in addition, P is also symmetric, then for all $z \in \mathbb{R}$ we have

$$F_{P,Q}^-(z) = F_{P,Q}^+(z) = \frac{1}{2} F_{P/Q}(z). \quad (\text{A.41})$$

ii) If P and Q are Lebesgue absolutely continuous with densities f_P and f_Q , then P/Q is Lebesgue absolutely continuous with density

$$f_{P/Q}(z) = \int_{\mathbb{R}} |t| f_P(tz) f_Q(t) dt \quad \text{for } \lambda\text{-almost all } z \in \mathbb{R}. \quad (\text{A.42})$$

iii) If P is a Dirac distribution at $b > 0$, that is $P = \delta_{\{b\}}$, then we have both

$$F_{P/Q}(z) = \begin{cases} F_Q(0) - \lim_{\varepsilon \searrow 0} F_Q(bz^{-1} - \varepsilon) & \text{if } z < 0 \\ F_Q(0) & \text{if } z = 0 \\ F_Q(0) + 1 - \lim_{\varepsilon \searrow 0} F_Q(bz^{-1} - \varepsilon) & \text{if } z > 0 \end{cases} \quad (\text{A.43})$$

and

$$F_{P,Q}^+(z) = \begin{cases} 0 & \text{if } z \leq 0 \\ 1 - \lim_{\varepsilon \searrow 0} F_Q(bz^{-1} - \varepsilon) & \text{if } z > 0. \end{cases} \quad (\text{A.44})$$

In particular, if F_Q is continuous, then taking $\lim_{\varepsilon \searrow 0}$ is superfluous in all three cases, and $F_{P/Q}$ is continuous. Finally, if Q is even Lebesgue absolutely continuous and has a density f_Q that is piecewise continuous, then P/Q is Lebesgue absolutely continuous and its density is λ -almost surely given by

$$f_{P/Q}(z) = bz^{-2} f_Q(bz^{-1}). \quad (\text{A.45})$$

Proof of Proposition A.1: We begin by showing (A.37). To this end, we consider, like in the derivation of (10), the projections $\pi_X, \pi_Y : \mathbb{R}^2 \rightarrow \mathbb{R}$ defined by $\pi_X(x, y) := x$ and $\pi_Y(x, y) := y$. With respect to the product measure $P \otimes Q$ on \mathbb{R}^2 these projections π_X and π_Y are independent random variables and their distributions are P and Q . Using $Q(\{0\}) = 0$ this leads to

$$\begin{aligned} P/Q(\{0\}) &= P \otimes Q\left(\frac{\pi_X}{\pi_Y} = 0\right) = P \otimes Q(\{(x, y) \in \mathbb{R}^2 : x/y = 0\}) = P \otimes Q(\{(x, y) \in \mathbb{R}^2 : x = 0\}) \\ &= P(\{0\}). \end{aligned}$$

Moreover, for the proof of the first equality in (A.38), we simply note that

$$\begin{aligned} F_{P,Q}^-(z) &= P \otimes Q(\{(x, y) \in \mathbb{R}^2 : x \geq zy \text{ and } y < 0\}) = \int_{\mathbb{R}} \int_{\mathbb{R}} \mathbf{1}_{[zy, \infty)}(x) \mathbf{1}_{(-\infty, 0)}(y) dP(x) dQ(y) \\ &= \int_{(-\infty, 0)} P([zy, \infty)) dQ(y). \end{aligned}$$

The second equality can be shown analogously.

i). Our first goal is to show (A.39). To this end, we first observe that the symmetry of Q gives

$$\int_{(-\infty, 0)} P([zt, \infty)) dQ(t) = \int_{(0, \infty)} P([-zt, \infty)) dQ(t).$$

Let us first consider the case $z < 0$. Using (10) and (A.38) we then obtain

$$F_{P/Q}(z) = F_{P,Q}^+(z) + F_{P,Q}^-(z) = \int_{(0, \infty)} P((-\infty, zt]) + P([-zt, \infty)) dQ(t) = \int_{(0, \infty)} 1 - P((zt, -zt)) dQ(t),$$

and since we have $Q([0, \infty)) = 1/2$ we get (A.39) in the case $z < 0$. The case $z \geq 0$ can be shown analogously, namely

$$F_{P/Q}(z) = \int_{(0, \infty)} P((-\infty, zt]) + P([-zt, \infty)) dQ(t) = \int_{(0, \infty)} 1 + P([-zt, zt]) dQ(t).$$

For the proof of the symmetry of P/Q we recall that a distribution ν on \mathbb{R} is symmetric, if and only if $\nu((-\infty, -z]) = \nu([z, \infty))$ for all $z > 0$, and the latter is equivalent to

$$F_{\nu}(-z) + \lim_{\varepsilon \searrow 0} F_{\nu}(z - \varepsilon) = 1, \quad z > 0. \quad (\text{A.46})$$

Now observe that, for $z > 0$, the already established (A.39) and Beppo Levi's theorem yield

$$\lim_{\varepsilon \searrow 0} F_{P/Q}(z - \varepsilon) = \frac{1}{2} + \lim_{\varepsilon \searrow 0} \int_{(0, \infty)} P([- (z - \varepsilon)t, (z - \varepsilon)t]) dQ(t) = \frac{1}{2} + \int_{(0, \infty)} P((-zt, zt)) dQ(t),$$

and by combining this with (A.39) applied to $-z$ we find (A.46) for $\nu = P/Q$. Consequently P/Q is symmetric.

Let us now establish (A.40). We begin with the second equality in (A.40). To this end, we simply use the already established (A.38) and the symmetry of Q to obtain

$$\begin{aligned} F_{P,Q}^+(z) &= \int_{(0, \infty)} P((-\infty, zt]) dQ(t) = \int_{\mathbb{R}} \mathbf{1}_{(0, \infty)}(t) P((-\infty, zt]) dQ(t) \\ &= \int_{\mathbb{R}} \mathbf{1}_{(0, \infty)}(-t) P((-\infty, -zt]) dQ(t) \\ &= \int_{(-\infty, 0)} P_-([zt, \infty)) dQ(t) \\ &= F_{P_-, Q}^-(z). \end{aligned}$$

Now using $(P_-)_- = P$, we also find the first equality in (A.40), namely $F_{P_-/Q}^+ = F_{(P_-)_-/Q}^- = F_{P/Q}^-$, and using these just established identities in combination with (10) gives $F_{P_-/Q} = F_{P/Q}$. Finally, if P is symmetric, we find $F_{P/Q}^- = F_{P_-/Q}^+ = F_{P/Q}^+$ and using (10) yet another time gives $F_{P,Q}^+ = \frac{1}{2} F_{P/Q}$.

ii). For a proof we refer to [3, Theorem 3.1], but the assertion can also be quickly derived from (10) and (A.38).

iii). We begin by showing (A.43). In the case $z = 0$ we first observe that $P((-\infty, 0]) = 0$ and $P([0, \infty)) = 1$, and hence (10) together with (A.38) gives

$$F_{P/Q}(0) = \int_{(0, \infty)} P((-\infty, 0]) dQ(t) + \int_{(-\infty, 0)} P([0, \infty)) dQ(t) = Q((-\infty, 0]) = F_Q(0),$$

where in the last step we used $Q(\{0\}) = 0$. Let us now consider the case $z < 0$. For $t > 0$ we then find

$$P((-\infty, zt]) = \mathbf{1}_{[b, \infty)}(zt) = 0,$$

while for $t < 0$ we obtain $P([zt, \infty)) = \mathbf{1}_{(-\infty, b]}(zt) = \mathbf{1}_{[bz^{-1}, \infty)}(t)$. By (10) and (A.38) we thus get

$$F_{P/Q}(z) = \int_{(-\infty, 0)} \mathbf{1}_{[bz^{-1}, \infty)}(t) dQ(t) = Q([bz^{-1}, 0]) = F_Q(0) - \lim_{\varepsilon \searrow 0} F_Q(bz^{-1} - \varepsilon).$$

Similarly, for $z > 0$ and $t > 0$ we find

$$P((-\infty, zt]) = \mathbf{1}_{[bz^{-1}, \infty)}(t)$$

while for $z > 0$ and $t < 0$ we get $P([zt, \infty)) = 1$. Together with (10) and (A.38) this yields

$$\begin{aligned} F_{P/Q}(z) &= \int_{(0, \infty)} \mathbf{1}_{[bz^{-1}, \infty)}(t) dQ(t) + Q((-\infty, 0]) = Q([bz^{-1}, \infty)) + F_Q(0) \\ &= F_Q(0) + 1 - \lim_{\varepsilon \searrow 0} F_Q(bz^{-1} - \varepsilon), \end{aligned}$$

and hence we have shown (A.43).

To establish (A.44), it suffices to observe that

$$F_{P,Q}^+(z) = Q(\{y \in \mathbb{R} : b/y \leq z \text{ and } y > 0\}) = \begin{cases} 0 & \text{if } z \leq 0 \\ Q([bz^{-1}, \infty)) & \text{if } z > 0. \end{cases}$$

Let us finally assume that the density f_Q is piecewise continuous, that is

$$N := \{t \in \mathbb{R} : f_Q \text{ is not continuous at } t\}$$

is finite. Then the fundamental theorem of calculus shows that F_Q is differentiable on $\mathbb{R} \setminus N$ and $F'_Q(z) = f_Q(z)$ for all $z \notin N$. Using (A.43) we consequently find for $z_0 \neq 0$ with $bz_0^{-1} \notin N$ that

$$F'_{P/Q}(z_0) = -\frac{\partial F_Q(bz^{-1})}{\partial z}(z_0) = bz_0^{-2} f_Q(bz_0^{-1}).$$

In particular, $F'_{P/Q}$ is piecewise continuous and the fundamental theorem of calculus thus shows that $F'_{P/Q}$ is a Lebesgue density of P/Q . \square

The next lemma establishes some simple lower bounds on certain ratio probabilities.

Lemma A.2. *Let P and Q be two probability measures on \mathbb{R} with $Q(\{0\}) = 0$. Then for all $\varepsilon > 0$ the following two estimates hold:*

$$P/Q((-\infty, z]) \geq P([-\varepsilon z, \infty)) \cdot Q([-\varepsilon, 0]) + P(-\infty, \varepsilon z] \cdot Q((0, \varepsilon]) \quad \text{if } z < 0 \quad (\text{A.47})$$

$$P/Q([z, \infty)) \geq P([\varepsilon z, \infty)) \cdot Q((0, \varepsilon]) + P(-\infty, -\varepsilon z] \cdot Q([-\varepsilon, 0]) \quad \text{if } z > 0. \quad (\text{A.48})$$

Proof of Lemma A.2: We begin by showing (A.47). To this end, we observe that for $z < 0$ and $y \in [-\varepsilon, 0)$ we have $zy \leq -\varepsilon z$, and hence we find

$$\begin{aligned} P \otimes Q(\{(x, y) \in \mathbb{R}^2 : x \geq zy \text{ and } y < 0\}) &\geq P \otimes Q(\{(x, y) \in \mathbb{R}^2 : x \geq zy \text{ and } y \in [-\varepsilon, 0)\}) \\ &\geq P \otimes Q(\{(x, y) \in \mathbb{R}^2 : x \geq -\varepsilon z \text{ and } y \in [-\varepsilon, 0)\}) \\ &= P([-\varepsilon z, \infty)) \cdot Q([-\varepsilon, 0)). \end{aligned}$$

Analogously, we obtain for $z < 0$ that

$$\begin{aligned} P \otimes Q(\{(x, y) \in \mathbb{R}^2 : x \leq zy \text{ and } y > 0\}) &\geq P \otimes Q(\{(x, y) \in \mathbb{R}^2 : x \leq \varepsilon z \text{ and } y \in (0, \varepsilon]\}) \\ &= P(-\infty, \varepsilon z] \cdot Q((0, \varepsilon]). \end{aligned}$$

Combining both estimates with (10) then yields (A.47). The proof of (A.48) is similar, namely, for $z > 0$ we have

$$\begin{aligned} P \otimes Q(\{(x, y) \in \mathbb{R}^2 : x \geq zy \text{ and } y > 0\}) &\geq P \otimes Q(\{(x, y) \in \mathbb{R}^2 : x \geq \varepsilon z \text{ and } y \in (0, \varepsilon]\}) \\ &= P([\varepsilon z, \infty)) \cdot Q((0, \varepsilon]) \end{aligned}$$

as well as

$$\begin{aligned} P \otimes Q(\{(x, y) \in \mathbb{R}^2 : x \leq zy \text{ and } y < 0\}) &\geq P \otimes Q(\{(x, y) \in \mathbb{R}^2 : x \leq -\varepsilon z \text{ and } y \in [-\varepsilon, 0)\}) \\ &= P(-\infty, -\varepsilon z] \cdot Q([-\varepsilon, 0)). \end{aligned}$$

Combining these two estimates with an equation analogous to (10), namely

$$\begin{aligned} P/Q([z, \infty)) &= P \otimes Q(\{(x, y) \in \mathbb{R}^2 : x \geq zy \text{ and } y > 0\}) \\ &\quad + P \otimes Q(\{(x, y) \in \mathbb{R}^2 : x \leq zy \text{ and } y < 0\}), \end{aligned}$$

then yields (A.48). □

Example A.3 (Normal Ratios). For $\sigma_P, \sigma_Q > 0$ consider the distributions $P := \mathcal{N}(0, \sigma_P^2)$ and $Q := \mathcal{N}(0, \sigma_Q^2)$. Then we have

$$f_{P/Q}(z) = \frac{\sigma_P \cdot \sigma_Q}{\pi} \cdot \frac{1}{\sigma_Q^2 z^2 + \sigma_P^2}, \quad z \in \mathbb{R},$$

see e.g. [3, Equation (3.3)]. In other words, P/Q is the Cauchy distribution with location parameter $x_0 = 0$ and scale parameter $\gamma = \sigma_P/\sigma_Q$. This leads to

$$F_{P/Q}(z) = \frac{1}{\pi} \arctan\left(\frac{\sigma_Q \cdot z}{\sigma_P}\right) + \frac{1}{2}, \quad z \in \mathbb{R}.$$

Finally, by the symmetry of $\mathcal{N}(0, \sigma_P^2)$ and $\mathcal{N}(0, \sigma_Q^2)$ and Equation (A.41) we find $F_{P,Q}^-(z) = F_{P,Q}^+(z) = \frac{1}{2}F_{P/Q}(z)$ for all $z \in \mathbb{R}$.

Example A.4 (Normal Denominators). For $b > 0$ and $\sigma > 0$ consider the distributions $P := \delta_{\{b\}}$ and $Q := \mathcal{N}(0, \sigma^2)$. Since Q has the Lebesgue density f_Q given by $f_Q(t) = \frac{1}{\sqrt{2\pi\sigma^2}} \exp(-\frac{t^2}{2\sigma^2})$ for $t \in \mathbb{R}$, we then find using (A.45) that

$$f_{P/Q}(z) = \frac{b}{\sqrt{2\pi\sigma^2} z^2} \exp\left(-\frac{b^2}{2\sigma^2 z^2}\right), \quad z \neq 0.$$

Note that this density has two modes at $\pm \frac{b}{\sqrt{2}\sigma}$ and it vanishes at 0. Furthermore, part *iii*) of Proposition 2.7 shows that

$$F_{P/Q}(z) = \begin{cases} \frac{1}{2} - \Phi\left(\frac{b}{\sigma z}\right) & \text{if } z < 0 \\ \frac{1}{2} & \text{if } z = 0 \\ \frac{1}{2} + \Phi\left(-\frac{b}{\sigma z}\right) & \text{if } z > 0, \end{cases}$$

$$F_{P,Q}^+(z) = \begin{cases} 0 & \text{if } z \leq 0 \\ 1 - \Phi\left(\frac{b}{\sigma z}\right) & \text{if } z > 0, \end{cases}$$

where Φ denotes the cumulative distribution function of the standard normal distribution $\mathcal{N}(0, 1)$.

Example A.5 (Asymmetric Uniform Ratios). For $\beta > 0$ and $\alpha > 0$ consider the distributions $P := \mathcal{U}[0, \beta]$ and $Q := \mathcal{U}[-\alpha, \alpha]$. Plugging their densities $f_P = \frac{1}{\beta}\mathbf{1}_{[0, \beta]}$ and $f_Q = \frac{1}{2\alpha}\mathbf{1}_{[-\alpha, \alpha]}$ into (A.42) gives

$$f_{P/Q}(z) = \frac{1}{4\alpha\beta} \min\{\alpha^2, \beta^2 z^{-2}\} = \begin{cases} \frac{\alpha}{4\beta} & \text{if } z \in \left[-\frac{\beta}{\alpha}, \frac{\beta}{\alpha}\right] \\ \frac{\beta}{4\alpha} \cdot z^{-2} & \text{if } z < -\frac{\beta}{\alpha} \text{ or } z > \frac{\beta}{\alpha}, \end{cases} \quad (\text{A.49})$$

and by integrating this density we obtain

$$F_{P/Q}(z) = \begin{cases} -\frac{\beta}{4\alpha z} & \text{if } z \leq -\frac{\beta}{\alpha} \\ \frac{2\beta + \alpha z}{4\beta} & \text{if } z \in \left[-\frac{\beta}{\alpha}, \frac{\beta}{\alpha}\right] \\ 1 - \frac{\beta}{4\alpha z} & \text{if } z \geq \frac{\beta}{\alpha}. \end{cases} \quad (\text{A.50})$$

Finally, for $z \leq 0$, Equation (A.38) immediately shows $F_{P_b, P_a}^+(z) = 0$, and for $z > 0$ we obtain

$$F_{P_b, P_a}^+(z) = \frac{1}{2\alpha\beta} \int_0^\alpha \int_0^{zt \wedge \beta} 1 \, ds \, dt = \frac{1}{2\alpha\beta} \int_0^\alpha \min\{zt, \beta\} \, dt.$$

Now, in the case $z \leq \frac{\beta}{\alpha}$ we have $zt \leq \beta$ for all $t \in [0, \alpha]$, and hence we find $F_{P_b, P_a}^+(z) = \frac{\alpha}{4\beta}z$, while in the case $z \geq \frac{\beta}{\alpha}$, we obtain

$$F_{P_b, P_a}^+(z) = \frac{1}{2\alpha\beta} \int_0^{\beta z^{-1}} zt \, dt + \frac{1}{2\alpha\beta} \int_{\beta z^{-1}}^\alpha \beta \, dt = \frac{1}{2\alpha\beta} \cdot \frac{\beta^2}{2z} + \frac{\beta}{2\alpha\beta} \left(\alpha - \frac{\beta}{z}\right) = \frac{1}{2} - \frac{\beta}{4\alpha z}.$$

Summarizing these calculation, we have found

$$F_{P/Q}^+(z) = \begin{cases} 0 & \text{if } z \leq 0 \\ \frac{\alpha}{4\beta}z & \text{if } z \in \left[0, \frac{\beta}{\alpha}\right] \\ \frac{1}{2} - \frac{\beta}{4\alpha z} & \text{if } z \geq \frac{\beta}{\alpha}. \end{cases}$$

Example A.6 (Symmetric Uniform Ratios). For $\beta > 0$ and $\alpha > 0$ consider the distributions $P := \mathcal{U}[-\beta, \beta]$ and $Q := \mathcal{U}[-\alpha, \alpha]$. Then an easy calculation shows that the density $f_{P/Q}$ coincides with (A.49), and therefore $F_{P/Q}$ coincides with (A.50). Unlike in Example A.5, however, the distributions P and Q are now symmetric, and therefore part *i*) of Proposition A.1 shows that $F_{P,Q}^+ = \frac{1}{2}F_{P/Q}$.

Example A.7 (Uniform Denominators). For $b > 0$ and $\alpha > 0$ consider the distributions $P := \delta_{\{b\}}$ and $Q := \mathcal{U}[-\alpha, \alpha]$. Then the Lebesgue density f_Q of Q is given by $f_Q = \frac{1}{2\alpha}\mathbf{1}_{[-\alpha, \alpha]}$ and by *iii*) of Proposition 2.7 therefore we obtain that

$$f_{P/Q}(z) = \begin{cases} 0 & \text{if } z \in [-\frac{b}{\alpha}, \frac{b}{\alpha}] \\ \frac{b}{2\alpha} \cdot z^{-2} & \text{if } z < -\frac{b}{\alpha} \text{ or } z > \frac{b}{\alpha} . \end{cases}$$

Moreover, using $F_Q(z) = \max\{0, \min\{1, \frac{\alpha+z}{2\alpha}\}\}$, part *iii*) of Proposition 2.7 further yields

$$F_{P/Q}(z) = \begin{cases} -\frac{b}{2\alpha z} & \text{if } z \leq -\frac{b}{\alpha} \\ \frac{1}{2} & \text{if } z \in [-\frac{b}{\alpha}, \frac{b}{\alpha}] \\ 1 - \frac{b}{2\alpha z} & \text{if } z \geq \frac{b}{\alpha} \end{cases}$$

$$F_{P,Q}^+(z) = \begin{cases} 0 & \text{if } z \leq \frac{b}{\alpha} \\ 1 - \frac{b}{2\alpha z} & \text{if } z \geq \frac{b}{\alpha} . \end{cases}$$

B Appendix: Geometric set operations

Given a set $A \subset \mathbb{R}^d$, the convex hull \mathcal{A} of A is the smallest convex set containing A . If A is finite, say $A = \{y_1, \dots, y_k\}$, then \mathcal{A} can be computed by

$$\text{co } A = \left\{ y \in \mathbb{R}^d : \exists \lambda_1, \dots, \lambda_k \geq 0 \text{ with } \lambda_1 + \dots + \lambda_k = 1 \text{ and } y = \sum_{j=1}^k \lambda_j y_j \right\}.$$

Moreover, a set $K \subset \mathbb{R}^d$ is called a cone, if for all $x \in K$ and $\alpha > 0$ we have $\alpha x \in K$. It is well known, see e.g. [13, page 30] that a cone K is convex, if and only if $K + K \subset K$. Moreover, the conic hull $\text{coni } A$ of a set A is the smallest convex cone containing A . If A is of the form $A = \{y_1, \dots, y_k\}$, then $\text{coni } A$ can be computed by

$$\text{coni } A = \left\{ y \in \mathbb{R}^d : \exists \lambda_1, \dots, \lambda_k \geq 0 \text{ with } y = \sum_{j=1}^k \lambda_j y_j \right\},$$

and for such sets A , both $\text{co } A$ and $\text{coni } A$ are closed. Moreover, for all $A \subset \mathbb{R}^d$ we have $\text{co } A \subset \text{coni } A$. In addition, given an $A \subset \mathbb{R}^d$, the dual cone of A is defined by

$$A^* := \{y \in \mathbb{R}^d : \langle y, x \rangle \geq 0 \text{ for all } x \in A\}.$$

Obviously, A^* is always a convex, closed cone. Moreover, we obviously have $(\text{coni } A)^* \subset A^*$, and since the converse implication is also straightforward, we actually have $(\text{coni } A)^* = A^*$. Furthermore, $A^{**} = A$ if and only if A is a closed convex cone, see e.g. [13, page 43], and by combining these results we find $A^{**} = (\text{coni } A)^{**} = \text{coni } A$ for arbitrary sets $A \subset \mathbb{R}^d$. Finally, it is straightforward to check that $([0, \infty)^d)^* = [0, \infty)^d$, cf. also [13, page 91]. The next lemma, which is probably well-known but could not be found in the literature, characterizes the finite sets A satisfying $\text{coni } A = [0, \infty)^d$.

Lemma B.1. Let $A = \{x_1, \dots, x_n\}$ be a finite set with $A \subset [0, \infty)^d$. Then the following statements are equivalent

i) We have $\text{coni } A = [0, \infty)^d$.

ii) For all $k = 1, \dots, d$ there exist $j_k \in \{1, \dots, n\}$ and $\alpha_k \geq 0$ such that $\alpha_k x_{j_k} = e_k$.

Proof of Lemma B.1: We first observe that i) holds if and only if for all $y \in [0, \infty)^d$ there exist $\lambda_1, \dots, \lambda_n \geq 0$ such that $y = \lambda_1 x_1 + \dots + \lambda_n x_n$. Since for $y \in [0, \infty)^d$ there also exist $\mu_1, \dots, \mu_d \geq 0$ with $y = \mu_1 e_1 + \dots + \mu_d e_d$, we conclude that i) holds if and only if the following condition is satisfied:

EC) For all $k = 1, \dots, d$ there exist $\alpha_{k,1}, \dots, \alpha_{k,n} \geq 0$ with $e_k = \alpha_{k,1} x_1 + \dots + \alpha_{k,n} x_n$.

ii) \Rightarrow i). Clearly, ii) implies Condition **EC)**, and this implies i) as previously discussed.

i) \Rightarrow ii). It suffices to show that **EC)** implies ii). To this end, we denote the l -th coordinate of x_j by $x_{j,l}$, that is $x_j = (x_{j,1}, \dots, x_{j,d})$. Moreover, we fix a $k \in \{1, \dots, d\}$ and by **EC)** we choose $\alpha_{k,1}, \dots, \alpha_{k,n} \geq 0$ such that

$$e_k = \alpha_{k,1} x_1 + \dots + \alpha_{k,n} x_n. \quad (\text{B.51})$$

Considering (B.51) for the l -th coordinate with $l \neq k$ then gives

$$0 = \sum_{j=1}^n \alpha_{k,j} x_{j,l}. \quad (\text{B.52})$$

Now, our assumptions guarantee $\alpha_{k,j} x_{j,l} \geq 0$, and hence (B.52) implies $\alpha_{k,j} = 0$ for all $j \in \{1, \dots, n\}$ with $x_{j,l} > 0$. Consequently, in the k -th coordinate, (B.51) reduces to

$$1 = \sum_{j \in J} \alpha_{k,j} x_{j,k},$$

where $J := \{j : x_{j,l} = 0 \text{ for all } l \neq k\}$. However, this equation implies that there is a $j \in J$ with $\alpha_{k,j} x_{j,k} > 0$. The choice $\alpha_k := x_{j,k}^{-1}$ then yields $\alpha_k x_{j_k} = e_k$. \square

The conic hull of an $A \subset \mathbb{R}^d$ is the smallest convex cone containing A . If one is only interested in the smallest cone containing A , one needs to consider the ray of A , which is

$$\text{ray } A := \{tx : x \in A, t > 0\}.$$

The next simple lemma, which is needed for Lemma D.5, shows that $\text{ray } A$ is measurable if $A \subset \mathbb{S}^{d-1}$ is measurable.

Lemma B.2. Let $A \subset \mathbb{S}^{d-1}$ be measurable. Then $\text{ray } A$ is also measurable.

Proof of Lemma B.2: We define $\phi : (0, \infty) \times \mathbb{R}^d \setminus \{0\} \rightarrow \mathbb{R}^d$ by $\phi(t, x) := tx$. Then the pre-image of A under ϕ is given by

$$\phi^{-1}(A) := \{(\|x\|_2^{-1}, x) : x \in \text{ray } A\}. \quad (\text{B.53})$$

Indeed, if we have an $(t, x) \in \phi^{-1}(A)$, then $tx = \phi(t, x) \in A$ implies both $x \in t^{-1}A \subset \text{ray } A$ and $\|tx\| = 1$. This shows the inclusion “ \subset ”. Conversely, if $x \in \text{ray } A$, then there exist $t > 0$ and $y \in A$ with $x = ty$. This implies $t^{-1}\|x\|_2 = \|y\|_2 = 1$, and hence $t = \|x\|_2$. The latter gives $\|x\|_2^{-1} \cdot x = y \in A$.

Let us now consider the map $\psi : \mathbb{R}^d \setminus \{0\} \rightarrow (0, \infty) \times \mathbb{R}^d \setminus \{0\}$ defined by $\psi(x) := (\|x\|_2^{-1}, x)$. Clearly, ψ injective, and therefore (B.53) yields $\psi^{-1}(\phi^{-1}(A)) = \text{ray } A$. Now the measurability of A , ϕ , and ψ shows that $\text{ray } A$ is measurable. \square

Lemma B.3. For all $A, B \subset \mathbb{S}^{d-1}$ the following statements are true:

- i) If $A \cap B = \emptyset$, then $\text{ray } A \cap \text{ray } B = \emptyset$.
- ii) We have $\text{ray}(A \cup B) = \text{ray } A \cup \text{ray } B$.

Proof of Lemma B.3: i). Let us assume that there is a $z \in \text{ray } A \cap \text{ray } B$. Then we find some $x \in A$, $y \in B$, $s, t > 0$ such that $z = sx$ and $z = ty$. This implies $\|z\|_2 = |s| \cdot \|x\|_2 = s$ and $\|z\|_2 = |t| \cdot \|y\|_2 = t$, and consequently, we find $x = s^{-1}z = s^{-1}ty = y$. In other words, we have $x \in A \cap B$.

ii). The inclusion “ \subset ” is essentially trivial, and the converse inclusion follows from $A \subset A \cup B$ and the monotonicity of $\text{ray}(\cdot)$. \square

C Appendix: Some function classes

Definition C.1. A function $f : \mathbb{R}^d \rightarrow \mathbb{R}^m$ is called *positively homogeneous*, if for all $\alpha > 0$ and all $x \in \mathbb{R}^d$ we have

$$f(\alpha x) = \alpha f(x).$$

Obviously, every linear function $f : \mathbb{R}^d \rightarrow \mathbb{R}^m$ is positively homogeneous. Moreover, every norm $\|\cdot\| : \mathbb{R}^d \rightarrow \mathbb{R}$ is positively homogeneous, and $|\cdot|_+ : \mathbb{R} \rightarrow \mathbb{R}$ is also positively homogeneous. Combining these examples with the help of the following trivial lemma gives a wealth of positively homogeneous functions.

Lemma C.2. Let $f, g : \mathbb{R}^d \rightarrow \mathbb{R}^m$, $h : \mathbb{R}^m \rightarrow \mathbb{R}^k$, and $f_1, \dots, f_m : \mathbb{R}^d \rightarrow \mathbb{R}$ be positively homogeneous functions and $\lambda \in \mathbb{R}$. Then the following functions are also positively homogeneous:

$$\begin{aligned} \lambda f + g &: \mathbb{R}^d \rightarrow \mathbb{R}^m \\ h \circ f &: \mathbb{R}^m \rightarrow \mathbb{R}^k \\ (f_1, \dots, f_m) &: \mathbb{R}^d \rightarrow \mathbb{R}^m. \end{aligned}$$

The next simple lemma shows that positively homogeneous functions vanish at the origin.

Lemma C.3. Let $f : \mathbb{R}^d \rightarrow \mathbb{R}^m$ be a positively homogeneous function. Then we have $f(0) = 0$.

Proof of Lemma C.3: For $x = 0$ and $\alpha = 2$ we have $f(0) = f(2x) = 2f(x) = 2f(0)$. This implies $f(0) = 0$. \square

In the following, we denote the set of positively homogeneous, \mathbb{R} -valued functions $f : \mathbb{R}^d \rightarrow \mathbb{R}$ by $\mathcal{PH}(\mathbb{R}^d)$. Moreover, for a subset $X \subset \mathbb{R}^d$ we define

$$\mathcal{PH}(X) := \{f : X \rightarrow \mathbb{R} \mid \exists g \in \mathcal{PH}(\mathbb{R}^d) \text{ such that } g|_X = f\}.$$

The next result will be used to show that $\mathcal{PH}(X)$ is a closed subset of some commonly considered spaces.

Lemma C.4. Let $X \subset \mathbb{R}^d$ be subset and $(f_n) \subset \mathcal{PH}(X)$ be a sequence such that there exists a function $f : X \rightarrow \mathbb{R}$ with

$$f(x) = \lim_{n \rightarrow \infty} f_n(x)$$

for all $x \in X$. Then we have $f \in \mathcal{PH}(X)$.

Proof of Lemma C.4: Let us pick $g_n \in \mathcal{PH}(\mathbb{R}^d)$ such that $(g_n)|_X = f_n$ for all $n \geq 1$. For $y \in \text{ray } X$ we then find some $t > 0$ and $x \in X$ with $y = tx$. This gives

$$g_n(y) = tg_n(x) = tf_n(x) \rightarrow tf(x).$$

Since this holds for all possible such representations $y = tx$, while the limit $\lim_{n \rightarrow \infty} g_n(y)$ is unique, we conclude that setting $g(y) := tf(x)$ is actually independent of the chosen representation $y = tx$ of y . Now, this definition ensures $g_n(y) \rightarrow g(y)$ for all $y \in \text{ray } X$. For $y \in \text{ray } X$ and $\alpha > 0$ we thus have

$$g(\alpha y) = \lim_{n \rightarrow \infty} g_n(\alpha y) = \alpha \lim_{n \rightarrow \infty} g_n(y) = \alpha g(y).$$

Let us define $g(y) := 0$ for all $y \notin \text{ray } X$. Since for such y we have $g(\alpha y) = 0 = \alpha g(y)$ for all $\alpha > 0$, we then see that g is positively homogeneous. Moreover, for $x \in X$ we have

$$g(x) = \lim_{n \rightarrow \infty} g_n(x) = \lim_{n \rightarrow \infty} f_n(x) = f(x),$$

and thus we find $g|_X = f$. This gives $f \in \mathcal{PH}(X)$. □

Corollary C.5. *Let $X \subset \mathbb{R}^d$ be a compact subset. Then $\mathcal{PH}(X) \cap C(X)$ is a closed subspace of $C(X)$.*

Proof of Corollary C.5: Let us fix a sequence $(f_n) \subset \mathcal{PH}(X) \cap C(X)$ and an $f \in C(X)$ with $\|f_n - f\|_\infty \rightarrow 0$. Then Lemma C.4 shows $f \in \mathcal{PH}(X)$ and hence we have $f \in \mathcal{PH}(X) \cap C(X)$. □

Corollary C.6. *Let P be a probability measure on \mathbb{R}^d . Then, for all $p \in [1, \infty)$, the space $\mathcal{PH}(\mathbb{R}^d) \cap L_p(P)$ is a closed subspace of $L_p(P)$.*

Proof of Corollary C.6: Let us fix a sequence $(f_n) \subset \mathcal{PH}(\mathbb{R}^d) \cap L_p(P)$ and an $f \in L_p(P)$ with $\|f_n - f\|_{L_p(P)} \rightarrow 0$. By considering a subsequence we may assume without loss of generality that there exists a measurable $N \subset \mathbb{R}^d$ with $P(N) = 0$ and $f_n(x) \rightarrow f(x)$ for all $x \in X := \mathbb{R}^d \setminus N$. Lemma C.4 then shows $f|_X \in \mathcal{PH}(X)$, and thus we can pick a $g \in \mathcal{PH}(\mathbb{R}^d)$ with $g|_X = f|_X$. Since $P(X) = 1$ we conclude both $\|f_n - g\|_{L_p(P)} \rightarrow 0$ and $g \in L_p(P)$. □

D Appendix: Some specific distributions

Recall, that for $a \in \mathbb{R}$ the incomplete gamma function is defined by

$$\Gamma(a, x) := \int_x^\infty e^{-t} t^{a-1} dt, \quad x \geq 0.$$

Note that $\Gamma(a, x) < \infty$ for all $x > 0$, and for $a > 0$ the gamma function $\Gamma(a) := \Gamma(a, 0)$ is also finite. Our first result provides bounds on certain ratios of the gamma function.

Lemma D.1. *For all $d \geq 1$ we have*

$$\sqrt{d-1/2} \leq \frac{\sqrt{2} \cdot \Gamma(\frac{d+1}{2})}{\Gamma(\frac{d}{2})} \leq \sqrt{d-1/4}.$$

Proof of Lemma D.1: We first note that in [10] the following refinement of Gautschi's inequality, see [6], has been established:

$$\sqrt{x+1/4} \leq \frac{\Gamma(x+1)}{\Gamma(x+1/2)} \leq \sqrt{x + \frac{\sqrt{3}-1}{2}}, \quad x > 0.$$

Moreover, using $\Gamma(1) = 1$ and $\Gamma(1/2) = \sqrt{\pi}$ one easily checks that this inequality also holds for $x = 0$. Considering $x := d/2 - 1/2$ and using $\sqrt{3}-2 \leq -1/4$ for the upper bound then gives the assertion. \square

The gamma function can also be approximated by a generalization of Stirling's formula. Namely we have

$$\Gamma(a) = \sqrt{\frac{2\pi}{a}} \cdot \left(\frac{a}{e}\right)^a \cdot e^{\mu(a)}, \quad (\text{D.54})$$

where $0 < \mu(a) < \frac{1}{12a}$. It is also well-known that for fixed $a > 0$ and $x \geq a$ the incomplete gamma function satisfies

$$\min\{1, a\}x^{a-1}e^{-x} \leq \Gamma(a, x) \leq \max\{1, a\}x^{a-1}e^{-x},$$

see e.g. [15, Lemma A.1.1]. Note that for $a > 1$, $\delta > 0$, and $x = (1 + \delta)a$, the upper bounds reads as

$$\Gamma(a, (1 + \delta)a) \leq a^a(1 + \delta)^{a-1}e^{-(1+\delta)a}. \quad (\text{D.55})$$

The following lemma presents an alternative upper bound on $\Gamma(a, x)$, which improves the last inequality. In [1], it is attributed to [14], but since the latter article is difficult to obtain, we present the short proof for the sake of completeness.

Lemma D.2. *For all $a > 1$ and $x > a - 1$ we have*

$$\Gamma(a, x) \leq \frac{x}{x - a + 1} \cdot x^{a-1} e^{-x}.$$

Proof of Lemma D.2: We define $B := \frac{x}{x-a+1}$. A simple calculation then shows $a - 1 = \frac{B-1}{B}x$, and by integration by parts we find

$$\begin{aligned} \Gamma(a, x) &= \int_x^\infty e^{-t}t^{a-1} dt = -e^{-t}t^{a-1}\Big|_x^\infty + (a-1) \int_x^\infty e^{-t}t^{a-2} dt = x^{a-1}e^{-x} + \frac{B-1}{B}x \int_x^\infty e^{-t}t^{a-2} dt \\ &\leq x^{a-1}e^{-x} + \frac{B-1}{B} \cdot \Gamma(a, x), \end{aligned}$$

Now the assertion follows by a simple transformation. \square

To appreciate Lemma D.2 we apply it to $a > 1$, $\delta > 0$, and $x = (1 + \delta)a$. This gives

$$\Gamma(a, (1 + \delta)a) \leq \frac{1 + \delta}{1 + a\delta} \cdot a^a(1 + \delta)^{a-1}e^{-(1+\delta)a}. \quad (\text{D.56})$$

In other words, compared to (D.55) the new bound is better by the factor of $\frac{1+\delta}{1+a\delta}$, and for cases with $\delta \rightarrow 0$ and $a\delta \rightarrow \infty$ this extra factor changes the asymptotics.

Lemma D.3. *Let X_1, \dots, X_d be i.i.d. random variables with $X_i \sim \mathcal{N}(0, \sigma^2)$ for some $\sigma > 0$. For $X := (X_1, \dots, X_d) \in \mathbb{R}^d$ we then have*

$$\mathbb{E}\|X\|_2 = \sigma \cdot \frac{\sqrt{2} \cdot \Gamma(\frac{d+1}{2})}{\Gamma(\frac{d}{2})}, \quad \text{Var}\|X\|_2 = d\sigma^2 - \sigma^2 \cdot \left(\frac{\sqrt{2} \cdot \Gamma(\frac{d+1}{2})}{\Gamma(\frac{d}{2})}\right)^2.$$

Moreover, the mode is given by $\text{mode } \|X\|_2 = \sigma\sqrt{d-1}$ and the density of the distribution of $\|X\|_2$ is

$$f(x) = \mathbf{1}_{[0,\infty)}(x) \cdot \frac{2^{1-d/2}}{\Gamma(\frac{d}{2})} \cdot \sigma^{-d} \cdot x^{d-1} e^{-\sigma^{-2}x^2/2}, \quad z \in \mathbb{R}. \quad (\text{D.57})$$

Finally, for all $s > 0$ we have

$$P(\|X\|_2 \geq s) = \frac{\Gamma(\frac{d}{2}, \frac{s^2}{2\sigma^2})}{\Gamma(\frac{d}{2})}. \quad (\text{D.58})$$

Proof of Lemma D.3: Let us consider $Y_i := \sigma^{-1}X_i$ and $Y := (Y_1, \dots, Y_d)$. Then $Z := \|Y\|_2$ is χ_d -distributed, and it is well-known that

$$\mathbb{E}Z = \frac{\sqrt{2} \cdot \Gamma(\frac{d+1}{2})}{\Gamma(\frac{d}{2})}, \quad \text{mode } Z = \sqrt{d-1}, \quad \text{Var } Z = d - 2 \cdot \left(\frac{\Gamma(\frac{d+1}{2})}{\Gamma(\frac{d}{2})} \right)^2,$$

where the latter can also be easily derived using the formula for $\mathbb{E}Z$ and the fact $Z^2 \sim \chi_d^2$, and thus $\mathbb{E}Z^2 = d$. Moreover, the distribution of Z has the Lebesgue density

$$f_Z(z) = \mathbf{1}_{[0,\infty)}(z) \cdot \frac{2^{1-d/2}}{\Gamma(\frac{d}{2})} \cdot z^{d-1} e^{-z^2/2}, \quad z \in \mathbb{R}.$$

Now, (D.57) easily follows from $\|X\|_2 = \sigma Z$ and $f(x) = |\sigma|^{-1} f_Z(x/\sigma)$ for $x \in \mathbb{R}$. For the proof of (D.58) we first note that (D.57) yields

$$P(\|X\|_2 \geq s) = \int_s^\infty f(x) dx = \frac{2^{1-d/2}}{\Gamma(\frac{d}{2})} \cdot \sigma^{-d} \cdot \int_s^\infty x^{d-1} e^{-\sigma^{-2}x^2/2} dx.$$

Moreover, by the substitution $t := \varphi(x) := \frac{x^2}{2\sigma^2}$ we obtain

$$\int_s^\infty x^{d-1} e^{-\sigma^{-2}x^2/2} dx = 2^{d/2-1} \cdot \sigma^d \cdot \int_s^\infty (\varphi(x))^{d/2-1} e^{-\varphi(x)} \varphi'(x) dx = 2^{d/2-1} \cdot \sigma^d \cdot \int_{\varphi(s)}^\infty t^{d/2-1} e^{-t} dt,$$

and combining both equations gives (D.58). \square

The next lemma, which will be needed to compute the directions of randomly initialized weight vectors, is a classical result from multi-dimensional calculus, see e.g. [5, Satz 14.8].

Lemma D.4. *Let \mathbb{S}^{d-1} be the Euclidean sphere in \mathbb{R}^d and σ^{d-1} be the surface measure on \mathbb{S}^{d-1} . For all Lebesgue integrable functions $f : \mathbb{R}^d \rightarrow [0, \infty)$ we then have*

$$\int_{\mathbb{R}^d} f d\lambda^d = \int_{\mathbb{S}^{d-1}} \int_0^\infty f(r\xi) r^{d-1} dr d\sigma^{d-1}(\xi).$$

For the following theorem recall that we have seen in Lemma B.2 that ray A is measurable for all measurable $A \subset \mathbb{S}^{d-1}$.

Theorem D.5. *Let $f : \mathbb{R}^d \rightarrow [0, \infty)$ be a Lebesgue probability density. On \mathbb{S}^{d-1} we define*

$$\mu_f(A) := \int_{\text{ray } A} f d\lambda^d,$$

for all measurable $A \subset \mathbb{S}^{d-1}$. Then the following statements hold true:

i) μ_f is a probability measure.

ii) The measure μ_f is absolutely continuous with respect to the surface measure σ^{d-1} on \mathbb{S}^{d-1} . Moreover, the σ^{d-1} -density h of μ_f is σ^{d-1} -almost surely given by

$$h(\xi) = \int_0^\infty f(r\xi) r^{d-1} dr, \quad \xi \in \mathbb{S}^{d-1}.$$

Proof of Theorem D.5: i). This immediately follows from Lemma B.3 and $\text{ray } \mathbb{S}^{d-1} = \mathbb{R}^d \setminus \{0\}$.

ii). Using Lemma D.4 we see that the measure μ_f can be evaluated by

$$\begin{aligned} \mu_f(A) &= \int_{\mathbb{R}^d} \mathbf{1}_{\text{ray } A} \cdot f d\lambda^d \\ &= \int_{\mathbb{S}^{d-1}} \int_0^\infty \mathbf{1}_{\text{ray } A}(r\xi) \cdot f(r\xi) r^{d-1} dr d\sigma^{d-1}(\xi) \\ &= \int_{\mathbb{S}^{d-1}} \mathbf{1}_A(\xi) \cdot \int_0^\infty f(r\xi) r^{d-1} dr d\sigma^{d-1}(\xi) \\ &= \int_A h(\xi) d\sigma^{d-1}(\xi) \end{aligned}$$

where in the second to last step we used $\mathbf{1}_{\text{ray } A}(r\xi) = \mathbf{1}_A(\xi)$ for all $\xi \in \mathbb{S}^{d-1}$ and all $r > 0$. \square

Let us now recall some facts about sub-Gaussian random variables. To this end, we denote, for a given a random variable X , its sub-Gaussian norm by $\|X\|_{\Psi_2}$, that is

$$\|X\|_{\Psi_2} := \inf \left\{ t > 0 : \mathbb{E} \exp(X^2/t^2) \leq 2 \right\}.$$

We say that X is sub-Gaussian if $\|X\|_{\Psi_2} < \infty$. Some simple properties of $\|\cdot\|_{\Psi_2}$ and characterizations of sub-Gaussian random variables can be found in [16, Chapter 2.5]. In particular recall from there that $\|X\|_{\Psi_2} \leq \frac{1}{\sqrt{\ln 2}} \|X\|_\infty$ for all bounded X . In addition, we have $\|\alpha X\|_{\Psi_2} = |\alpha| \cdot \|X\|_{\Psi_2}$ whenever $\|X\|_{\Psi_2} < \infty$. Finally, since the moment generating function of a $Z \sim \chi_1^2$ is

$$\mathbb{E} e^{tZ} = \frac{1}{\sqrt{1-2t}}, \quad t \in [0, 1/2),$$

it is easy to check that $\|X\|_{\Psi_2} = \sqrt{8/3}$ for $X \sim \mathcal{N}(0, 1)$.

Now, [16, Theorem 3.1.1], or more precisely, Inequality (3.3) in its proof, provides the following concentration of the Euclidean norm. Note that some tedious calculations along the lines of its proof will actually provide a value for the universal constant in this estimate.

Theorem D.6. *There exists a universal constant $K > 0$ such that for all $d \geq 1$, all i.i.d. random variables X_1, \dots, X_d with $c_X := \max\{1, \|X_1\|_{\Psi_2}\} < \infty$ and $\mathbb{E}X_1^2 = 1$, and all $t > 0$ the random vector $X = (X_1, \dots, X_d)$ satisfies*

$$P\left(\left| \|X\|_2 - \sqrt{d} \right| \geq t\right) \leq 2 \exp\left(-\frac{Kt^2}{c_X^4}\right).$$

Lemma D.7. *Let Y be a symmetric random variable. Then we have $2\mathbb{E}|Y|_+^2 = \mathbb{E}Y^2$.*

Proof of Lemma D.7: Let P_Y be the distribution of Y . Then a simple calculation shows

$$\mathbb{E}|Y|_+^2 = \int_{\mathbb{R}} |y|_+^2 dP_Y(y) = \int_{(0,\infty)} y^2 dP_Y(y).$$

Moreover, an analogous calculation shows

$$\mathbb{E}Y^2 = \int_{\mathbb{R}} y^2 dP_Y(y) = \int_{(-\infty,0)} y^2 dP_Y(y) + \int_{(0,\infty)} y^2 dP_Y(y) = \int_{(0,\infty)} y^2 dP_Y(y) + \int_{(0,\infty)} y^2 dP_Y(y),$$

where in the last step we used the symmetry of P_Y . By combining both equations we obtain the assertion. \square

	Size	Dimension	Naive Error
air-quality-bc	8991	10	.23426
air-quality-co2	7674	10	.24630
air-quality-no2	7715	10	.28620
air-quality-nox	7718	10	.28838
appliances-energy	19735	29	.19163
beijing-pm25	41757	12	.18521
bike-sharing-casual	17379	12	.26868
bike-sharing-total	17379	12	.37169
carbon-nanotubes-u	10721	5	.63039
carbon-nanotubes-v	10721	5	.63114
carbon-nanotubes-w	10721	5	.57816
chess-krvk	28056	22	4.63674
cycle-power-plant	9568	4	.45208
facebook-comment-volume	40949	52	.05440
five-cities-beijing-pm25	19062	14	.24504
five-cities-chengdu-pm25	21074	14	.19888
five-cities-guangzhou-pm25	20074	14	.16495
five-cities-shanghai-pm25	21436	14	.16315
five-cities-shenyang-pm25	19038	14	.13064
gas-sensor-drift-class	13910	128	1.72854
gas-sensor-drift-conc	13910	128	.34322
indoor-loc-alt	21048	520	.60629
indoor-loc-lat	21048	520	.49678
indoor-loc-long	21048	520	.62644
insurance-benchmark	9822	85	.23686
naval-propulsion-comp	11934	14	.58878
naval-propulsion-turb	11934	14	.60000
nursery	12960	8	1.23560
online-news-popularity	39644	58	.02757
parkinson-motor	5875	19	.47159
parkinson-total	5875	19	.44588
protein-tertiary-structure	45730	9	.58272
skill-craft	3338	18	1.44795
sml2010-dining	4137	17	.37693
sml2010-room	4137	17	.37896
wall-follow-robot-2	5456	2	1.00466
wall-follow-robot-24	5456	24	1.00466
wall-follow-robot-4	5456	4	1.00466
wine-quality-all	6497	12	.87319
wine-quality-white	4898	11	.88555

Table 2: Characteristics of the regression data sets. The naive error is the standard deviation of the labels. Note that this equals the root mean square error one obtains when predicting all labels by the label mean.

	Size	Dimension	Naive Error
abalone	2870	8	.46760
adult	45222	88	.24784
anuran-calls-families	6585	22	.32878
anuran-calls-genus	5743	22	.27738
anuran-calls-species	4599	22	.24375
avila	12495	10	.31397
bank-marketing	41579	29	.11407
bank-marketing-additional	39457	34	.11124
chess	3196	36	.47778
chess-krvk	8747	22	.47948
crowd-sourced-mapping	9003	28	.16594
default-credit-card	30000	23	.22120
eeg-eye-state	14980	14	.44880
epileptic-seizure-recognition	4600	178	.50000
firm-teacher-clave	8606	16	.49965
first-order-theorem-proving	6118	51	.41746
gas-sensor-drift-class	5935	128	.49301
gesture-phase-segmentation-raw	5719	19	.48418
gesture-phase-segmentation-va3	5691	32	.48164
htru2	17898	8	.09157
human-activity-smartphone	3850	561	.49506
indoor-loc-building	15545	520	.37215
indoor-loc-relative	19937	520	.16698
insurance-benchmark	9822	85	.05966
landsat-satimage	3041	36	.49589
madelon	2600	500	.50000
magic-gamma-telescope	19020	10	.35163
mushroom	8124	111	.48203
musk	6598	166	.15414
nomao	34465	120	.28562
nursery	8588	8	.49674
occupancy-detection	20560	7	.23103
page-blocks	5242	10	.06276
pishing	11055	30	.44306
polish-companies-bankruptcy-1year	7027	64	.03857
polish-companies-bankruptcy-2year	10173	64	.03932
polish-companies-bankruptcy-3year	10503	64	.04713
polish-companies-bankruptcy-4year	9792	64	.05259
polish-companies-bankruptcy-5year	5910	64	.06937
seismic-bumps	2584	15	.06579
smartphone-human-activity-postural	3937	561	.49733
spambase	4601	57	.39404
thyroid-all-bp	3621	31	.04336
thyroid-all-hyper	3621	31	.02624
thyroid-all-hypo	3528	31	.05300
thyroid-all-rep	3621	31	.03314
thyroid-ann	7034	21	.05232
thyroid-dis	3621	31	.01547
thyroid-hypo	2700	25	.05037
thyroid-sick	3621	31	.06214
thyroid-sick-eu	3163	26	.09263
turkiye-student-evaluation	5045	32	.28622
wall-follow-robot-2	4302	2	.48745
wall-follow-robot-24	4302	24	.48745
wall-follow-robot-4	4302	4	.48745
waveform	3353	21	.49418
waveform-noise	3347	40	.49447
wilt	4839	5	.05394
wine-quality-all	4974	12	.42984
wine-quality-type	6497	11	.24611
wine-quality-white	3655	11	.39863

Table 3: Characteristics of the classification data sets. The naive error is the classification error one obtains when predicting all labels by the most frequent label in the data set.

	ReLU BN He zero	ReLU He zero	ReLU sphere hull -5	SeLU SNN zero	SeLU ball hull -5
air-quality-bc	.02530 ± .00292	.01196 ± .00180	.00440 ± .00145	.01194 ± .00147	.00500 ± .00237
air-quality-co2	.08348 ± .00397	.08002 ± .00367	.07965 ± .00344	.08288 ± .00379	.08301 ± .00382
air-quality-no2	.11367 ± .00402	.10787 ± .00335	.10280 ± .00428	.11682 ± .00413	.11251 ± .00483
air-quality-nox	.09470 ± .00494	.09003 ± .00510	.08819 ± .00520	.09709 ± .00517	.09496 ± .00656
appliances-energy	.16003 ± .00480	.15697 ± .00521	.15340 ± .00503	.15975 ± .00544	.15571 ± .00500
beijing-pm25	.08911 ± .00494	.08247 ± .00287	.07907 ± .00212	.08960 ± .00507	.08452 ± .00507
bike-sharing-casual	.08728 ± .00277	.08206 ± .00272	.07928 ± .00277	.09032 ± .00352	.08406 ± .00393
bike-sharing-total	.11556 ± .00437	.08749 ± .00333	.08482 ± .00336	.09592 ± .00428	.09043 ± .00417
carbon-nanotubes-u	.02898 ± .00304	.00870 ± .00066	.00698 ± .00032	.01480 ± .00122	.00790 ± .00090
carbon-nanotubes-v	.02865 ± .00274	.00882 ± .00075	.00684 ± .00028	.01469 ± .00110	.00774 ± .00081
carbon-nanotubes-w	.04039 ± .00588	.02767 ± .00784	.02653 ± .00826	.03153 ± .00682	.02719 ± .00817
chess-krvk	.86500 ± .06194	.64335 ± .05549	.65755 ± .07172	.61139 ± .04152	.60320 ± .05796
cycle-power-plant	.10698 ± .00347	.10796 ± .00309	.10231 ± .00280	.10844 ± .00314	.10641 ± .00322
facebook-comment-volume	.04380 ± .00522	.03969 ± .00407	.03960 ± .00439	.03931 ± .00442	.03876 ± .00410
five-cities-beijing-pm25	.12805 ± .00451	.11656 ± .00528	.10534 ± .00414	.12682 ± .00711	.11904 ± .00930
five-cities-chengdu-pm25	.09419 ± .00327	.08413 ± .00437	.07236 ± .00258	.09695 ± .00462	.08745 ± .00785
five-cities-guangzhou-pm25	.10083 ± .00378	.09168 ± .00420	.08352 ± .00315	.10180 ± .00513	.09401 ± .00557
five-cities-shanghai-pm25	.08837 ± .00492	.08078 ± .00471	.07116 ± .00309	.10006 ± .00758	.08700 ± .00969
five-cities-shenyang-pm25	.08365 ± .00389	.08042 ± .00423	.07186 ± .00409	.09358 ± .00535	.08494 ± .00562
gas-sensor-drift-class	.30161 ± .03595	.26132 ± .01914	.25606 ± .02185	.26386 ± .02746	.22851 ± .02435
gas-sensor-drift-conc	.06566 ± .00671	.06371 ± .00727	.06101 ± .00763	.06929 ± .00789	.06206 ± .00793
indoor-loc-alt	.10042 ± .00448	.11511 ± .00469	.11593 ± .00454	.12702 ± .00482	.11949 ± .00606
indoor-loc-lat	.05177 ± .00307	.05622 ± .00237	.05638 ± .00249	.06228 ± .00251	.05837 ± .00280
indoor-loc-long	.04911 ± .00268	.05376 ± .00248	.05392 ± .00257	.06013 ± .00208	.05619 ± .00341
insurance-benchmark	.24313 ± .00383	.23266 ± .00169	.23282 ± .00185	.23248 ± .00178	.23311 ± .00210
naval-propulsion-comp	.03547 ± .00415	.01820 ± .00267	.01282 ± .00125	.02112 ± .00281	.01733 ± .00318
naval-propulsion-turb	.05278 ± .00651	.02964 ± .00338	.02085 ± .00213	.03209 ± .00485	.02602 ± .00545
nursery	.14147 ± .00881	.14218 ± .00607	.13022 ± .00639	.14373 ± .00797	.12493 ± .00959
online-news-popularity	.02950 ± .00528	.02838 ± .00559	.02758 ± .00582	.02748 ± .00585	.02753 ± .00587
parkinson-motor	.22291 ± .01097	.19748 ± .01999	.17068 ± .00970	.21589 ± .02503	.19149 ± .01818
parkinson-total	.21398 ± .00892	.18817 ± .01803	.16559 ± .01358	.20614 ± .02277	.18171 ± .02464
protein-tertiary-structure	.34592 ± .00509	.36797 ± .00410	.36324 ± .00378	.37246 ± .00565	.36773 ± .00682
skill-craft	1.0793 ± .03394	.98190 ± .02792	.96239 ± .02505	.96871 ± .02526	.96336 ± .02762
sml2010-dining	.05634 ± .00463	.03843 ± .00348	.02596 ± .00254	.05654 ± .00346	.03899 ± .00968
sml2010-room	.05644 ± .00487	.03822 ± .00315	.02560 ± .00268	.05613 ± .00400	.03938 ± .00869
wall-follow-robot-2	.24423 ± .01781	.28668 ± .02252	.13948 ± .01446	.30612 ± .01957	.15895 ± .01872
wall-follow-robot-24	.46616 ± .02051	.45095 ± .01833	.42010 ± .01924	.46025 ± .02151	.42825 ± .02262
wall-follow-robot-4	.29135 ± .02797	.33636 ± .02852	.20635 ± .01813	.32603 ± .02370	.20907 ± .02429
wine-quality-all	.69474 ± .01304	.69292 ± .01101	.68479 ± .01074	.70403 ± .01195	.69209 ± .01074
wine-quality-white	.70564 ± .01742	.72052 ± .01344	.69593 ± .01238	.72320 ± .02031	.70725 ± .01243
Average raw rank	4.0000	2.8500	1.4500	4.1500	2.5500
Average adjusted rank	4.0000	2.8250	1.4500	4.1625	2.5625
Fraction adjusted best runs	.1000	.0250	.7500	.0500	.1000
Fraction adjusted worst runs	.5000	.0250	.0000	.4750	.0000
Aver. rel. perform.	1.5582	1.1975	1.0168	1.3395	1.1087
90 percent av. rel. perform.	1.2688	1.1123	1.0058	1.2319	1.0754
Worst rel. perform.	5.6457	2.6813	1.1543	2.6769	1.5360
90 percentile rel. perform.	2.6389	1.4847	1.0895	2.1522	1.2345
80 percentile rel. perform.	1.6353	1.2642	1.0126	1.5581	1.1629
70 percentile rel. perform.	1.3409	1.1448	1.0000	1.2833	1.1305

Table 4: Comparison of all considered methods on the regression data sets. The numbers in the upper part of the table are the average root mean squared test errors the corresponding standard deviations. Red and orange entries indicate the best-performing method for each data set, where red entries indicate those methods that are significantly better than the second best method according to a paired two-sample t -test with a significance level of 95%. Similarly, blue and green entries indicate the worst-performing method, and blue entries indicate those methods that are significantly worse than the best method according to a paired two-sample t -test with with a significance level of 95%.

	ReLU BN He zero	ReLU He zero	ReLU He hull -5	ReLU ball hull +5	SeLU SNN zero	SeLU ball hull -5
abalone	.19530 ± .02380	.19628 ± .01635	.18828 ± .01255	.18963 ± .01213	.19743 ± .01377	.19012 ± .01211
adult	.15258 ± .00406	.15405 ± .00345	.15461 ± .00345	.15337 ± .00399	.14984 ± .00383	.15054 ± .00338
anuran-calls-families	.00714 ± .00239	.00949 ± .00254	.00876 ± .00254	.00960 ± .00234	.01034 ± .00294	.01016 ± .00359
anuran-calls-genus	.00230 ± .00137	.00251 ± .00135	.00249 ± .00128	.00270 ± .00155	.00320 ± .00159	.00306 ± .00147
anuran-calls-species	.00143 ± .00117	.00126 ± .00138	.00128 ± .00100	.00148 ± .00127	.00141 ± .00119	.00117 ± .00107
avila	.21498 ± .03992	.14942 ± .02356	.08478 ± .01887	.10157 ± .01682	.14361 ± .02613	.07778 ± .03048
bank-marketing	.09800 ± .00262	.09662 ± .00271	.09647 ± .00260	.09576 ± .00241	.09443 ± .00266	.09513 ± .00272
bank-marketing-additional	.09278 ± .00300	.09293 ± .00290	.09190 ± .00292	.09118 ± .00263	.09005 ± .00278	.09040 ± .00270
chess	.00850 ± .00478	.01128 ± .00543	.01044 ± .00462	.01116 ± .00526	.01109 ± .00488	.01053 ± .00550
chess-krvk	.12936 ± .01610	.12726 ± .01502	.12375 ± .01179	.12745 ± .00999	.10803 ± .01281	.11160 ± .01219
crowd-sourced-mapping	.01552 ± .00222	.01949 ± .00313	.01984 ± .00295	.01986 ± .00262	.02107 ± .00314	.02131 ± .00321
default-credit-card	.18356 ± .00478	.17971 ± .00428	.18096 ± .00410	.18011 ± .00449	.17968 ± .00420	.18045 ± .00446
eeg-eye-state	.42543 ± .01986	.43007 ± .00874	.34647 ± .03366	.34489 ± .03762	.42316 ± .00948	.31452 ± .04123
epileptic-seizure-recognition	.05085 ± .00862	.04407 ± .00728	.04198 ± .00765	.04304 ± .00595	.05459 ± .00775	.05409 ± .00824
firm-teacher-clave	.02111 ± .00371	.02110 ± .00301	.02179 ± .00388	.02046 ± .00342	.02059 ± .00370	.02029 ± .00322
first-order-theorem-proving	.20655 ± .01246	.21915 ± .01241	.20946 ± .01355	.20902 ± .01192	.22261 ± .01286	.21559 ± .01108
gas-sensor-drift-class	.00146 ± .00110	.00261 ± .00135	.00229 ± .00124	.00236 ± .00148	.00251 ± .00148	.00224 ± .00132
gesture-phase-segmentation-raw	.00470 ± .00213	.00514 ± .00192	.00531 ± .00213	.00540 ± .00230	.00628 ± .00233	.00666 ± .00227
gesture-phase-segmentation-va3	.15788 ± .01175	.17166 ± .01173	.15120 ± .01146	.15559 ± .01124	.17122 ± .01054	.15342 ± .01214
htru2	.02027 ± .00201	.02013 ± .00192	.02015 ± .00184	.02011 ± .00174	.02007 ± .00174	.02039 ± .00158
human-activity-smartphone	.00000 ± .00000	.00000 ± .00000	.00000 ± .00000	.00000 ± .00000	.00000 ± .00000	.00000 ± .00000
indoor-loc-building	.00007 ± .00015	.00007 ± .00013	.00008 ± .00014	.00009 ± .00015	.00009 ± .00015	.00010 ± .00016
indoor-loc-relative	.09112 ± .00520	.09473 ± .00492	.09438 ± .00510	.09586 ± .00468	.09540 ± .00573	.09347 ± .00485
insurance-benchmark	.06116 ± .00280	.06010 ± .00035	.06016 ± .00048	.06008 ± .00024	.06048 ± .00106	.06054 ± .00089
landsat-satimage	.00085 ± .00121	.00099 ± .00128	.00089 ± .00142	.00095 ± .00115	.00138 ± .00134	.00141 ± .00166
madelon	.43400 ± .02286	.42346 ± .01897	.42535 ± .02426	.41812 ± .02118	.43146 ± .03040	.42846 ± .02108
magic-gamma-telescope	.12444 ± .00548	.13173 ± .00474	.12745 ± .00512	.12834 ± .00414	.13234 ± .00549	.12454 ± .00544
mushroom	.00000 ± .00000	.00000 ± .00000	.00000 ± .00000	.00000 ± .00000	.00000 ± .00000	.00000 ± .00000
musk	.00531 ± .00265	.00812 ± .00392	.00793 ± .00344	.00769 ± .00337	.00905 ± .00430	.00672 ± .00383
nomao	.03761 ± .00228	.03929 ± .00191	.03909 ± .00246	.03875 ± .00253	.03933 ± .00244	.03934 ± .00199
nursery	.00024 ± .00037	.00024 ± .00031	.00026 ± .00031	.00026 ± .00031	.00029 ± .00038	.00026 ± .00031
occupancy-detection	.00873 ± .00129	.00899 ± .00136	.00888 ± .00129	.00892 ± .00140	.00929 ± .00158	.00915 ± .00145
page-blocks	.01680 ± .00368	.01752 ± .00424	.01668 ± .00364	.01661 ± .00385	.01786 ± .00434	.01704 ± .00384
pishing	.03572 ± .00406	.03766 ± .00454	.03753 ± .00408	.03667 ± .00408	.03625 ± .00396	.03703 ± .00361
polish-companies-bankruptcy-1year	.03918 ± .00037	.03913 ± .00017	.03919 ± .00025	.03918 ± .00027	.03910 ± .00010	.03912 ± .00032
polish-companies-bankruptcy-2year	.03935 ± .00013	.03935 ± .00013	.03933 ± .00010	.03933 ± .00010	.03932 ± .00007	.03939 ± .00018
polish-companies-bankruptcy-3year	.04721 ± .00021	.04719 ± .00017	.04718 ± .00016	.04717 ± .00014	.04719 ± .00017	.04736 ± .00047
polish-companies-bankruptcy-4year	.05262 ± .00014	.05258 ± .00000	.05262 ± .00017	.05264 ± .00020	.05258 ± .00000	.05301 ± .00054
polish-companies-bankruptcy-5year	.06934 ± .00045	.06973 ± .00098	.06985 ± .00117	.06988 ± .00121	.06978 ± .00104	.06978 ± .00187
seismic-bumps	.06820 ± .00396	.06642 ± .00133	.06669 ± .00218	.06592 ± .00129	.06747 ± .00258	.06723 ± .00340
smartphone-human-activity-postural	.00000 ± .00000	.00000 ± .00000	.00003 ± .00018	.00000 ± .00000	.00000 ± .00000	.00000 ± .00000
spambase	.08345 ± .04778	.06777 ± .00926	.06565 ± .01041	.06460 ± .00859	.07012 ± .00913	.06580 ± .00847
thyroid-all-bp	.03106 ± .00467	.03208 ± .00556	.03247 ± .00494	.03172 ± .00491	.03266 ± .00514	.03272 ± .00577
thyroid-all-hyper	.01818 ± .00374	.01768 ± .00374	.01777 ± .00361	.01724 ± .00398	.01724 ± .00401	.01821 ± .00362
thyroid-all-hypo	.05423 ± .00287	.05451 ± .00188	.05457 ± .00206	.05400 ± .00178	.05380 ± .00242	.05301 ± .00301
thyroid-all-rep	.02977 ± .00499	.03261 ± .00358	.03170 ± .00426	.03137 ± .00406	.03120 ± .00387	.02954 ± .00473
thyroid-ann	.05237 ± .00103	.03575 ± .00644	.02572 ± .00397	.02605 ± .00395	.02838 ± .00664	.02490 ± .00514
thyroid-dis	.02025 ± .00298	.01785 ± .00177	.01862 ± .00262	.01749 ± .00171	.01790 ± .00265	.01801 ± .00229
thyroid-hypo	.02126 ± .00489	.02063 ± .00489	.02085 ± .00533	.02059 ± .00521	.01963 ± .00448	.02074 ± .00484
thyroid-sick	.04701 ± .01530	.04121 ± .00734	.03906 ± .00809	.04061 ± .00783	.03903 ± .00818	.03366 ± .00600
thyroid-sick-eu	.00009 ± .00050	.00000 ± .00000	.00000 ± .00000	.00000 ± .00000	.00006 ± .00045	.00000 ± .00000
turkiye-student-evaluation	.10483 ± .04106	.11648 ± .05614	.03529 ± .00584	.03947 ± .00625	.02994 ± .00590	.02390 ± .00478
wall-follow-robot-2	.29972 ± .15443	.00704 ± .00367	.00172 ± .00139	.00170 ± .00141	.00669 ± .00369	.00149 ± .00115
wall-follow-robot-24	.24149 ± .06723	.05886 ± .00940	.05264 ± .00935	.05231 ± .00928	.05036 ± .00868	.04769 ± .00882
wall-follow-robot-4	.36927 ± .10264	.01617 ± .00631	.00792 ± .00298	.00727 ± .00346	.00985 ± .00476	.00609 ± .00283
waveform	.08217 ± .01124	.07732 ± .00985	.07586 ± .00992	.07411 ± .00984	.07554 ± .01045	.07708 ± .00915
waveform-noise	.08728 ± .00990	.08182 ± .00943	.08045 ± .01126	.08128 ± .00946	.08513 ± .01060	.08218 ± .01092
wilt	.01447 ± .00293	.02731 ± .00526	.01292 ± .00304	.01389 ± .00320	.02460 ± .00565	.01288 ± .00323
wine-quality-all	.28849 ± .01452	.28878 ± .01248	.28396 ± .01204	.28554 ± .01177	.29699 ± .01188	.28924 ± .01120
wine-quality-type	.00475 ± .00195	.00729 ± .00229	.00560 ± .00232	.00554 ± .00177	.00685 ± .00251	.00540 ± .00199
wine-quality-white	.27967 ± .02046	.28454 ± .01782	.27932 ± .01482	.27959 ± .01555	.29123 ± .01654	.28992 ± .02082
Average raw rank	3.6885	3.9508	3.2213	2.9590	3.8115	3.3689
Average adjusted rank	3.6230	3.9180	3.2295	3.0000	3.8852	3.3443
Fraction adjusted best runs	.4098	.1967	.1967	.2459	.2459	.3115
Fraction adjusted worst runs	.3115	.1639	.0984	.0656	.1967	.1803
Aver. rel. perform.	5.2716	1.2728	1.0801	1.0878	1.2155	1.0731
90 percent av. rel. perform.	1.0655	1.0890	1.0467	1.0499	1.1114	1.0339
Worst rel. perform.	188.9658	4.8571	1.5272	1.6485	4.2794	1.5853
90 percentile rel. perform.	1.9479	1.5230	1.2253	1.2772	1.6083	1.2878
80 percentile rel. perform.	1.1972	1.2537	1.1274	1.1616	1.3453	1.0557
70 percentile rel. perform.	1.0541	1.1033	1.0753	1.0965	1.1594	1.0379

Table 5: Comparison between *He-et-al.* with and without batch normalization, the original SeLU, and our new initialization strategies. Our new strategies outperform the three standard approaches both in terms of ranking and reliability.